

DESIGN AND ANALYSIS OF TEST RIG FOR SMALL SCALE WIND
TURBINE BLADE

A THESIS SUBMITTED TO
THE GRADUATE SCHOOL OF NATURAL AND APPLIED SCIENCES
OF
MIDDLE EAST TECHNICAL UNIVERSITY

BY

MUSTAFA İÇEN

IN PARTIAL FULFILLMENT OF THE REQUIREMENTS
FOR
THE DEGREE OF MASTER OF SCIENCE
IN
AEROSPACE ENGINEERING

DECEMBER 2019

Approval of the thesis:

**DESIGN AND ANALYSIS OF TEST RIG FOR SMALL SCALE WIND
TURBINE BLADE**

submitted by **MUSTAFA İÇEN** in partial fulfillment of the requirements for the degree of **Master of Science in Aerospace Engineering Department, Middle East Technical University** by,

Prof. Dr. Halil Kalıpçılar
Dean, Graduate School of **Natural and Applied Sciences**

Prof. Dr. İsmail Hakkı Tuncer
Head of Department, **Aerospace Engineering**

Prof. Dr. Demirkan Çöker
Supervisor, **Aerospace Engineering, METU**

Examining Committee Members:

Prof. Dr. Altan Kayran
Aerospace Engineering, METU

Prof. Dr. Demirkan Çöker
Aerospace Engineering, METU

Prof. Dr. Oğuz Uzol
Aerospace Engineering, METU

Prof. Dr. Kemal Levend Parnas
Mechanical Engineering, TED University

Assist. Prof. Dr. Gökhan Özgen
Mechanical Engineering, METU

Date: 27.12.2019

I hereby declare that all information in this document has been obtained and presented in accordance with academic rules and ethical conduct. I also declare that, as required by these rules and conduct, I have fully cited and referenced all material and results that are not original to this work.

Name, Surname: Mustafa İen

Signature:

ABSTRACT

DESIGN AND ANALYSIS OF TEST RIG FOR SMALL SCALE WIND TURBINE BLADE

İçen, Mustafa
Master of Science, Aerospace Engineering
Supervisor: Prof. Dr. Demirkan Çöker

December 2019, 150 pages

In this thesis, a test setup for the experimental 5 meter RÜZGEM wind turbine blade and that can be used for small scale wind turbine blades up to 9 meter is designed and analyzed. The purpose of this thesis is to help establishing the test infrastructure under METUWIND project such as NREL, RISØ, CRES. The literature on the existing facilities is reviewed. After that, RÜZGEM wind turbine blade is introduced and design loads are presented. To apply these loads appropriately to the blade, the moment distributions are converted to concentrated loads at 2 saddle points optimizing the load locations and corresponding loads using Excel Solver Add-in. The objective of these solutions is to obtain the best moment distribution on the blade compared to the given design moment distribution. With this design input, the load interface design of test fixture is performed. Next, hydraulic equipment and load cell selection are carried out and support structure is designed which is composed of main reaction wall and ground support. Resultant test fixture capacity is verified by structural analysis using FEM and hand calculation methods under static loading. Finally, required infrastructural cost is estimated.

Keywords: Wind Turbine Blade, Test Load Optimization, Wind Turbine Blade Testing, Test Rig Design

ÖZ

KÜÇÜK ÖLÇEKLI RÜZGAR TÜRBİNİ KANADI İÇİN TEST DÜZENEĞİ TASARIMI VE ANALİZİ

İçen, Mustafa
Yüksek Lisans, Havacılık ve Uzay Mühendisliği
Tez Danışmanı: Prof. Dr. Demirkan Çöker

Aralık 2019, 150 sayfa

Bu tezde, 5 metre boyundaki RÜZGEM tam boy deneysel rüzgar türbini kanadı ve 9 metreye kadar olan küçük ölçekli rüzgar türbini kanatları için test düzeneği tasarlanmış ve analiz edilmiştir. Bu tezin amacı, RÜZGEM projesi kapsamında, dünyadaki diğer örnekleri gibi bir test altyapısı oluşturulmasına yardımcı olmaktır. Çalışmanın en başında, literatür taraması yapılmış ve mevcut merkezleri incelenmiştir. Daha sonra, RÜZGEM kanadı tanıtılmış ve tasarım yükleri sunulmuştur. Kanada, tasarım moment dağılımına yaklaşan en iyi yükleri vermek için Excel çözücü eklentisinde yük uygulama noktaları ve karşılık gelen yükler iki nokta için optimize edilmiştir. Bu tasarım girdisiyle beraber, yük arayüzleri tasarımı gerçekleştirilmiştir. Sonrasında, hidrolik ekipman ve yük hücresi seçimi yürütülmüş olup, test düzeneği tasarımı ana reaksiyon duvarı ve yer destek yapısıyla beraber tamamlanmıştır. Tasarlanmış olan test düzeneğinin belirtilen kanat için static yüklerde çalışma kapasitesi sonlu elemanlar yöntemi ve el hesabıyla doğrulanmıştır. Son olarak, test altyapısını oluşturmak için gerekli tahmini maliyet hesabı ortaya dökülmüştür.

Anahtar Kelimeler: Rüzgar Türbini Kanadı, Test Yük Optimizasyonu, Rüzgar Türbini Kanat Testi, Test Düzeneđi Tasarımı

To my family...

ACKNOWLEDGEMENTS

First and foremost, I would like to express my deepest gratitude to my supervisor Assoc. Prof. Dr. Demirkan öker, for his guidance, criticism, advice and encouragements throughout my study.

I am grateful to my parents, Mehmet İen and Hatice İen and my brother, Hüseyin Oğuz İen for their endless love and support. They were always encouraging me with their best wishes.

I would like to offer my thanks to my colleagues in Turkish Aerospace, Fırat Temel, Afif Umur Limon, Levent Ulu and Yusuf Ulu. Without their help, this study would not have been finished.

I would also like to thank my friends and special thank my housemate Süleyman Altınışık for their great support. They always encourage me and keep me lively with his different point of view and amusing moments.

Finally, for her great understanding and affection, I would like to special thank Hesna İzel Atıcı who has always been by my side. I managed to overcome the difficulties in the process with her love and understanding.

TABLE OF CONTENTS

ABSTRACT	v
ÖZ	vii
ACKNOWLEDGEMENTS	x
TABLE OF CONTENTS	xi
LIST OF TABLES	xiv
LIST OF FIGURES	xv
CHAPTERS	
1. INTRODUCTION	1
1.1. Modern Wind Energy	1
1.2. Wind Turbine Blade Structure	2
1.3. Wind Turbine Blade Loads	3
1.4. Wind Turbine Blade Testing	4
1.5. Wind Turbine Blade Testing Methods	6
1.5.1. Static Testing	7
1.5.2. Fatigue Testing	10
1.6. Motivation	10
1.7. Methodology	10
2. LITERATURE SURVEY	13
2.1. Wind Turbine Blade Test System	13
2.2. Differences between Wind Turbine Blade Test System and Helicopter Blade Test System	23
3. RÜZGEM BLADE AND LOAD CALCULATION	27

3.1. Wind Turbine Blade in METU RÜZGEM	27
3.2. RÜZGEM Blade Coordinate System	29
3.3. Design Loads of RÜZGEM Blade	30
3.4. Calculation of Applied Loads and Locations for Two Saddle Points.....	33
3.5. Calculation of Applied Loads and Locations for One Saddle Point	52
3.6. Discussions.....	55
4. DESIGN OF TEST SETUP	57
4.1. Test Rig Design.....	57
4.1.1. Dummy Hub and Loading Interfaces Design.....	58
4.1.2. Load Cell and Hydraulic Actuator Selection	66
4.1.3. Support Structure Design	71
4.2. Architecture of the Test System.....	79
5. ANALYSIS OF THE TEST SYSTEM.....	83
5.1. Structural Analysis.....	83
5.2. Material Selection	83
5.3. Load Data.....	84
5.4. Material, Fastener and Allowable Data.....	85
5.5. Finite Element Model (FEM) Description	86
5.6. Strength Analysis	93
5.6.1. Reserve Factor Summary	118
5.7. Fatigue Analysis.....	119
6. CONCLUSION	121
6.1. Summaries and Conclusion.....	121
6.2. Future Work	122

REFERENCES.....123

APPENDICES

A. Extreme Loads Including Safety Factor129

B. Cost Analysis143

C. M16 Bolt Loads of Reaction Wall Assembly.....145

D. Hilti HAS – U 8.8 Anchor Loads for Ground Plate.....148

E. Hilti HAS – U 8.8 Anchor Loads for Reaction Wall Assembly.....149

LIST OF TABLES

TABLES

Table 2.1. Loading Steps	20
Table 3.1. Fx And My Along Over Blade Radial Position.[28]	32
Table 3.2. Location and Corresponding Loads for Initial Values $x_1 = 1.5\text{ m}$, $x_2 = 3.5\text{ m}$, $F_1/F_r = 0.6$, $F_2/F_r = 0.4$ using $f_{AD}(x)$ as Objective Function	44
Table 3.3. Different Initial Values of Changing Parameters	47
Table 3.4. Solutions with Different Initial Values.....	50
Table 5.1. Material Allowable Values [39], [40].....	85
Table 5.2. Fastener Material Allowable Values [40], [41]	85
Table 5.3. Reaction Wall Assembly Maximum M16 Bolt Loads	115
Table 5.4. Stiffness Constant Calculation Details of Bolts on Support Structure ...	117
Table 5.5. Results and Variables of Failure Check of the Bolts on Support Structure	117
Table 5.6. M30 Hilti HAS-U 8.8 Maximum Anchor Loads.....	117
Table 5.7. Reserve Factor Summary.....	118
Table 5.8. Endurance Strength.....	120
Table 0.1. Estimated Cost for Equipment.....	144
Table 0.2. Bolt Loads Obtained from FE Results.....	145
Table 0.3. Ground Plate Hilti Anchor Rod Loads	148
Table 0.4. Reaction Wall Assembly Hilti Anchor Rod Loads	149

LIST OF FIGURES

FIGURES

Figure 1.1. Representative Size, Height and Diameter of Wind Turbines [1]	1
Figure 1.2. Share of Major Wind Turbine Component Failures [2]	2
Figure 1.3. Typical Wind Turbine Blade Cross-Section [3]	3
Figure 1.4. Lift and Drag Directions [5]	3
Figure 1.5. Representation of Flapwise (upper) and Edgewise (lower) Bending of a Rotor Blade [6].....	4
Figure 1.6. Distributed Surface Loads [14].....	7
Figure 1.7. Single Point Method [8]	8
Figure 1.8. Multiple Point Method with Whiffletree System [8].....	9
Figure 1.9. Multiple Point Method without Whiffletree System [15].....	9
Figure 1.10. Wind Turbine Blade Test Rig Design Steps.....	11
Figure 2.1. Blade Test Facility in CECET [16]	14
Figure 2.2. Blade Wall Mount Adapters [16]	14
Figure 2.3. Conventional Bell Crank System for Biaxial Testing [4].....	15
Figure 2.4. Alternative Method for Fatigue Testing [4]	16
Figure 2.5. Concentrated load at the tip	17
Figure 2.6. Concentrated load far from the tip.....	17
Figure 2.7. Concentrated load simultaneously at different locations.....	17
Figure 2.8. Sketch of bi-axial test setup from blade tip [19].....	18
Figure 2.9. Whiffletree arrangement on 9 meters wind turbine blade [20].....	19
Figure 2.10. A full-scale wind turbine blade under flap-wise loading static test [21]	20
Figure 2.11. Sketch of Whiffletree with 4 Saddle Points.....	22
Figure 2.12. Shear Force Comparison along the Blade in 4 Saddle Point [22]	22
Figure 2.13. Bending Moment Comparison along the Blade in 4 Saddle Point [22]	23

Figure 2.14. Helicopter Load Pattern during Testing [24], [25].....	25
Figure 2.15. Helicopter Blade Root Section Test System [24].....	25
Figure 2.16. Example of Wind Turbine Blade Test Setup [27].....	26
Figure 3.1. RÜZGEM Blade Composition [29]	28
Figure 3.2. Maximum Tip Deflection [29]	28
Figure 3.3. Existing Blade in METU RÜZGEM [30]	29
Figure 3.4. Coordinate System of the RÜZGEM Blade [28]	30
Figure 3.5. Flapwise Load over Blade Radial Position	31
Figure 3.6. Flapwise Bending Moments over Blade Radial Position.....	32
Figure 3.7. Scheme of Notations on the Blade	34
Figure 3.8. Initial Values, Constraints and Corresponding Sum of Moment Percentage Error.....	39
Figure 3.9. Introducing Objective, Changing Variables and Constraints.....	41
Figure 3.10. Saddle Locations and Corresponding Loads after Solution for Initial Values $x_1 = 1.5m$, $x_2 = 3.5m$, $F_1/F_r = 0.6$, $F_2/F_r = 0.4$ using $fPE(x)$ as Objective Function.....	42
Figure 3.11. Shear Distribution for Initial Values $x_1 = 1.5m$, $x_2 = 3.5m$, $F_1/F_r = 0.6$, $F_2/F_r = 0.4$ using $fPE(x)$ as Objective Function	42
Figure 3.12. Moment Distribution for Initial Values $x_1 = 1.5m$, $x_2 = 3.5m$, $F_1/F_r = 0.6$, $F_2/F_r = 0.4$ using $fPE(x)$ as Objective Function.....	43
Figure 3.13. Shear Distribution for Initial Values $x_1 = 1.5 m$, $x_2 = 3.5 m$, $F_1/F_r = 0.6$, $F_2/F_r = 0.4$ using $fAD(x)$ as Objective Function	44
Figure 3.14. Moment Distribution for Initial Values $x_1 = 1.5 m$, $x_2 = 3.5 m$, $F_1/F_r = 0.6$, $F_2/F_r = 0.4$ using $fAD(x)$ as Objective Function	45
Figure 3.15. Comparison of the First Approach using $fPE(x)$ and the Second Approach using $fAD(x)$	46
Figure 3.16. Moment Distribution for Initial Values $x_1 = 1.5 m$, $x_2 = 3.5m$, $F_1/F_r = 0.8$, $F_2/F_r = 0.2$ using $fAD(x)$ as Objective Function (Set 2).....	48

Figure 3.17. Moment Distribution for Initial Values $x_1 = 0.8\text{ m}$, $x_2 = 4.8\text{ m}$, $F_1/F_r = 0.7$ $F_2/F_r = 0.3$ using $f_{AD}(x)$ as Objective Function (Set 4)	49
Figure 3.18. Moment Distributions of Set 1, Set 2, Set 3, Set 4	50
Figure 3.19. Comparison of Solutions in terms of Moment Errors	51
Figure 3.20. Schematic of Test Loads and Locations	52
Figure 3.21. One Saddle Point Representation	52
Figure 3.22. Moment Distribution of One Saddle Point	53
Figure 3.23. Moment Error of One Saddle Point	54
Figure 4.1. Concept Design of the Test Rig.....	57
Figure 4.2. General view of the test rig.....	58
Figure 4.3. Existing Blade's Root Detail	59
Figure 4.4. Dummy Hub Plate and Assembly.....	60
Figure 4.5. Saddle near the Root.....	61
Figure 4.6. Saddle near the Tip	62
Figure 4.7. INA FAG GIR17-UK Specifications [32].....	63
Figure 4.8. Cross Section of Clevis and Rod End Assembly.....	64
Figure 4.9. 3D Model of the Clevis	65
Figure 4.10. Clevis Attached to the Root Saddle.....	65
Figure 4.11. Clevis Attached to the Tip Saddle	66
Figure 4.12. Interface Load Cell Specifications [33].....	67
Figure 4.13. RotaTeknik Hydraulic Actuator Specifications [34]	69
Figure 4.14. Actuator Assembly	70
Figure 4.15. Connection of Actuator – Load Cell – Rod End.....	71
Figure 4.16. T-Slot Specification [35]	72
Figure 4.17. DIN 508 T Nut [36] and Assembly of T Nut in T Slot Channel	73
Figure 4.18. General Dimensions of Main Reaction Wall.....	74
Figure 4.19. Reaction Wall Plate and Weldment Assembly.....	74
Figure 4.20. Hilti HAS-U 8.8 Anchor [37]	75
Figure 4.21. Assembly of Hilti HAS-U 8.8 Anchor [38].....	75
Figure 4.22. Actuator Ground Plate	76

Figure 4.23. Assembly of the Actuator to the Ground Plate	77
Figure 4.24. Holes on the Plate.....	78
Figure 4.25. Final Position of the Blade at 100% Loading	79
Figure 4.26. Architecture of the Test System	80
Figure 5.1. Sketch of Load and Boundary Conditions (left), FEM of Actuator Circular Plate (right)	87
Figure 5.2. Load and Boundary Conditions of the Ground Plate (left), Finite Element Model of the Ground Plate (right)	88
Figure 5.3. FE Model of the Lower Part of the Root Saddle.....	89
Figure 5.4. FE Model of the Lower Part of the Tip Saddle	89
Figure 5.5. Load and Boundary Conditions (left), FE Model of the Dummy Hub Plate (right)	90
Figure 5.6. FE Model of the Reaction Wall Plate.....	91
Figure 5.7. FE Model and Load Condition of Reaction Wall Weldment Assembly.	92
Figure 5.8. Boundary Condition and Detailed FE Model of Reaction Wall Weldment Assembly	92
Figure 5.9. Displacement Contours of the Ground Plate [mm].....	93
Figure 5.10. Von-Mises Stress Contours of the Ground Plate (left:back, right:front) [MPa]	94
Figure 5.11. Displacement Contours of the Actuator Circular Plate [mm]	95
Figure 5.12. Von-Mises Stress Contours of the Actuator Circular Plate [MPa]	95
Figure 5.13. Displacement Contours of the Root Saddle of Lower Part [mm]	96
Figure 5.14. Von-Mises Stress Contours of Root Saddle of Lower Part [MPa]	97
Figure 5.15. Displacement Contours of Tip Saddle of Lower Part [mm]	98
Figure 5.16. Von-Mises Stress Contours of Tip Saddle of Lower Part [MPa].....	98
Figure 5.17. Displacement Contours of Dummy Hub Plate [mm]	99
Figure 5.18. Von-Mises Stress Contours of Dummy Hub Plate [MPa]	100
Figure 5.19. Displacement Contours of Reaction Wall Plate [mm]	101
Figure 5.20. Von-Mises Stress Contours of Reaction Wall Plate [MPa]	101

Figure 5.21. Displacement Contours of Reaction Wall Weldment Assembly [mm]	102
Figure 5.22. Von-Mises Stress Contours of Reaction Wall Weldment Assembly [MPa]	103
Figure 5.23. Detail View of Von-Mises Stress of Reaction Wall Weldment Assembly [MPa]	103
Figure 5.24. Von-Mises Stress Contours of Welding	104
Figure 5.25. Basic Profile for Metric Thread [41]	105
Figure 5.26. General Basic Dimensions of the Clevis	107
Figure 5.27. Shear-Bearing Efficiency Factor [42].....	108
Figure 5.28. Lug Efficiency Factor for Tension [42].....	110
Figure 5.29. Pin Moment Arm for Determination of Bending Moment [44]	114
Figure 0.1. Bolt Number Guideline.....	145
Figure 0.2. Ground Plate Anchor Rod Guideline.....	148
Figure 0.3. Reaction Wall Assembly Anchor Rod Guideline	149

CHAPTER 1

INTRODUCTION

1.1. Modern Wind Energy

Over the three decades, wind turbine systems have improved, and they have widespread usage around the world as a competitive energy resource. The size of wind turbines has been increased significantly from 50 kW to 2 MW, with new wind turbines up to 5 MW currently designed. The evolution of size of wind turbines can be seen in Figure 1.1 [1].

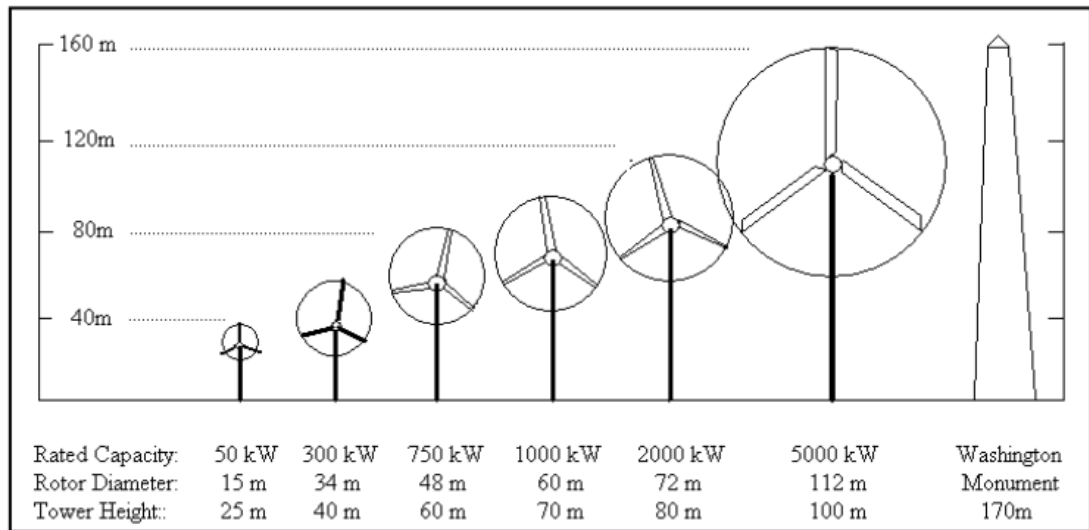


Figure 1.1. Representative Size, Height and Diameter of Wind Turbines [1]

As a renewable and environmentally friendly source of energy, wind turbine systems are used in many countries, and wind energy is recognized as an affordable and reliable for providing electricity. Manufacturing and logistic constraints require

components as light and affordable as possible. As a result of widespread usage and these constraints, wind turbines also brings failure. Rotor blades comprise roughly 7% of total wind turbine component failures, as shown in Figure 1.2 [2].

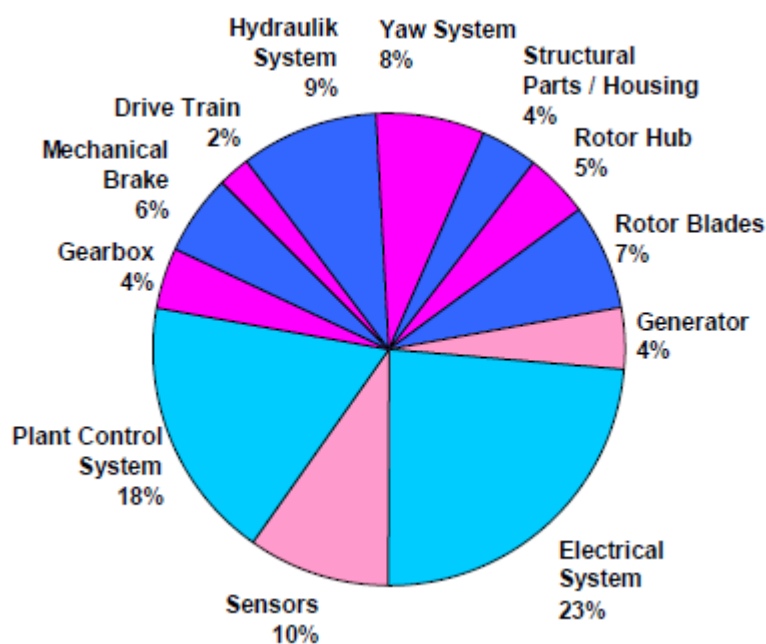


Figure 1.2. Share of Major Wind Turbine Component Failures [2]

1.2. Wind Turbine Blade Structure

Blades have three sections from the root to the tip: circular root cross-section to mount hub, transition region from circular to aerodynamic cross-section shape, and airfoil cross-section along with the transition to the tip. Generally, reinforced fiberglass composite materials comprise a wind turbine blade as a primary material of the blade that gives aerodynamic shape to the blade. Single or double shear webs are used to create a beam box structure which carries the loads along the span. The typical wind turbine blade cross-section is illustrated in Figure 1.3 [3].

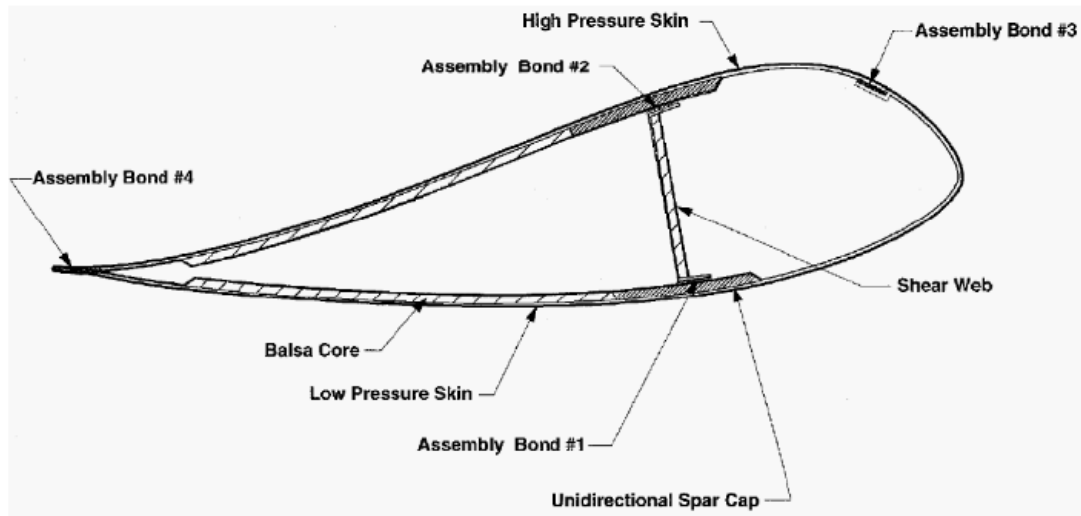


Figure 1.3. Typical Wind Turbine Blade Cross-Section [3]

1.3. Wind Turbine Blade Loads

Wind turbine blades are subjected mainly two types of loads, which are aerodynamic loads and inertial loads [4]. Aerodynamic loads involve lift, drag, shear, etc. whereas inertial loads contain gravity, blade dynamics, etc. Due to the drag and lift forces shown in Figure 1.4 on the blades [5], edgewise (lead-lag) and flapwise bending moments arise. These moments are shown in Figure 1.5 [6].

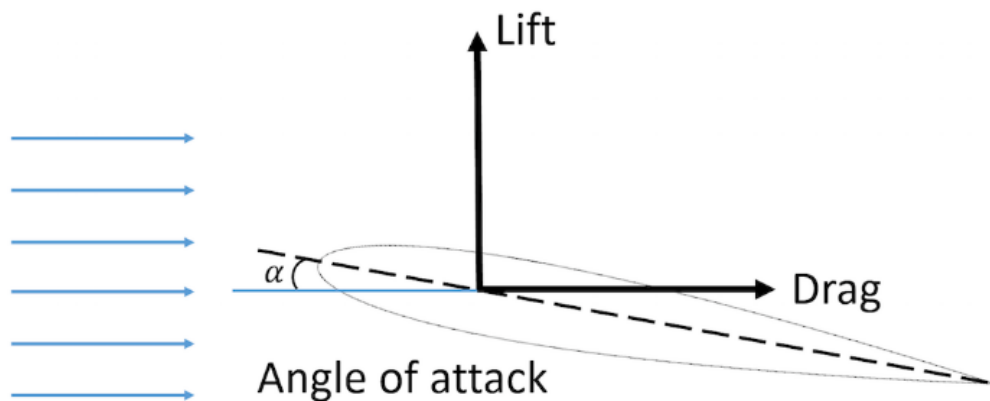


Figure 1.4. Lift and Drag Directions [5]

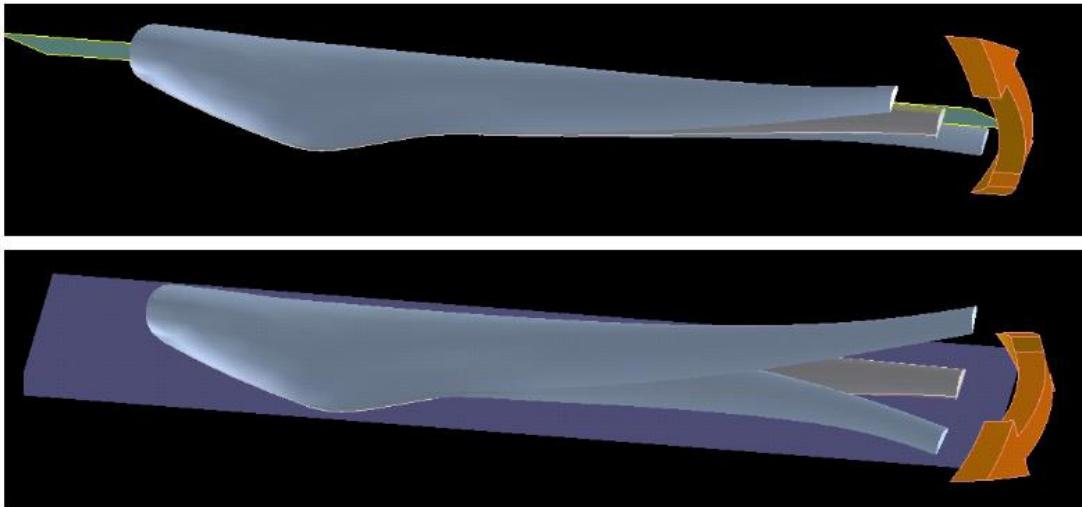


Figure 1.5. Representation of Flapwise (upper) and Edgewise (lower) Bending of a Rotor Blade [6]

Because of the airfoil shape, blades have higher stiffness in edgewise direction and can carry higher bending moments in this direction. Within these two flapwise and edgewise bending moments, a flapwise bending moment is readily induced by wind loads. Due to the lower strength in flapwise direction, these forces and moment are the deterministic components. Moreover, inertial loads are not considered as significant loads for small scale wind turbine blades.

1.4. Wind Turbine Blade Testing

As one of the most crucial parts of the wind turbine system, a reliable wind turbine blade to be developed is the main focus of designers and manufacturers. In this development, wind turbine blade testing is considered as a requirement. Full scale testing, which is the ultimate static test and fatigue test, is performed to certificate a new blade developed in accordance with the “International Electrotechnical Commission (IEC) 61400 Part-22 [7] document approved by the IEC Technical Committee 88-Wind Turbine Blades. Every new blade developed is subjected to these

testing for not only certification issues but also there are other reasons for that [8].

These reasons are listed below:

- To verify design analysis and structural integrity of the blade
- To check the strength of the rotor blade
- To substantiate the analysis of full scale blade
- To demonstrate the fatigue life of the blade
- To provide full scale test data to establish the predicted service life of the structure analytically

The main focus of certification testing is to conform certification requirements by conducting both static and fatigue tests. In other words, it should be shown that the blade should withstand extreme loads and should not fail during its service life [8]. In this thesis, the main focus will be static testing to ensure that the blade does not fail under extreme design loads given.

Structural testing of wind turbine blades is performed around the world in a few structural laboratories designed for these testing. National Renewable Energy Laboratory (NREL) (USA) [9], Center For Renewable Energy Sources (CREG) (Greece) [10], Delft (Netherlands) [11], Risø National Laboratory for Sustainable Energy (Denmark) [12] are several examples of these laboratories. With this thesis, setting up a testing infrastructure conducting a blade testing within RÜZGEM is aimed. The testing procedure implemented in these laboratories generally follows the standardization document “IEC/TS 61400-23 Wind Turbine Generator Systems – Part 23: Full-Scale Structural Testing of Rotor Blades [8]. This document generally describes how full-scale blade testing is to be performed, but it should not be considered as a requirement for every blade design. That means an alternative method for testing can be used. In this document, technical specifications for static strength tests, fatigue tests, and other tests determining blade properties are considered. It is stated that the blade shall be described by means of drawings and specifications.

Moreover, instructions for handling, lifting should be provided. For testing of the blades, six load components (F_x , F_y , F_z , M_x , M_y , M_z) shall be defined along the blade span. However, not all loads have equal importance, and some of them are applied to the blades. Flapwise and edgewise moments are usually applied to the blade. Due to the limitations of the test laboratory, it is not practical to establish the same loading conditions as in the design.

In order to collect data on the blade, several measurement techniques are used. Mainly, strain gauges are implemented to obtain strain data on the blade during testing. Moreover, there are some tools like displacement transducer, load cell, angle sensor, etc.

For loading of the blade in a static test, the test procedure shall contain some steps until 100% test loads. At the required maximum test load (100% of extreme design load), the test load should be maintained at least 10 seconds, and then the load is released until zero [13].

1.5. Wind Turbine Blade Testing Methods

There are two types of blade testing. These are static and fatigue testing. There are two types of loading methods, which are load-based and strength-based. In the certification process, a load-based test is used, and the main purpose of this method is to demonstrate that the blade will endure the extreme design loads without failure.

For all of these loading methods, blades should be fixed at the root, and loading should be applied with load introduction, which is called the load saddles on the blade.

1.5.1. Static Testing

In this testing, loads are applied to the blade statically until reaching ultimate strength or failure. With this test, it is ensured that the blade can withstand extreme loads during operation.

There are three types of static loading methods, and all of these have advantages and disadvantages [8]. The first one is distributed surface loads. This loading is carried out by heavy sandbags distributed over the blade surface. The main advantage of this method is that it is the best representation of shear forces, while the disadvantages of this method are that loading can be dangerous while adding a bag at extreme loads. This loading is limited to a single axis. An example of this method can be seen in Figure 1.6 [14]



Figure 1.6. Distributed Surface Loads [14]

The second method is called a single point method. In this method, loads are applied as concentrated to the blade in one section. This loading results higher shear loads on the blade. This loading can be conducted with a crank or hydraulic actuator. Multiple loading at different sections can be required. A single point method is shown in Figure 1.7 [8].



Figure 1.7. Single Point Method [8]

The third method is a multiple point method. In this method, loading is applied at different sections simultaneously so that more representative shear and moment distribution can be acquired. These distributions are more realistic than a single point method. The disadvantage of this method is that it requires a more complex test setup system. Multiple point methods can be conducted with several hydraulic actuators or cranks, as well as the whiffletree system. Example figures for multiple point methods with and without a whiffletree system are given in Figure 1.8 and Figure 1.9 [8] - [15].

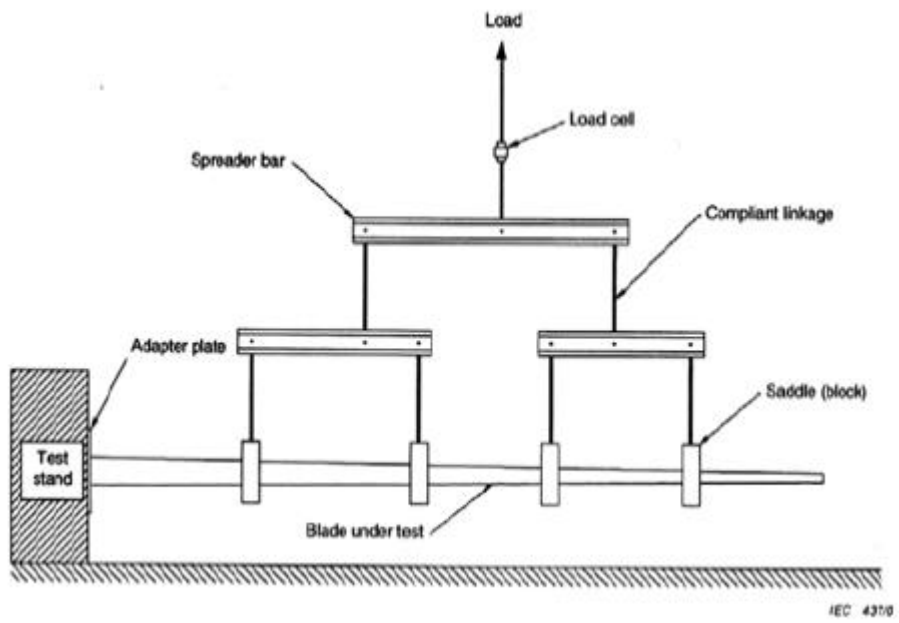


Figure 1.8. Multiple Point Method with Whiffletree System [8]



Figure 1.9. Multiple Point Method without Whiffletree System [15]

1.5.2. Fatigue Testing

In fatigue testing, the durability of the blade is verified with a cyclic loading profile. These cyclic load can be 1 million to 5 million load cycles. Fatigue test is conducted mainly in two directions, which are flapwise and edgewise. This testing can be respectively or simultaneously. Simultaneously method is called dual-axis, and better simulation of the loads facing in operation can be experienced. This method also can take a shorter time than uniaxial testing. Applying load can be divided into two that are forced displacement and resonant oscillation [4].

1.6. Motivation

With an increasing demand for energy in the world, countries are forced produce new alternative energy methods. Wind energy is one of these. For this reason, increasing wind energy generation is one of the motivations of Turkey. METUWIND is established to research on wind energy with government support. In this thesis, it is aimed to establish testing infrastructure, both static and fatigue tests in METU under the METUWIND project. It is planned to be capable of having a test of the blade up to 9 meters in this facility. In this thesis, a static test of 5 meters RÜZGEM blade is defined, and a test fixture is designed to cover tests of blades up to 9 meters.

1.7. Methodology

In this part, briefly how to conduct test setup design is explained in Figure 1.10 as follow,

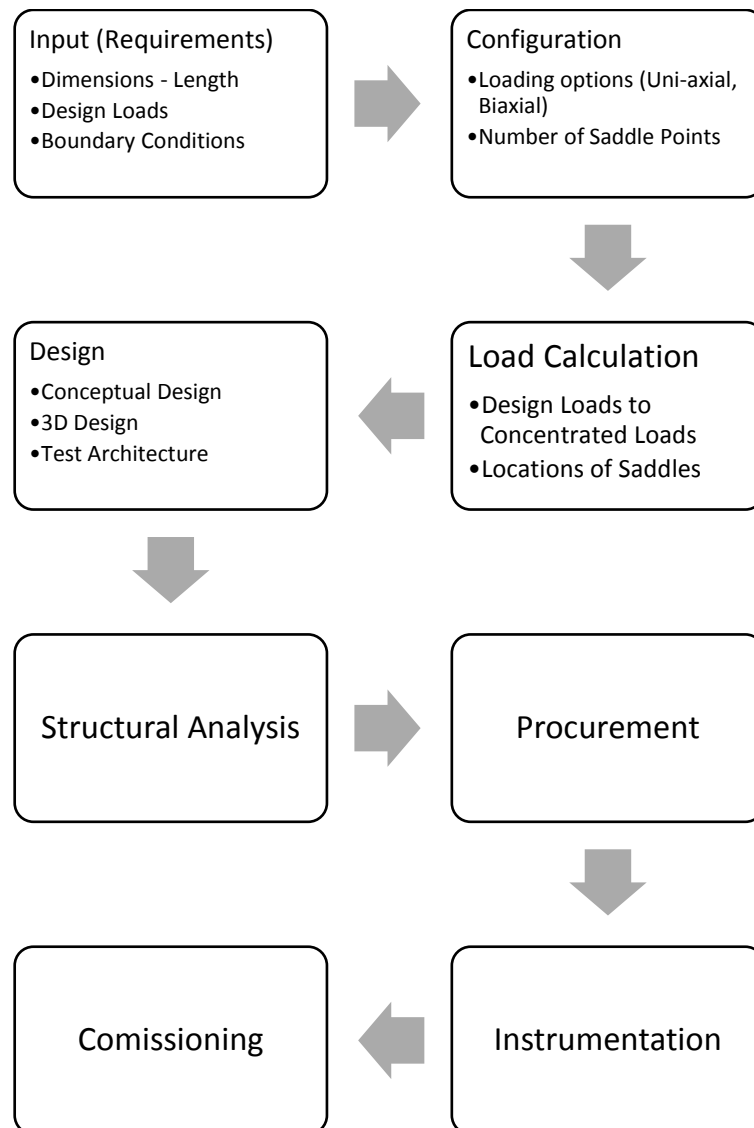


Figure 1.10. Wind Turbine Blade Test Rig Design Steps

Firstly, the required data are evaluated as an input to start a concept. With these data and literature research, the configuration is decided. In the direction of the configuration decided, load calculation is performed. The selection of actuators and load cells are made according to the load to be applied. With this information, conceptual design options are presented, and by acceptance of one concept, detailed design is started. According to the detail design, the architecture of the test system is

determined. When the detail design is finished, structural analysis is performed for the detail parts used in the test rig by using load to be applied to the system. If the structural analysis is satisfied, procurement is started. With the settlement of the test system, instrumentation of the test specimen is performed and finally, commissioning is conducted.

CHAPTER 2

LITERATURE SURVEY

In this chapter, a literature survey on test setup design of wind turbine blades is presented. The following brief information are summarized. In the first section, literature on work conducted on wind turbine blade test systems and in the second section, differences between test systems for wind turbine blades and helicopter rotor blades are summarized.

2.1. Wind Turbine Blade Test System

According to IEC 61400-23 [8], static and fatigue tests required to be carried out in order to conform certification requirements. In the last 20 years, many test facilities have been developed to perform static and fatigue test on wind turbine blade. There are two types of blade testing facilities. The first type is small scale wind turbine blade testing that commonly utilizes servo hydraulic or electromechanical actuators to apply loads. The second type is large scale wind turbine blade which is greater than 20-meters that commonly utilizes cranks that pull the blades transversely to apply bending moments to the blades. The test setup and load applications in the literature are summarized in the following paragraphs.

Valyou et al [16] used the Blade Test Facility of CECET at Clarkson University, which was established in 2013 [17]. The test facility has a capability of static and fatigue loading of wind turbine blades with length up to 15-meters. Figure 2.1 shows the facility's layout. This test facility consists of an 8 m x 14 m strong floor with 6 m wide x 5 m high reaction walls. The reaction walls and strong floor were designed to sustain up to 1 MNm and floor can withstand 445 kN for testing of small and mid-size wind turbine facility. The reaction wall has two test stands. Hub connections of the test

stand can be modified in accordance with the blade types. Blade wall mount drawing for the hub constraint of the blades is shown in Figure 2.2. This facility is equipped with MTS System Corporation. With the equipment based in the blade test facility, static, fatigue, modal testing of the blades can be performed with the desired configuration. Also, note that the development of the Blade Test Facility's bi-axial fatigue test system is underway.

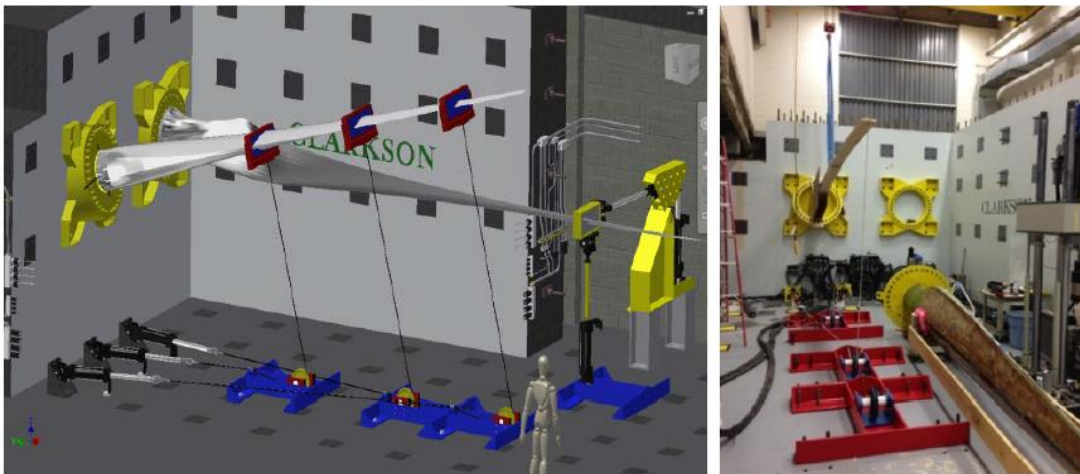


Figure 2.1. Blade Test Facility in CECET [16]

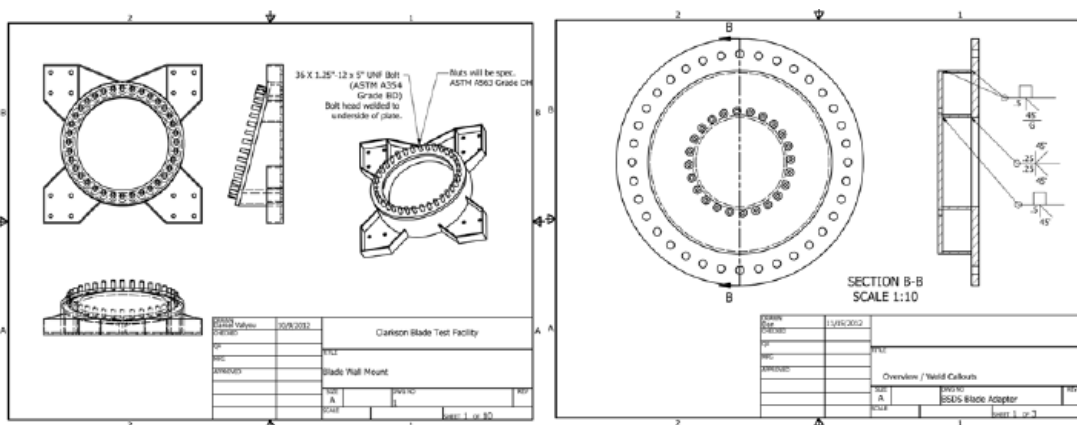


Figure 2.2. Blade Wall Mount Adapters [16]

In [4], Malthora studied different testing methods and improvements to a conventional concept for testing of large wind turbine blades in University of Massachusetts Amherst. He stated that blades should be tested in terms of both statically and dynamically in order to improve the design and the manufacturing processes. In this study, two different approaches to the design of a bell crank system have been improved to test large scale blades. The conventional bell crank system for testing the blade in both directions is shown in Figure 2.3. Alternative method to test large scale blades is conducted, and the design of this method has been modeled in SolidWorks and analyzed. This alternative design conducted in this study is illustrated in Figure 2.4. This concept is about to excite the blade simultaneously both in flapwise and edgewise directions. BREX resonant technology is used for flapwise excitation in NREL, and two inclined actuators and linear rail guide system are used to excite edgewise motion. This system is analyzed and discussed in this study.

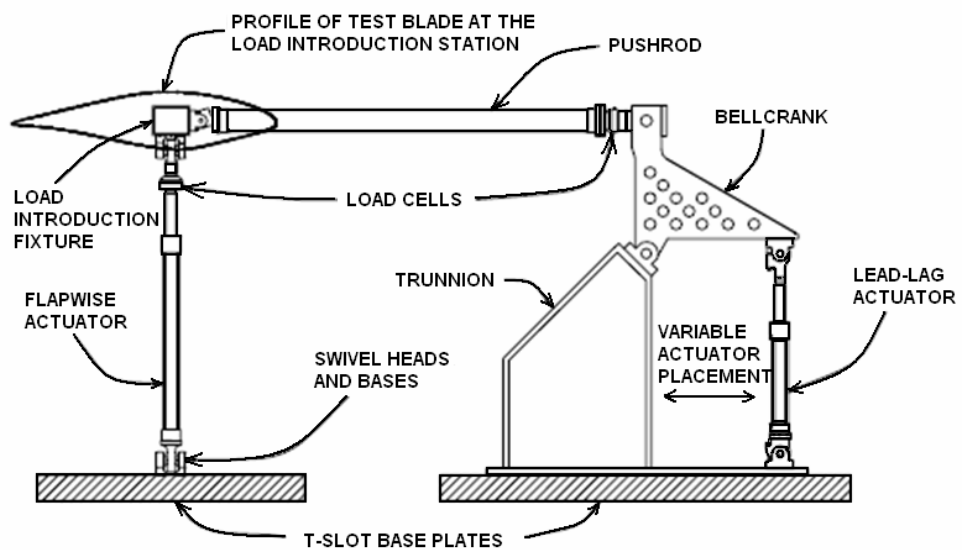


Figure 2.3. Conventional Bell Crank System for Biaxial Testing [4]

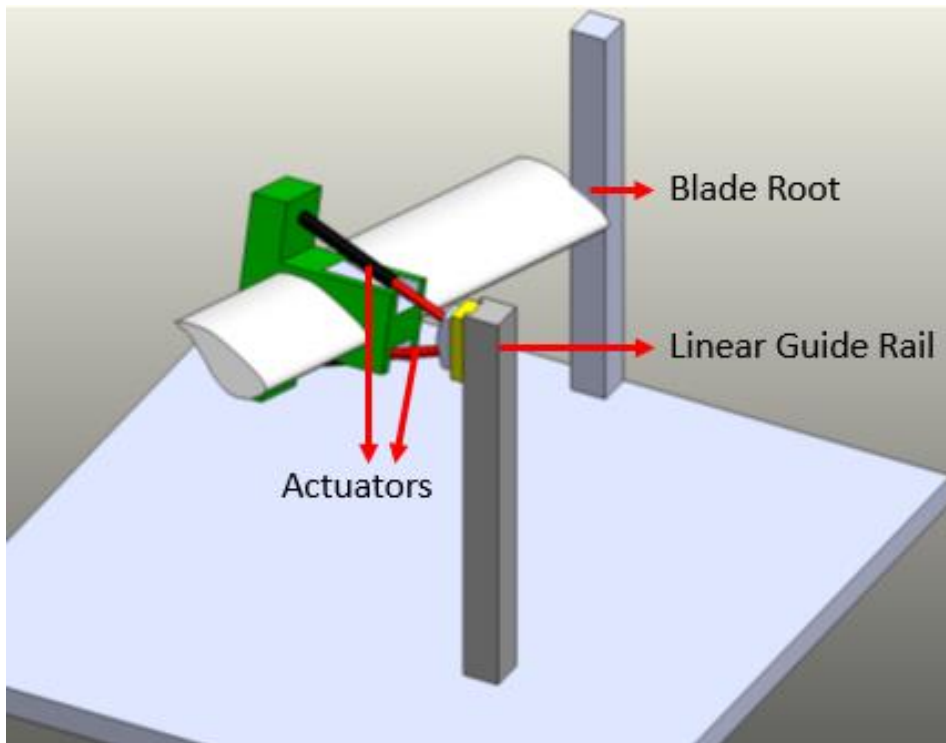


Figure 2.4. Alternative Method for Fatigue Testing [4]

In [18], Bürkner et al. stated that the blade is loaded by a distributed load. However, concentrated loads are applied to the blade during testing. Moment distribution has become inaccurate because of this reason. Concentrated load at the tip causes deviation from the actual bending moment distribution subjected to in the practical application as shown in Figure 2.5. In order to counter this effect, there are two options. The first option is to carry out the testing with two separate tests subsequently. In these two independent testing, different load introduction position is used as seen in Figure 2.5 and Figure 2.6. The main disadvantage of this method is that it requires too much effort and time. The second option is to put loads at two different positions simultaneously, which results in fairly accurate moment distribution, as in Figure 2.7. For this reason, a generally simultaneous test procedure is followed.

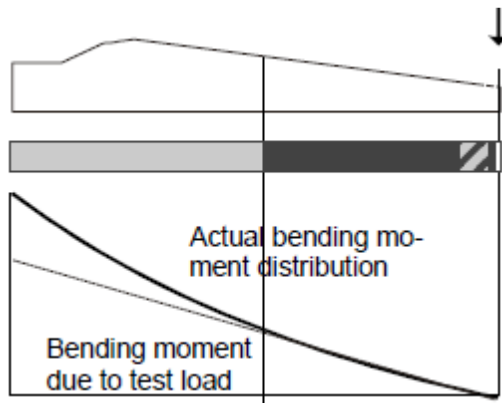


Figure 2.5. Concentrated load at the tip

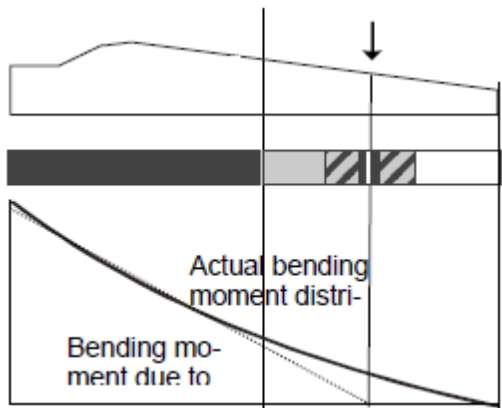


Figure 2.6. Concentrated load far from the tip

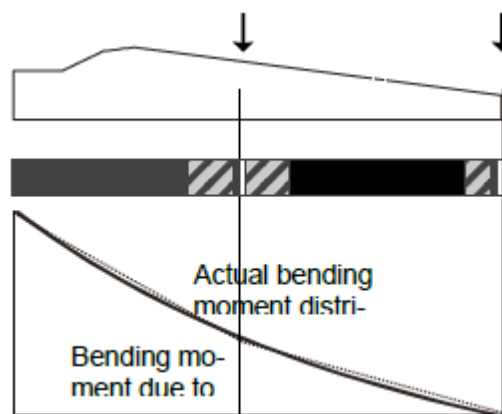


Figure 2.7. Concentrated load simultaneously at different locations

In [19], Bürkner et al. presented a new method for testing. Conventional testing is composed of up and down flapwise and edgewise loading. In conventional methods, these loadings are applied separately, and therefore it may take too much time, which can easily exceed five months. The option presented to reduce testing time is to determine the eigenfrequency of the blade once and then apply flapwise and edgewise loading combined as a cyclic. A sketch of the bi-axial loading test setup is shown in Figure 2.8. The advantage of this configuration is reducing the time by factor two. Also, the loading of the material in terms of a three dimensional stress or strain state seems to be closer compared to loading of the blade in use on a turbine. The other advantage is that no influence of higher frequency movements of the blade. In other words, the higher frequency can be achieved with this configuration. On the other hand, in this system, the design of test rig is challenging. Because of bi-axial loading simultaneously, test rig more complicated than conventional test rigs. And also, the compatibility of hydraulic actuators may arise a problem. With this configuration, time consumption problems can be achieved, but the assembly of this test setup will be hard.

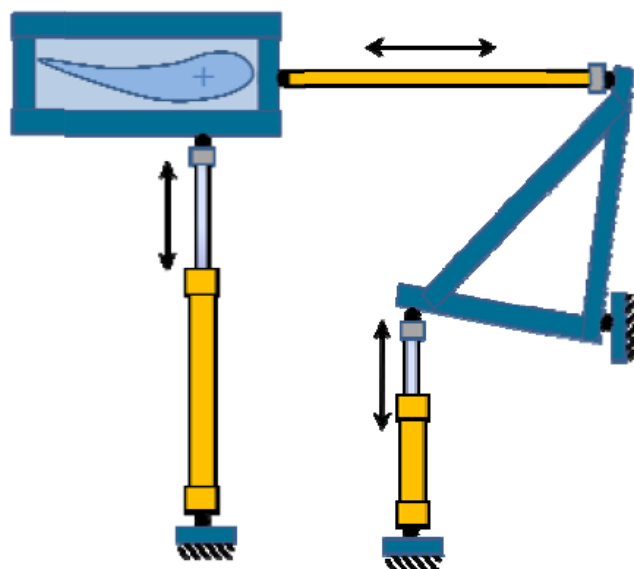


Figure 2.8. Sketch of bi-axial test setup from blade tip [19]

In [20], Sundaresan et al. studied on a different loading concept. In this loading concept, whiffletree arrangement was used as shown in Figure 2.9. For testing, 9 meters long blade was used. Whiffle tree provides a multiple loading by using one load introduction. These types of loading enable us to apply loading with less hydraulic actuators compared to conventional multiple loading or with one crank. But the design of whiffletree is a little bit complicated in terms of load application points. In their study, four loading points were used to introduce loads with four calibrated load cells. Load cells are placed just between the saddle points and tree branches. Whiffle tree arrangement is a good option to loading, it provides easiness of loading condition, but it should be noted that it is only useful for static tests. It may not be used in fatigue tests due to oscillatory loads.



Figure 2.9. Whiffletree arrangement on 9 meters wind turbine blade [20]

In [21], Yang et al. studied actual collapse testing under the flapwise loading for a large full-scale composite 40 meter wind turbine blade. The photo of testing is shown

in Figure 2.10. Full scale test has been carried out at the Blade Test Centre of Zhuzhou Times New Materials Technology Co., Ltd. in Hunan, China. The testing performed until failure under flapwise loading. Loads were applied in six sequential steps with increasing loads. These steps are tabulated in Table 2.1. This table includes not only loads applied but also normalized moments. At the first step, dead weights on the blade have been relieved.



Figure 2.10. A full-scale wind turbine blade under flap-wise loading static test [21]

Table 2.1. Loading Steps

Load Increment	Additional Load	M (%)
1. Step	Relieving the component from its dead weight and setting all measurement points back to zero	0
2. Step	40% extreme design load	25
3. Step	60% extreme design load	37.5

Table 2.1. *Loading Steps (cont'd)*

4. Step	80% extreme design load	50
5. Step	100% extreme design load	62.5
6. Step	160% extreme design load	100

Yeniceli [22] – [23] made calculations for loading arrangements for a selected wind turbine blade system. In this research, the optimization of the whiffletree system was conducted to apply appropriate loading on a wind turbine blade. The National Renewable Energy Laboratory (NREL) research wind turbine blade was used for this study. Firstly, he chose one of the loading cases that the wind turbine blade facing in operation. After that, the distributed loads on the blade was converted to concentrated loads by using MS Excel to apply blade in testing. In this optimization, the optimum locations to apply loads to the blade were found for two, three and four saddle points. These are compared to each other in terms of the best moment distribution on the blade. These optimizations are performed not only in MS Excel but also in MATLAB. A tool with Graphical User Interface (GUI) was prepared to build an algorithm to optimize. In this tool, determination of saddle point locations and corresponding saddle point loads, which gives the best moment distribution according to distribute design loads were calculated. These two calculations performed in MS Excel and Matlab tools are compared. As a result, Matlab optimization gives the closest moment distribution to design moment distribution on the blade. The optimum design solution for whiffletree was selected, and whiffletree design was conducted to apply appropriate loading to the blade. In this thesis, 4 points whiffletree design was selected to give the best distribution, and a sketch of this design is illustrated in Figure 2.11. Also, shear force and moment distribution comparisons for 4 points whiffletree arrangement are presented in Figure 2.12 and Figure 2.13.

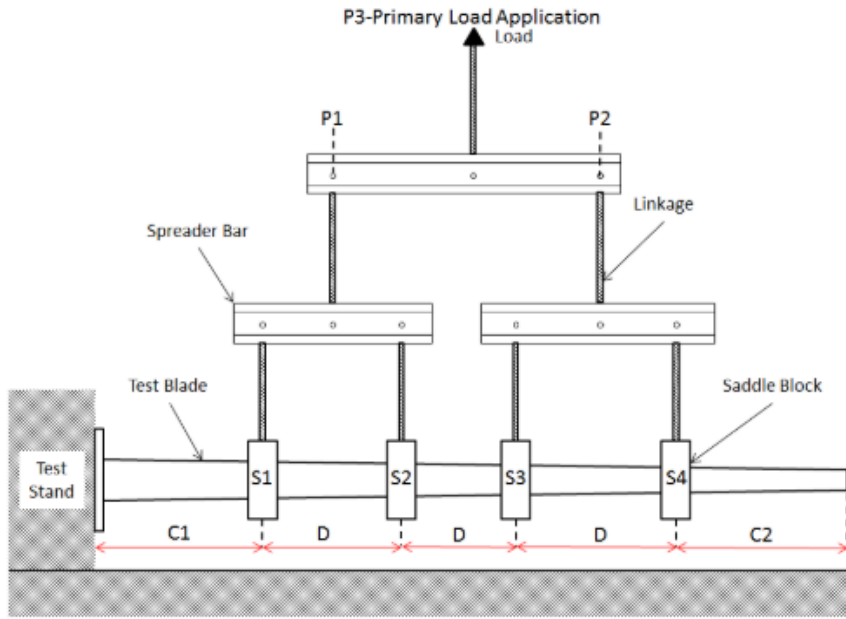


Figure 2.11. Sketch of Whiffletree with 4 Saddle Points

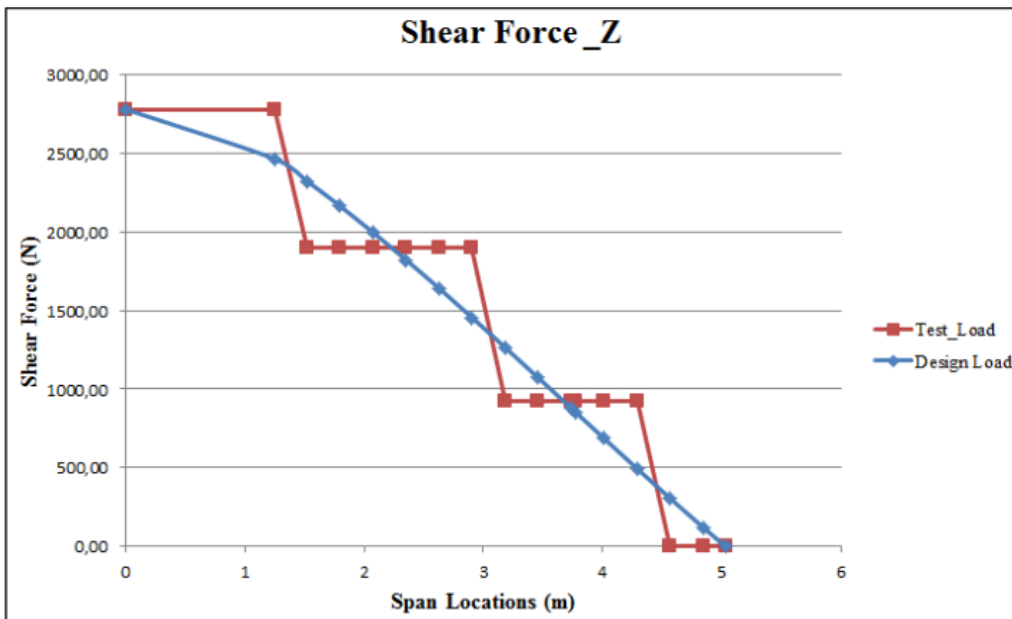


Figure 2.12. Shear Force Comparison along the Blade in 4 Saddle Point [22]

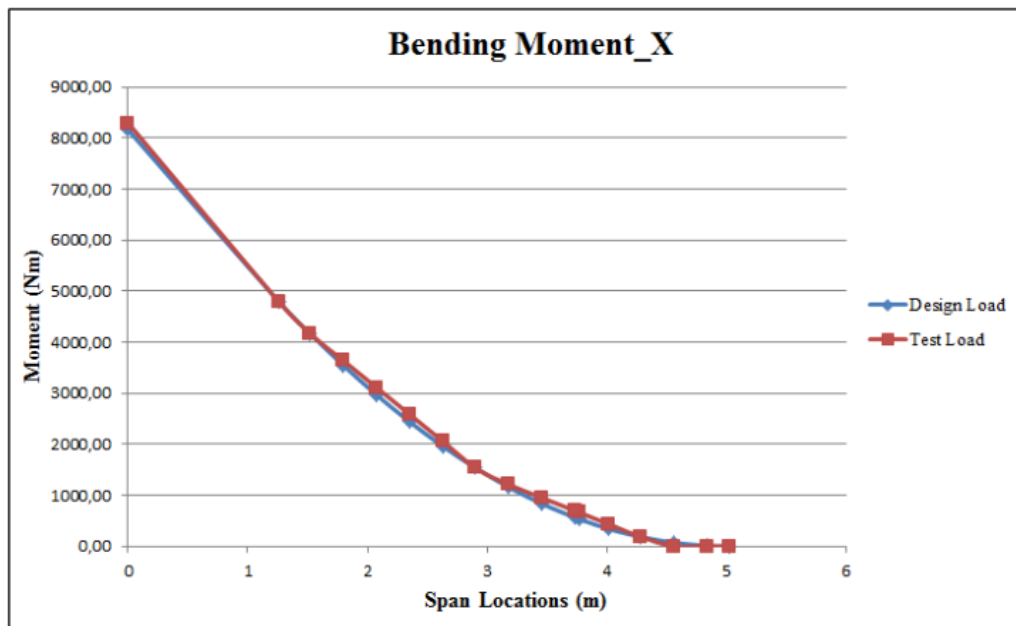


Figure 2.13. Bending Moment Comparison along the Blade in 4 Saddle Point [22]

2.2. Differences between Wind Turbine Blade Test System and Helicopter Blade Test System

Both wind turbines and helicopters have rotor blades for different purposes. These blades are probably the most critical parts of their design. In case of catastrophic failure during the operation, they must be tested before. In operation, these blades are exposed to similar loadings. The loadings acting on blades differ due to the purpose of usage. Helicopter blades rotate with higher RPM. Also, when considering the maneuvers of a helicopter, blades behavior are continuously changing due to the capability of helicopters and different loading like damper loading, pitch link loading acting on blades. Within loads of blades during the maneuvers or operations, the importance of centrifugal force comes forward due to higher RPM. On the other hand, a wind turbine blade rotates with lower RPM. For this reason, a centrifugal force is too small in accordance with moments on the blade. The most critical loading on the wind turbine blade occurs flapwise moment.

On the helicopter blade, not only centrifugal force but also the other forces must be taken into account while testing. These are flapwise moment, edgewise moment, torsion, damper loading and pitch link loading. During the testing, all of these loads have to be applied to the helicopter blade. The most affected load is a centrifugal force on the helicopter blade. The blade testing is performed under constant centrifugal forces. While the other forces are changing and follow specific load patterns, centrifugal force must be kept the same. An example of the load pattern of the helicopter blades is given in Figure 2.14. Moreover, it is not possible to test the full-scale helicopter blade due to the length and load distribution of the blade. If the full-scale blade is tried to be tested, there might be a problem with the measurement of load distribution and testing, and also the testing result may move away from the reality. A testing time is significantly increasing as well. Only the root section is tested with these loads. In TAI, there is a test system about the helicopter blade root section test fulfilling the requirement described as shown in Figure 2.15 [24], [25]. This test system has the capability to apply all types of loading. It should be noted that CF (centrifugal force) is kept constant, and the other load are oscillating during the test. Furthermore, the failure modes of the helicopter blades can vary with maneuvers. A helicopter is an aircraft that carries people. So any failure in the blades arises a problem with a fatal accident. For this reason, in order to show the structural integrity of the blades and certify the helicopters, the test of the blade must be conducted all types of loading in case of any failure due to even the smallest load acting on the blade. For the certification of a helicopter, it is mandatory to apply all loadings simultaneously.

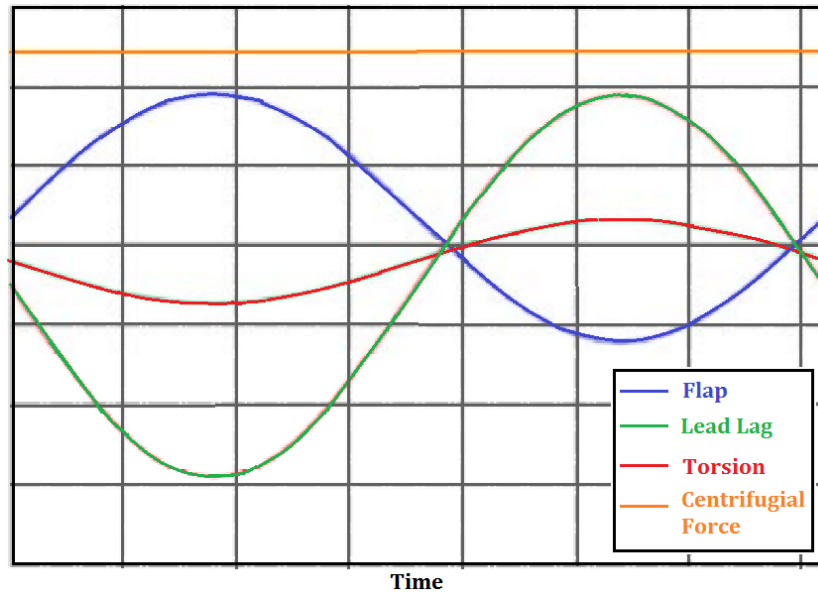


Figure 2.14. Helicopter Load Pattern during Testing [24], [25]

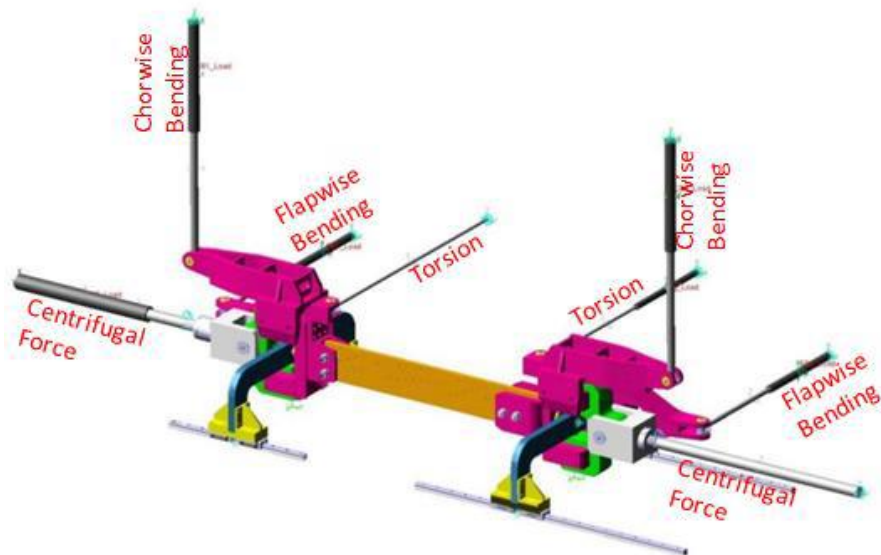


Figure 2.15. Helicopter Blade Root Section Test System [24]

For the wind turbine blades, centrifugal force can be assumed negligible when it compares to other wind turbine load cases. And also, due to lower RPM, a linear speed of a wind turbine blade is smaller. For this reason, torsion due to aerodynamic load is too small to consider. The main loads of the blade have become edgewise and flapwise bending. These bending loadings can be performed simultaneously or separately. There is not directly guidance about this process in the literature. So it is not necessary to apply these loads simultaneously. Unlike helicopter blades, wind turbine blades are fixed at the root to the hub. In the helicopter blade, this procedure is more complicated due to constraints and types of loading. In the wind turbine blades, the hub connection is one and only boundary condition, and concentrated load points are only the loading conditions for bending. An example of a wind turbine blade test setup is illustrated in Figure 2.16. In this figure, a reaction block represents the hub connection of the blade, and loading fixtures provide bending loading on the blade.

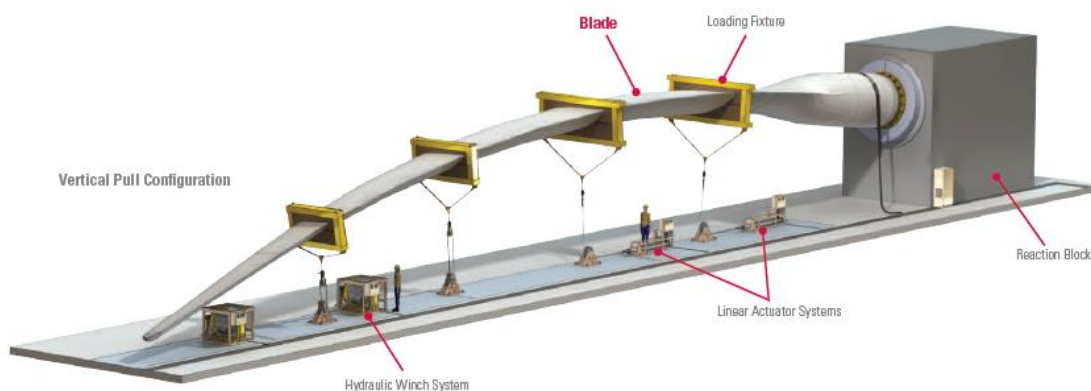


Figure 2.16. Example of Wind Turbine Blade Test Setup [27]

CHAPTER 3

RÜZGEM BLADE AND LOAD CALCULATION

In this chapter, a brief summary of RÜZGEM blade to be tested is presented, and test loads to be applied to the blade are calculated.

3.1. Wind Turbine Blade in METU RÜZGEM

METU RÜZGEM Blade is designed in cooperation with RÜZGEM – METU Center for Wind Energy and Core Team of the University of PATRAS. This blade was designed in accordance with IEC 61400-2, Wind Turbines - Design requirements for small wind turbines [7]. The blade has a 30 kW nominal power capacity at 10 m/s wind speed. This blade was created to obtain light, reliable and suitable for working under strong wind conditions within the METUWIND project. Aerodynamic design was completed by Smartblade GmbH, providing detailed aerodynamic geometry and stress distributions for extreme IEC loading cases, which will be encountered in operations [28].

The blade has 5-meter length, and the first aerodynamic section starts at 0.7 m from the root. The composite blade is made up gel coat, steel and composite laminates. The composition of the blade as a suction side, a pressure side, an internal flange, a hat shape chassis and the flange is shown in Figure 3.1. The total mass of the blade, including the adhesive paste, the gel coat and the CSM 300 finishing ply, is 82.198 kg [29].

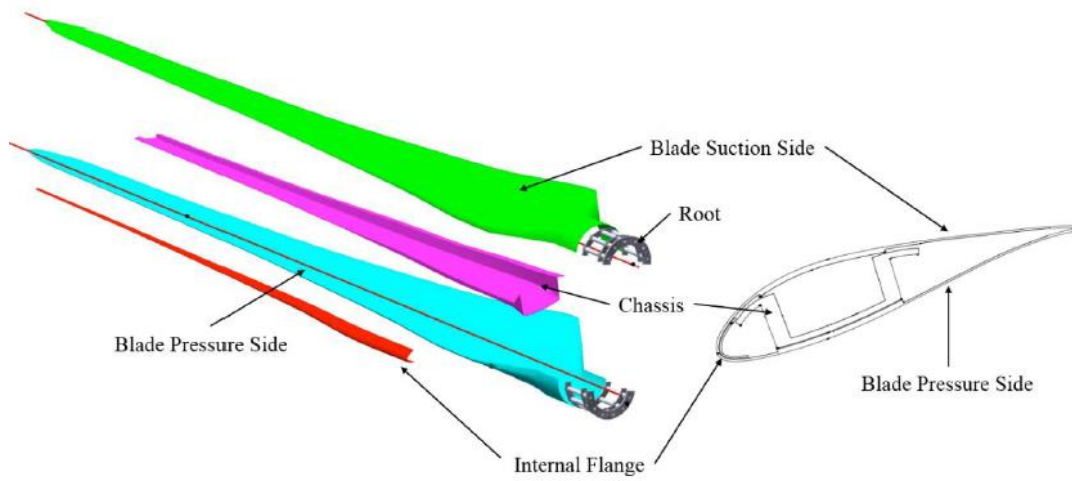


Figure 3.1. RÜZGEM Blade Composition [29]

During the design process of the blade, a linear static analysis was performed in ANSYS by using extreme ultimate loads. According to the linear elastic static analysis, the maximum deflection is equal to 0.503 m at the tip under extreme ultimate loads, as presented in Figure 3.2 [29].

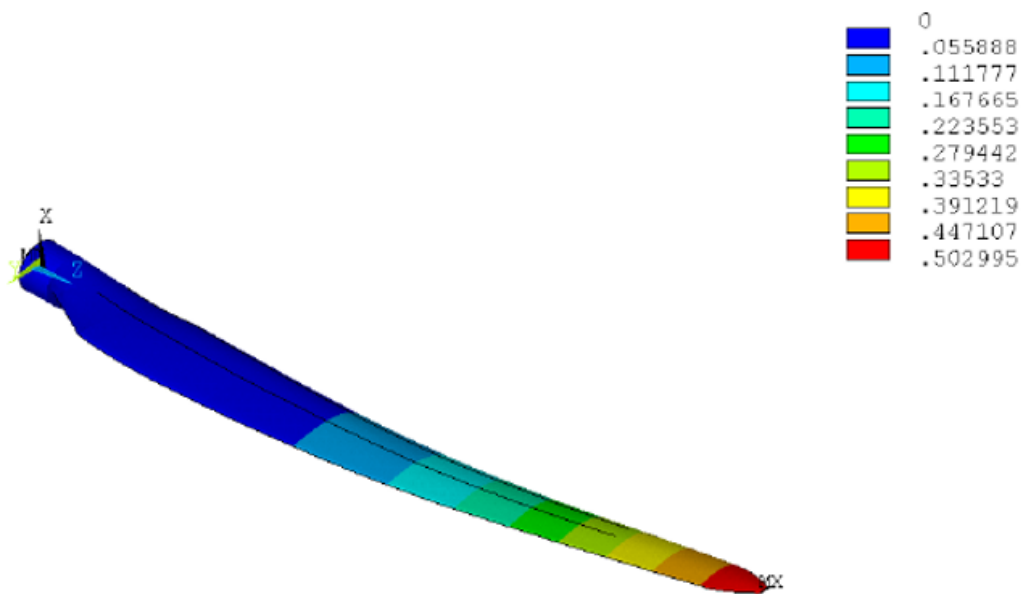


Figure 3.2. Maximum Tip Deflection [29]

The connection of the blade to the wind turbine hub will be made by 12 M16x1.5, 8.8 grade bolts. The external root diameter is equal to 273 mm, while the 12 M16 bolt hole patterns are placed in 245 mm diameter. The existing blade in RÜZGEM is shown in Figure 3.3 [30].



Figure 3.3. Existing Blade in METU RÜZGEM [30]

3.2. RÜZGEM Blade Coordinate System

The wind turbine coordinate system should be well defined before defining design loads. The forces and moments are given in the blade pitch coordinate system, according to Figure 3.4. The blade pitch coordinate system has its origin at the intersection of the blades pitch axis and the blade root. It rotates with the rotor and the local pitch angle adjustment.

Origin: Intersection of the blades pitch axis and the blade root.

YB: Pointing towards the trailing edge of the blade and parallel with the chord line at the zero-twist blade station.

ZB: Pointing along the pitch axis towards the tip of the blade.

X_B : Orthogonal with y_b and z_b axes such that they form a right-handed coordinate system.

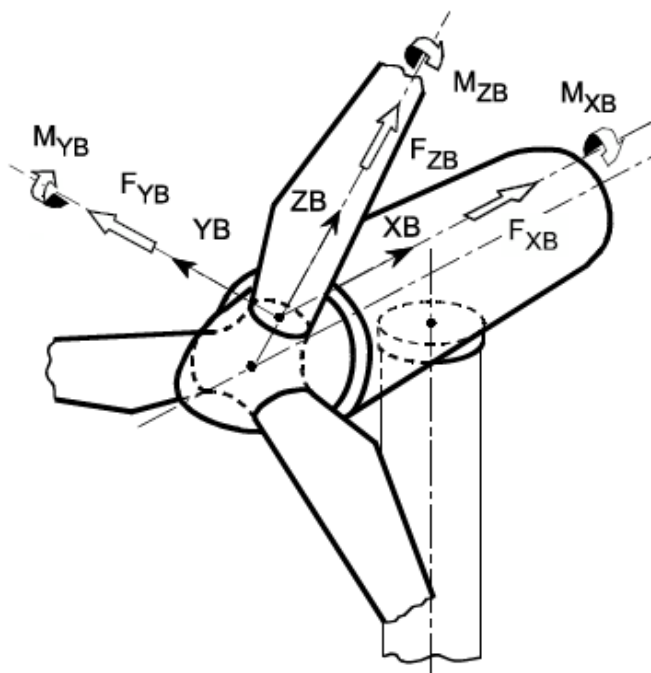


Figure 3.4. Coordinate System of the RÜZGEM Blade [28]

3.3. Design Loads of RÜZGEM Blade

While creating the design loads to be tested, the worst case load scenario is chosen. This worst case load scenario is acquired from aero-elastic simulations of blades that conform IEC 61400-2 standard in the blade design report [29]. According to these extreme loads, F_x , F_y , F_z , M_x , M_y , M_z loads and residual loads in both positive and negative directions are presented for 28 different sections along the blade. It should be noted that safety factor was taken 1.35 for these loads. These sectional loads in all directions are given in the Appendix.

Since the blade has lower stiffness in flapwise direction while higher stiffness and lower loads on the blade, two types of loading are more important than others. These are F_x (flapwise shear load) and M_y (flapwise bending moment) arising from the lift. This flapwise load is plotted along the blade radial position in Figure 3.5 and bending moment arising from flapwise load is drawn in Figure 3.6. These forces and moments are tabulated in Table 3.1. Moreover, these loads are to be used to apply on a blade after converting these sectional loads to concentrated loads.

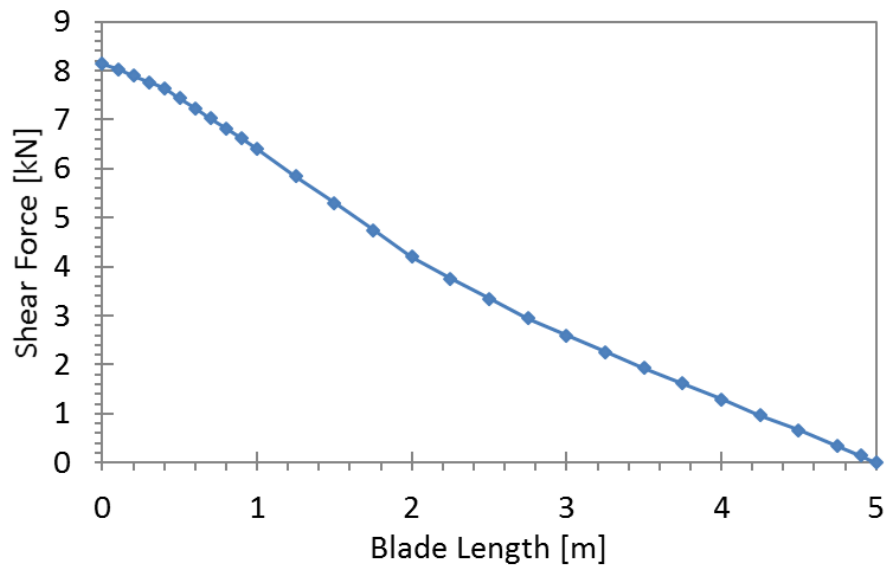


Figure 3.5. Flapwise Load over Blade Radial Position

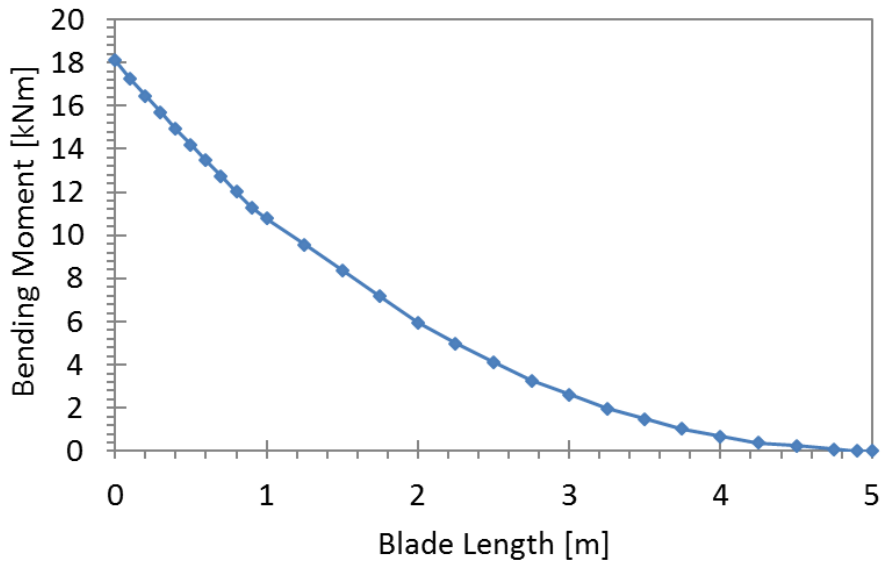


Figure 3.6. Flapwise Bending Moments over Blade Radial Position

Table 3.1. F_x And M_y Along Over Blade Radial Position.[28]

Section	R [m]	F_x [kN]	M_y [kNm]
1	0.00	8.14	18.09
2	0.10	8.03	17.24
3	0.20	7.90	16.47
4	0.30	7.77	15.70
5	0.40	7.64	14.93
6	0.50	7.44	14.21
7	0.60	7.23	13.48
8	0.70	7.03	12.75
9	0.80	6.82	12.02
10	0.90	6.62	11.29
11	1.00	6.40	10.79
12	1.25	5.85	9.58
13	1.50	5.30	8.38
14	1.75	4.75	7.17
15	2.00	4.20	5.97
16	2.25	3.76	5.00

Table 3.1. *Fx And My Along Over Blade Radial Position.[28] (cont'd)*

17	2.50	3.35	4.12
18	2.75	2.95	3.27
19	3.00	2.60	2.61
20	3.25	2.26	1.98
21	3.50	1.93	1.49
22	3.75	1.60	1.02
23	4.00	1.29	0.69
24	4.25	0.97	0.39
25	4.50	0.66	0.24
26	4.75	0.34	0.10
27	4.90	0.15	0.01
28	5	0	0

3.4. Calculation of Applied Loads and Locations for Two Saddle Points

Flapwise loading is to be used for static testing of RÜZGEM Blade. These loads are given as both a shear force in x-direction and a flapwise moment in the previous section. Real operation cases and testing are different. In the real case, distributed aerodynamic loads affect blades directly. These aerodynamic loads are presented in 28 sections in the design report as concentrated loads converging to the distributed loads. Flapwise loads stated in the design report cannot be applied directly to the blade in these 28 sections with saddles. For this reason, a number of saddle points should be decreased by keeping shear force constant at the root and by converging the bending moment distribution as much as possible over the blade radial position. It is aimed to converge to realistic moment distribution by decreasing loading points. Before calculation, notations are shown in Figure 3.7 and these notations are defined as;

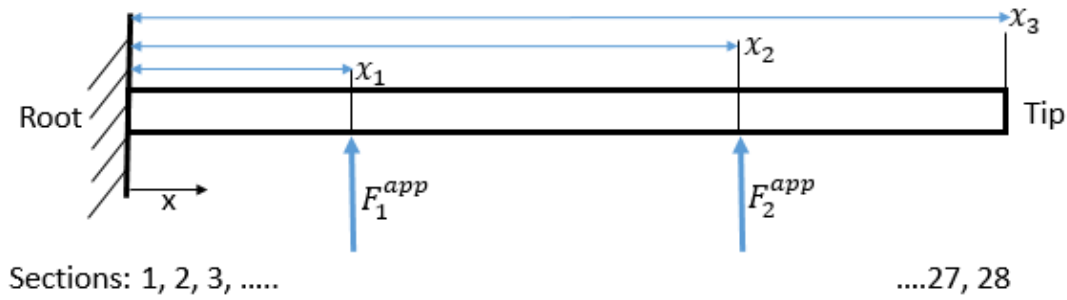


Figure 3.7. Scheme of Notations on the Blade

F_1^{app} is a force applied at saddle point 1,

F_2^{app} is a force applied at saddle point 2,

x_1 is a location of saddle point 1,

x_2 is a location of saddle point 2,

x_3 is a tip,

x is the distance from the root where moment is calculated,

and sections 1, 2, 3 to 28 are where the design loads are defined.

Two approaches

Load calculation, which is converting loads in 28 sections to the concentrated load, is performed by using two approaches with separate objective functions. In both two approaches, the main aim of these calculations are to acquire realistic moment distribution converging to design moment distribution presented in 28 sections. These calculations are performed for saddle points and corresponding loads at these saddles. With the help of Excel Solver, saddle point locations and corresponding loads to be applied are calculated. Before the calculation, the objective function, changing parameters and constraints are decided.

Objective Functions

The two approaches use different objective functions to determine the saddle points and corresponding loads. The first approach minimizes the sum of absolute values of the moment error between design moments and moments due to applied saddle loads at each section. This approach is defined as;

$$f_{PE}(x) = \sum_{i=1}^{28} g_{PE}(x)_i \quad (3-1)$$

$$g_{PE}(x)_i = \begin{cases} 0, & M_y^{des}(x)_i = 0 \\ \left| \frac{M_y^{des}(x)_i - M_y^{app}(x)_i}{M_y^{des}(x)_i} \times 100 \right|, & M_y^{des}(x)_i \neq 0 \end{cases} \quad (3-2)$$

where

$M_y^{des}(x)_i$ is a design moment at section defined,

$M_y^{app}(x)_i$ is a applied moment at section defined due to saddle loads,

$g_{PE}(x)_i$ is a percentage moment error of section defined,

$f_{PE}(x)$ is an objective function.

In the first approach, our aim is to minimize $f_{PE}(x)$, which is similar to approach studied in [22].

The second approach minimizes the sum of absolute values of moment differences between design moments and moments due to applied saddle loads at each section. This approach is defined as;

$$f_{AD}(x) = \sum_{i=1}^{28} g_{AD}(x)_i \quad (3-3)$$

$$g_{AD}(x)_i = |M_y^{des}(x)_i - M_y^{app}(x)_i| \quad (3-4)$$

where

$g_{AD}(x)_i$ absolute moment difference of section defined,

$f_{AD}(x)$ is an objective function.

In the second approach, our aim is to minimize $f_{AD}(x)$.

In these two approaches which is studied, all other changing parameters and constraints are kept the same for comparison.

Constraints

All of these calculations are carried out by changing loads to be applied at each saddle point and saddle point locations. Since the moment distribution is more critical than shear force distribution, it is aimed to obtain the best moment distribution in this calculation. While distributing loads to saddle points, total shear force is kept equal to the design shear force at the root. For the RÜZGEM blade load calculation, constraints are defined as follows;

- The sum of loads to be applied at saddle points shall be equal to the design shear force at the root, which is 8140. To introduce this constraint to Excel, the sum of the loads are normalized. Distribution of loads for saddle point 1 and saddle point 2 are also normalized and notations are given as,

$$\frac{F_1}{F_r} + \frac{F_2}{F_r} = 1 \quad (3-5)$$

where

F_1 is a load applied at saddle point 1,

F_2 is a load applied at saddle point 2,

F_r is a shear load at the root, which is equal to 8140 N for our case.

- The ratio of saddle point loads to total shear force at the root shall be lower than 1,

$$\frac{F_1}{F_r} < 1 \quad (3-6)$$

$$\frac{F_2}{F_r} < 1 \quad (3-7)$$

- The ratio of the saddle point loads to total shear force at the root shall be bigger than 0,

$$\frac{F_1}{F_r} > 0 \quad (3-8)$$

$$\frac{F_2}{F_r} > 0 \quad (3-9)$$

- Saddle point locations cannot be bigger than the length of blade, which is 5 meters,

$$x_1 < 5 \quad (3-10)$$

$$x_2 < 5 \quad (3-11)$$

- Saddle point locations cannot be lower than 0.7 meter, where aerodynamic profile starts for the RÜZGEM blade,

$$0.7 < x_1 \quad (3-12)$$

$$0.7 < x_2 \quad (3-13)$$

- The moment differences between design moment and test moments at the root shall be lower than 1%,

$$\left| \frac{M_y^{des}(x)_r - M_y^{app}(x)_r}{M_y^{des}(x)_r} \times 100 \right| < 1 \quad (3-14)$$

where

$M_y^{des}(x)_r$ is a design moment at the root,

$M_y^{app}(x)_r$ is an applied moment at the root due to load applied at saddle locations

Changing Parameters

Load calculations are performed by changing saddle locations, which are x_1 and x_2 , and corresponding load distributions, which are F_1/F_r and F_2/F_r . These values are assigned randomly as initial values for the solution. It should be noted that these initial values should be selected sensible. And also, locations must be selected in the order of $x_1 < x_2$.

Moment Calculations due to 2 Saddle Loads

Moment calculations due to the loads applied at the saddle points are performed according to notations, which is stated previously. The test moment equations for each section are defined by;

$$M_y(x) = F_1(x_1 - x) + F_2(x_2 - x) \quad (3-15)$$

where $0 < x < x_1$

$$M_y(x) = F_2(x_2 - x) \quad (3-16)$$

where $x_1 < x < x_2$

$$M_y(x) = 0 \quad (3-17)$$

where $x_2 < x < x_3$

For the first objective, Excel datasheet is created with design moments column, test moments due to load applied at saddle points column and moment percentage error between design moments and moments due to applied load at saddle points for each cells column. Each column has 28 rows. The design moments presented in Table 3.1 are inserted to related column and the moment equations are written to the moments due to load applied at saddle points column. In the same Excel datasheet, initial value cells for changing parameters and constraint cells are also defined. Initial values are chosen as $x_1 = 1.5 \text{ m}$, $x_2 = 3.5 \text{ m}$, $F_1/F_r = 0.6$ and $F_2/F_r = 0.4$. The sum of moment error with selected initial values, changing parameters and constraints defined can be seen in Figure 3.8.

Objective			
Sum of Moment Error %	1064.00		
Constraints			
minimum saddle location [m]	0.7		
maximum saddle location [m]	5		
Moment Error at the Root [%]	3.49364		
Changing Variables	Saddle 1	Saddle 2	
Location	1.5	3.50	
Distribution	0.6	0.4	1
Load	4884	3256	
Total Shear Force at the Root	8140.00		

Figure 3.8. Initial Values, Constraints and Corresponding Sum of Moment Percentage Error

In order to perform this calculation, Excel Solver Add-in tool is used. In this solver, the objective function is introduced as the sum of moment percentage error. The aim of the objective is selected as minimizing. After that, changing parameters, which are x_1 , x_2 , F_1/F_r and F_2/F_r , are introduced. Excel solver performs a calculation by changing these parameters. Then, constraints are introduced as stated previously in *Constraints* part. Solver parameters introduced to Excel are shown in Figure 3.9.

GRG Nonlinear solving method is used in this solver. GRG stands for generalized reduced gradient. This method uses the gradient of the objective function. When it obtains partial derivatives which is equal to the zero, it reaches a solution. This is the fastest method within solving method. After pressing a “Solve” button, Excel gives the location and magnitude of the saddle loads.

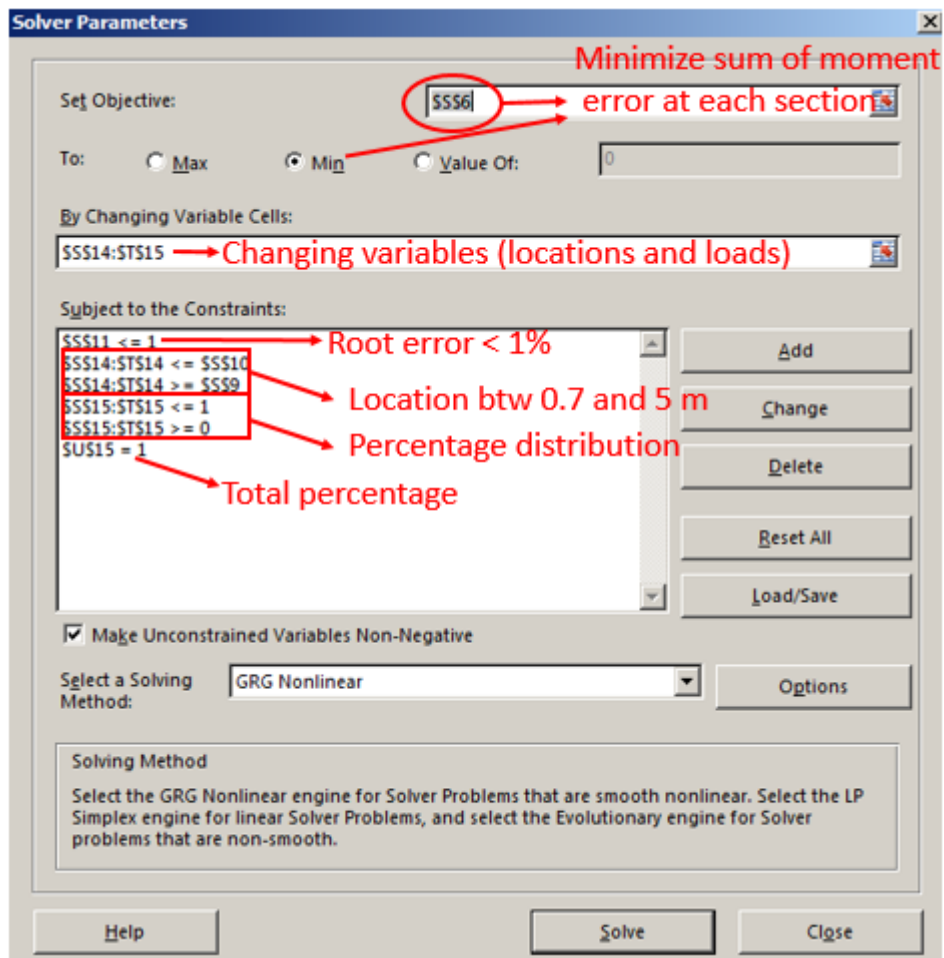


Figure 3.9. Introducing Objective, Changing Variables and Constraints

For the initial conditions $x_1 = 1.5 \text{ m}$, $x_2 = 3.5 \text{ m}$, $F_1/F_r = 0.6$ and $F_2/F_r = 0.4$, the optimized saddle locations are obtained 1.40 m and 4.16 m from the root and corresponding loads are $F_1 = 5659 \text{ N}$ and $F_2 = 2481 \text{ N}$, respectively. These values are shown in Figure 3.10. Note that these saddle locations and corresponding loads are for the first objective function, which is the sum of the moment percentage error at each section. Shear and moment distributions of design and test loads are given in Figure 3.11 and Figure 3.12. In Figure 3.11, the total shear force at the root, 8140 N, is observed between the root and the root saddle while there is no shear force between the tip saddle and the tip. In Figure 3.12, the moment at the root is found with an error

of less than 1% and the moment values are found as zero for the distance between the tip saddle and the tip.

Objective			
Sum of Moment Error %	670.57		
Constraints			
minimum saddle location [m]	0.7		
maximum saddle location [m]	5		
Moment Error at the Root [%]	1		
Changing Variables			
	Saddle 1	Saddle 2	
Location	1.4045	4.16	
Distribution	0.69526	0.304743	1
Load	5659.39	2480.607	
Total Shear Force at the Root	8140.00		

Figure 3.10. Saddle Locations and Corresponding Loads after Solution for Initial Values $x_1 = 1.5m$, $x_2 = 3.5m$, $F_1/F_r = 0.6$, $F_2/F_r = 0.4$ using $f_{PE}(x)$ as Objective Function.

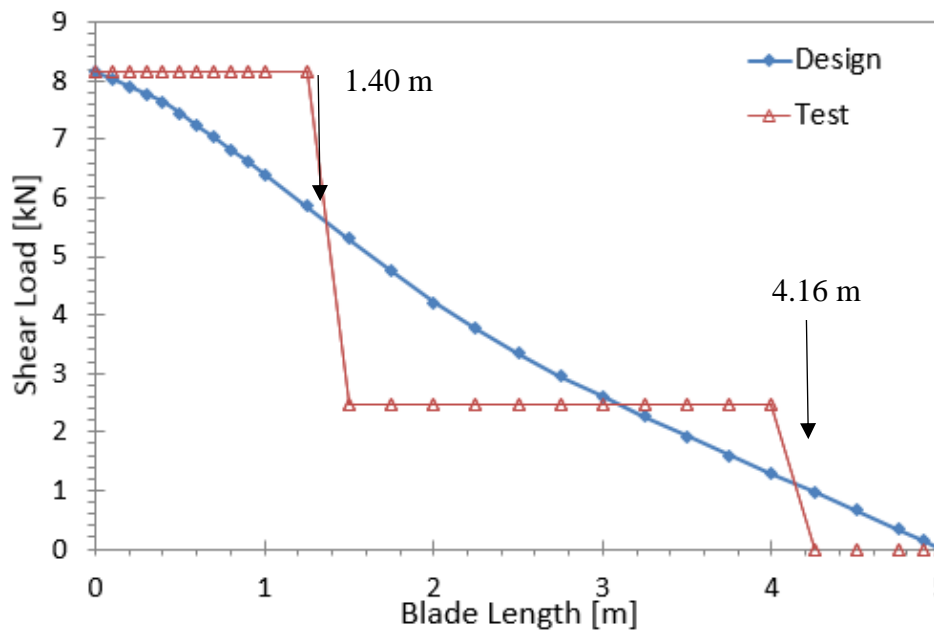


Figure 3.11. Shear Distribution for Initial Values $x_1 = 1.5m$, $x_2 = 3.5m$, $F_1/F_r = 0.6$, $F_2/F_r = 0.4$ using $f_{PE}(x)$ as Objective Function

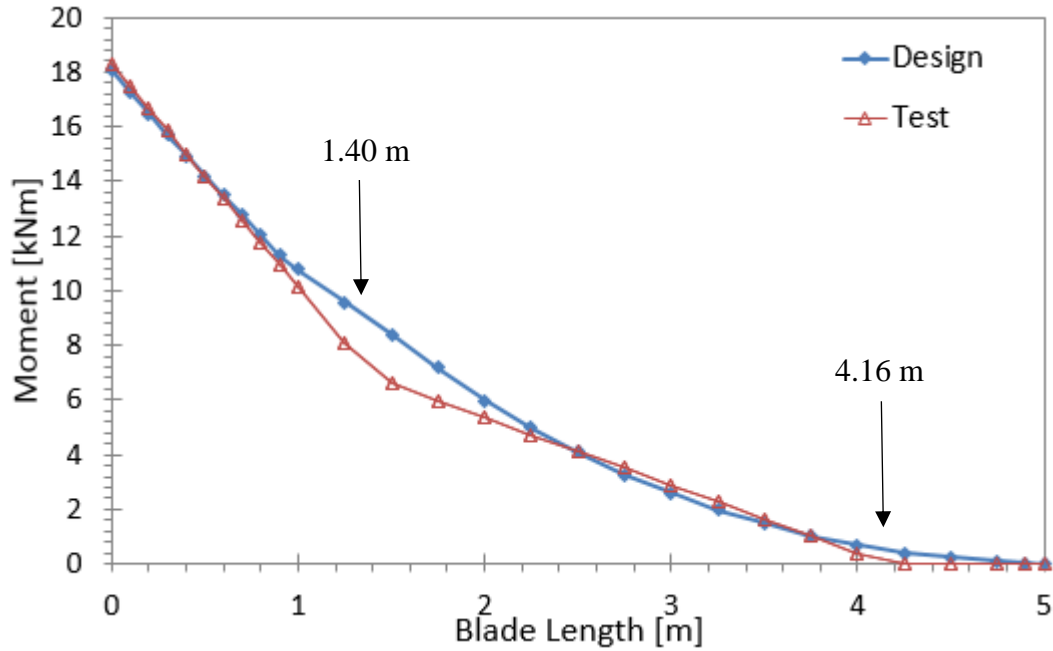


Figure 3.12. Moment Distribution for Initial Values $x_1 = 1.5m$, $x_2 = 3.5m$, $F_1/F_r = 0.6$, $F_2/F_r = 0.4$ using $f_{PE}(x)$ as Objective Function

After the load calculation with the first approach, the objective function is changed for the second approach. Absolute moment differences between design moments and test moments at each section are used for an objective function for the second approach. By keeping constraints and changing parameters the same, the solution is conducted. In order to compare these two approaches, initial values of saddle locations and corresponding load ratios, which are $x_1 = 1.5 m$, $x_2 = 3.5 m$, $F_1/F_r = 0.6$ and $F_2/F_r = 0.4$, are kept the same as well.

According to a solution carried out with the second approach, it is aimed to minimize the moment differences between design moments and test moments in each section. With initial values, which are $x_1 = 1.5 m$, $x_2 = 3.5 m$, $F_1/F_r = 0.6$ and $F_2/F_r = 0.4$, saddle locations are obtained as 1.05 m and 3.72 m, and corresponding saddle loads are obtained as $F_1 = 4492 N$ and $F_2 = 3648 N$. These values are given in Table 3.2. Besides, shear and moment distributions of design and test loads are also presented in

Figure 3.13 and Figure 3.14. In Figure 3.13, it is seen that the shear force between the root and the root saddle is equal to 8140 N while there is no shear force between the tip saddle and the tip. In Figure 3.14, the design moment are caught with an error of less than 1% at the root and there are no test moments between the tip saddle and the tip.

Table 3.2. Location and Corresponding Loads for Initial Values $x_1 = 1.5 \text{ m}$, $x_2 = 3.5 \text{ m}$, $F_1/F_r = 0.6$, $F_2/F_r = 0.4$ using $f_{AD}(x)$ as Objective Function

	<i>Saddle Point 1</i>	<i>Saddle Point 2</i>
Location [m]	1.05	3.72
Load Distribution [%]	55.2%	44.8%
Load [N]	4492	3648

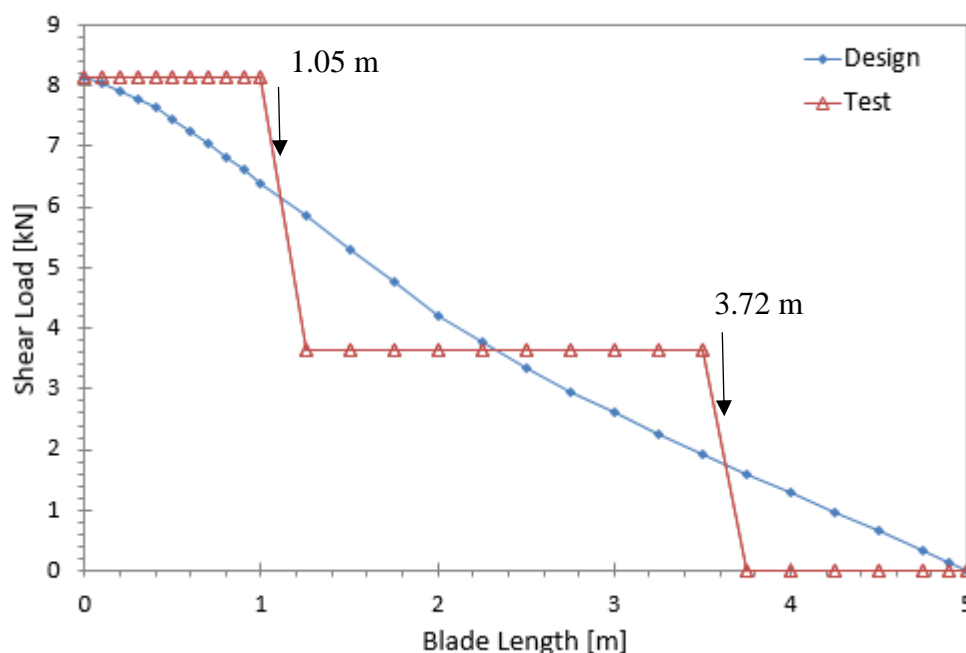


Figure 3.13. Shear Distribution for Initial Values $x_1 = 1.5 \text{ m}$, $x_2 = 3.5 \text{ m}$, $F_1/F_r = 0.6$, $F_2/F_r = 0.4$ using $f_{AD}(x)$ as Objective Function

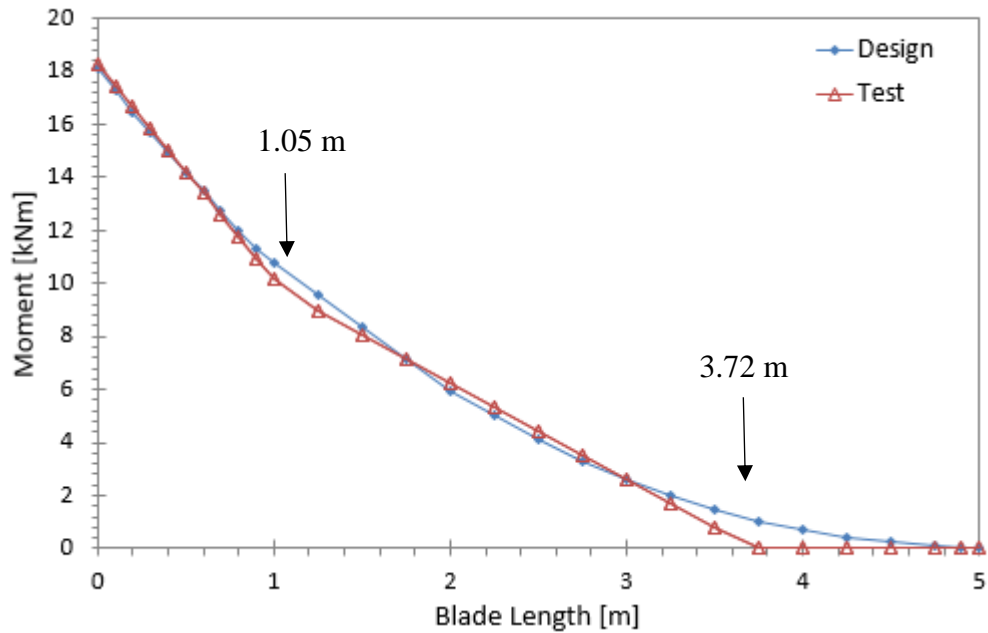


Figure 3.14. Moment Distribution for Initial Values $x_1 = 1.5$ m, $x_2 = 3.5$ m, $F_1/F_r = 0.6$, $F_2/F_r = 0.4$ using $f_{AD}(x)$ as Objective Function

When these two approaches with the same constraints and initial values are compared, the second approach with the objective $f_{AD}(x)$ gives better saddle moment distribution than $f_{PE}(x)$ near the root, while $f_{PE}(x)$ gives better saddle moment distribution than $f_{AD}(x)$ near the tip. In order to examine these two approaches detailed, sectional moment errors of both two approaches according to design moments along the blade graph is presented in Figure 3.15. Both two approaches works well for near the root. After 1 meter from the root, differences at loading are observed and it can be said that the second approach using $f_{AD}(x)$ works better. 100% error is observed near the tip for both approaches using different objective functions. It occurs because there is no loading between tip saddle and the tip. Because of the absence of the loading, it looks like the moment errors are 100% at these sections. The design moment loads at these sections are very small. Since we are not interested in these sections, the absence of the loading near the tip is not critical. An alternative method for the tip zone can be considered for this special region for comparison. When the whole blade is considered,

it is seen that $f_{PE}(x)$ has more error near the root. Since the root is more critical, the second approach using $f_{AD}(x)$ objective function can be used to determine saddle locations and corresponding saddle loads.

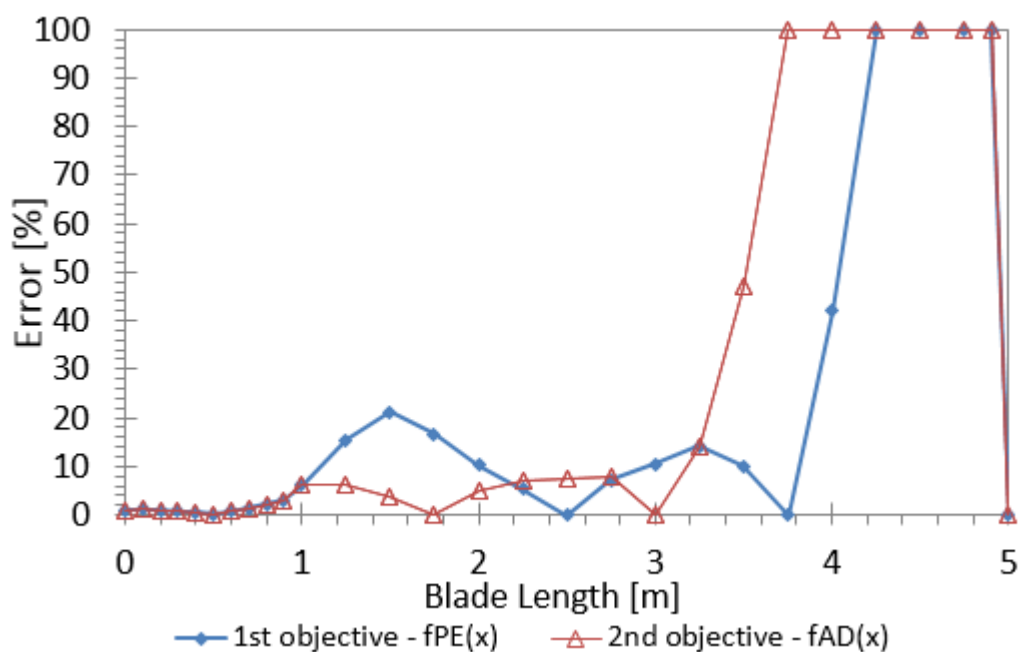


Figure 3.15. Comparison of the First Approach using $f_{PE}(x)$ and the Second Approach using $f_{AD}(x)$

Different Initial Points

The second approach is aimed to minimize $f_{AD}(x)$ objective function, which is moment differences between design moments and test moments. Different initial values of random changing parameters are selected for the new solver run. $x_1 = 1.5 m$, $x_2 = 3.5 m$, $F_1/F_r = 0.6$ and $F_2/F_r = 0.4$ is used before for the solution and this initial values set can be called Set 1. The other sets for run are determined as in Table 3.3.

Table 3.3. *Different Initial Values of Changing Parameters*

<i>Set#</i>	<i>Initials</i>			
	x_1 [m]	x_2 [m]	F_1/F_r	F_2/F_r
Set 1	1.5	3.5	0.6	0.4
Set 2	1.5	3.5	0.8	0.2
Set 3	2	4	0.6	0.4
Set 4	0.8	4.8	0.7	0.3

For the Set 2, saddle locations, $x_1 = 1.5 \text{ m}$ and $x_2 = 3.5 \text{ m}$, are kept the same while corresponding saddle load distribution ratios are changed to $F_1/F_r = 0.8$ and $F_2/F_r = 0.2$. For these initial values, the saddle locations are obtained 1.08 m and 3.82 m, and the corresponding saddle loads are obtained $F_1 = 4680 \text{ N}$ and $F_2 = 3460 \text{ N}$, respectively. The moment distribution graph of this solution with different initial values of saddle load distribution ratios can be seen in Figure 3.16. In this graph, the test moment is converged to design moment near the root and there are no test moments between the tip saddle and the tip.

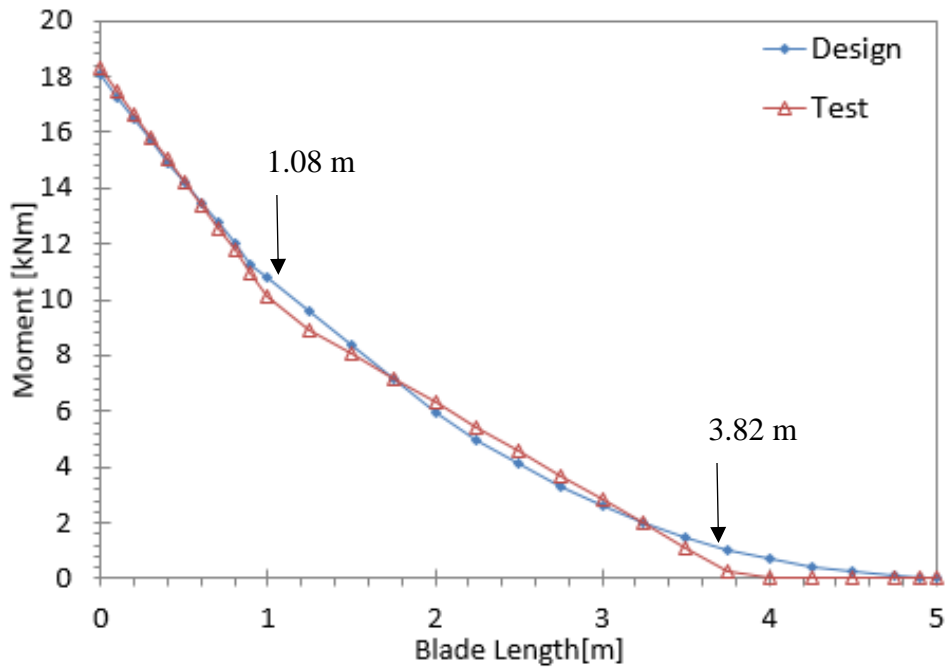


Figure 3.16. Moment Distribution for Initial Values $x_1 = 1.5 m$, $x_2 = 3.5m$, $F_1/F_r = 0.8$, $F_2/F_r = 0.2$ using $f_{AD}(x)$ as Objective Function (Set 2)

For the Set 3 initial values, saddle locations are $x_1 = 2 m$ and $x_2 = 4 m$ which are different from 1.5 m and 3.5 m. These initial values are run by keeping the corresponding saddle load distribution ratios the same as $F_1/F_r = 0.6$ and $F_2/F_r = 0.4$ for this solution. For these initial values, saddle locations are acquired 1.05 and 3.72 while corresponding saddle loads are 4492 N and 3648 N. They are the same as in Table 3.2.

For the Set 4 initial values, different saddle locations and corresponding saddle load distributions are tried with the values of $x_1 = 0.8 m$ and $x_2 = 4.8 m$ from the root, and corresponding load distribution ratios are chosen $F_1/F_r = 0.7$ and $F_2/F_r = 0.3$, respectively. These initial values give us a solution with 1.08 m and 3.82 m saddle locations and $F_1 = 4686 N$ and $F_2 = 3454 N$ saddle loads, respectively. Moment distributions of these initial values are presented in Figure 3.17. Nearly the same solution with Set 2 initial values is obtained.

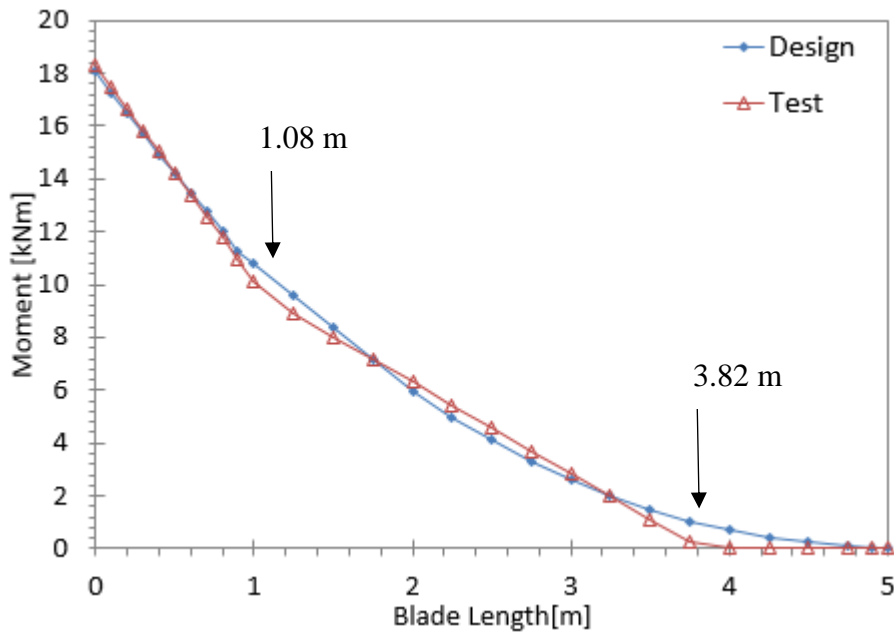


Figure 3.17. Moment Distribution for Initial Values $x_1 = 0.8 \text{ m}$, $x_2 = 4.8 \text{ m}$, $F_1/F_r = 0.7$ $F_2/F_r = 0.3$ using $f_{AD}(x)$ as Objective Function (Set 4)

All solutions obtained with corresponding set number are tabulated in Table 3.4 and the comparison of these solutions with respect to design moment distributions in the same graph is shown in Figure 3.18. All of initial values present nearly the same solution for test case.

Percentage errors concerning the design moments at each section are plotted in Figure 3.19 in order to examine solutions in detail. It is seen that the solution of Set 1, which are $x_1 = 1.05 \text{ m}$, $x_2 = 3.72 \text{ m}$, $F_1 = 4492 \text{ N}$ $F_2 = 3648 \text{ N}$, gives better moment distribution with smaller error near the root. More trial runs with different initial values give more solutions for this load calculations, however, the saddle locations and corresponding loads are found to be very close to each other.

Table 3.4. Solutions with Different Initial Values

Set #	Solutions Obtained			
	x_1 [m]	x_2 [m]	F_1 [N]	F_2 [N]
Set 1	1.05	3.72	4492	3648
Set 2	1.08	3.82	4680	3460
Set 3	1.05	3.72	4492	3648
Set 4	1.08	3.82	4686	3454

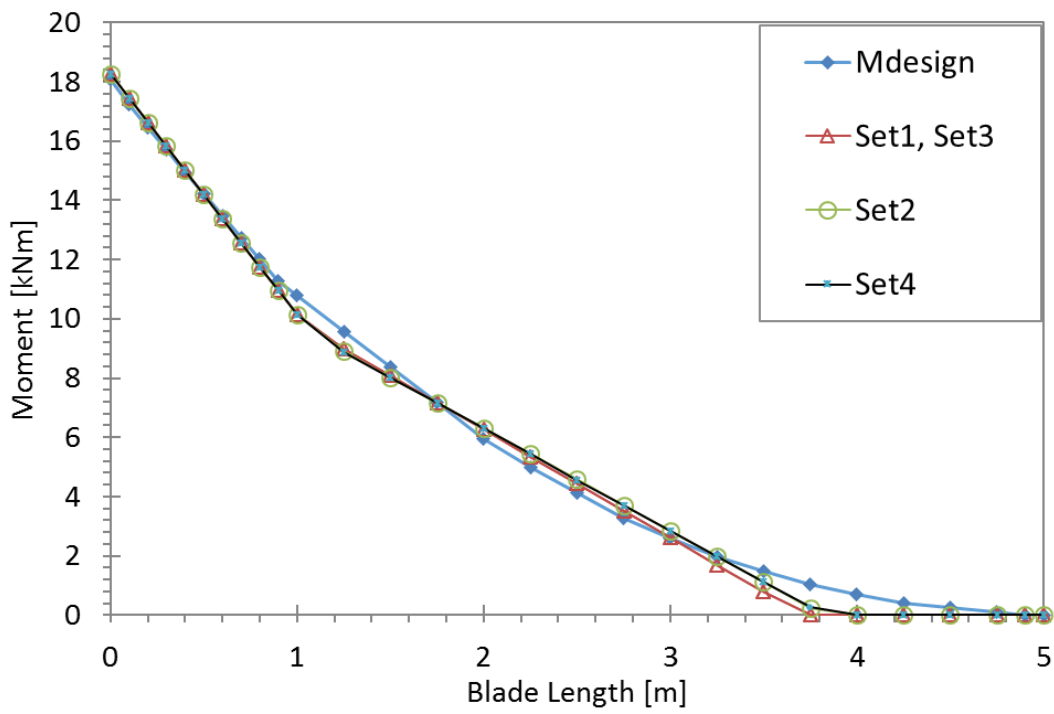


Figure 3.18. Moment Distributions of Set 1, Set 2, Set 3, Set 4

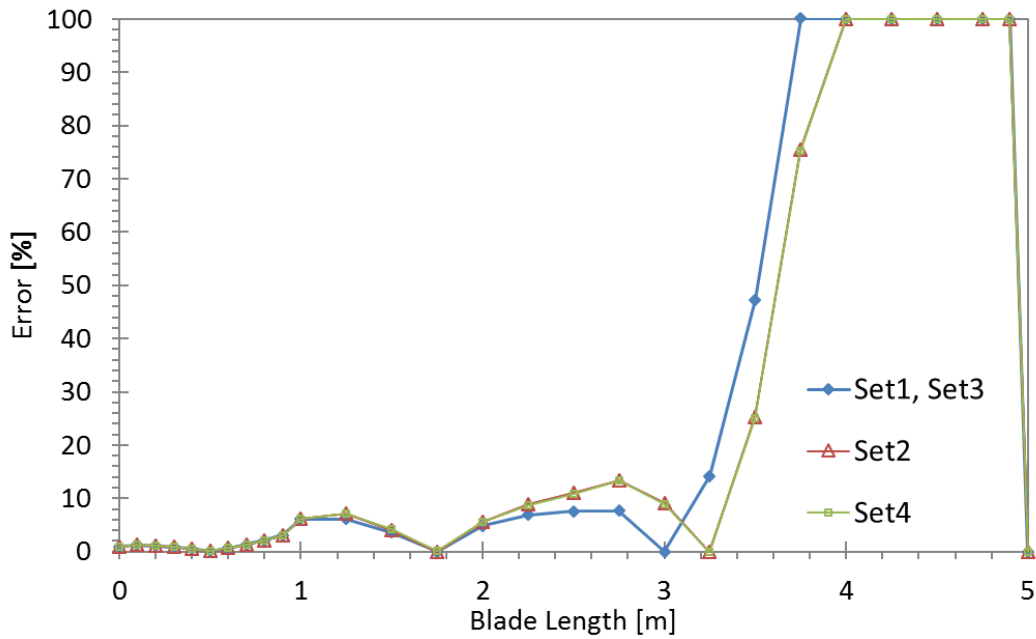


Figure 3.19. Comparison of Solutions in terms of Moment Errors

In summary, since we cannot apply distributed aerodynamic loads directly, load calculation are made for two load points. In this calculation, two approaches using separate objective function are compared for the same initial values and constraints. The approach that use the sum of absolute moment differences between design moments and moments due to applied load at each section as the objective function is chosen. Within the solutions conducted with different initial values, the best solution is the case where $x_1 = 1.05$ m, $x_2 = 3.72$ m, $F_1 = 4492$ N and $F_2 = 3648$ N is selected for the design input of the test rig. Representative figure of this saddle point locations and corresponding loads to be applied is shown in Figure 3.20.

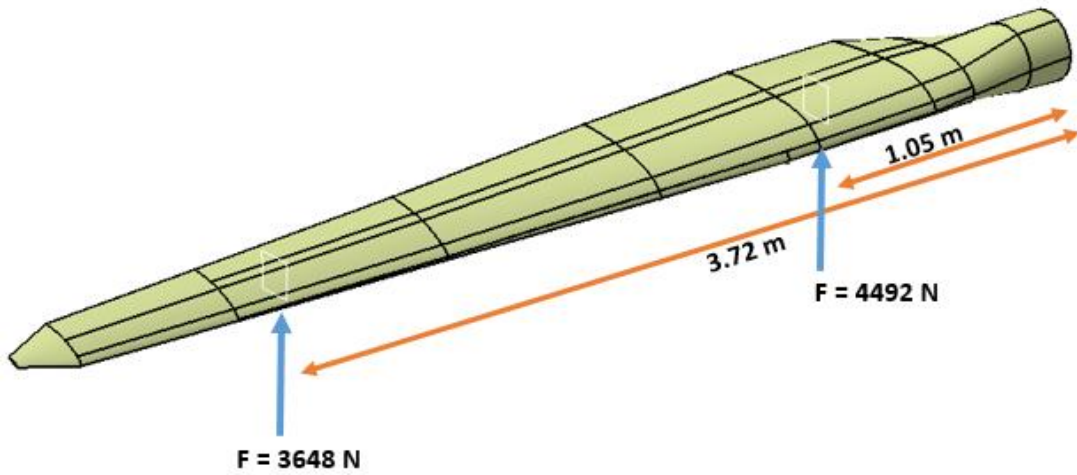


Figure 3.20. Schematic of Test Loads and Locations

3.5. Calculation of Applied Loads and Locations for One Saddle Point

In order to show how a single point method and multiple point method with two saddle points are entirely different, the same Excel solver is adapted to one saddle point, and calculation is performed again. For this adaptation, test moment calculations are performed according to Figure 3.21 with the moment distributions given by;

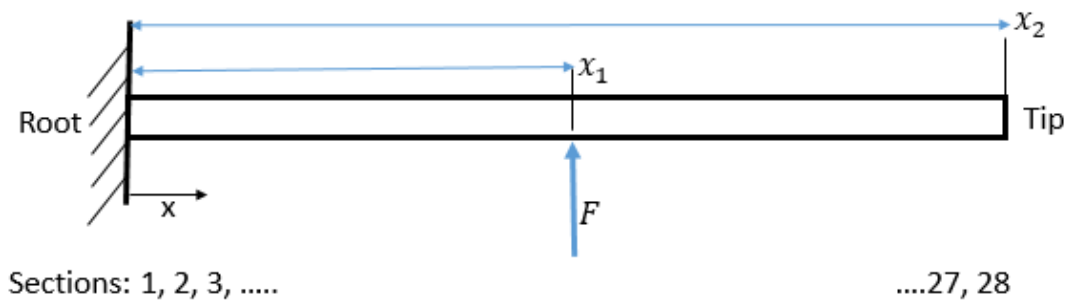


Figure 3.21. One Saddle Point Representation

$$M_y(x) = Fx \quad (3-18)$$

where $0 < x < x_1$

$$M_y(x) = 0 \quad (3-19)$$

where $x_1 < x < x_2$

In this Excel sheet, the changing variable is set as the location only because the load to be applied, ($F = 8140 \text{ N}$), is the same as shear force at the root. Since we have only one changing variable, all initial values for the distance will give the same solution. Two cases using different approach with one objective function defined previously are run and both methods converge to the same solution. The solver gives this location as 2.24 m. With this location, moment distributions are drawn, as shown in Figure 3.22. Also, percentage error of applied moment distribution at each section is presented in Figure 3.23. The test moment for distance between 2.24 m and 5 m at the tip is given as zero. Maximum error occurs at 2.24 m and afterwards.

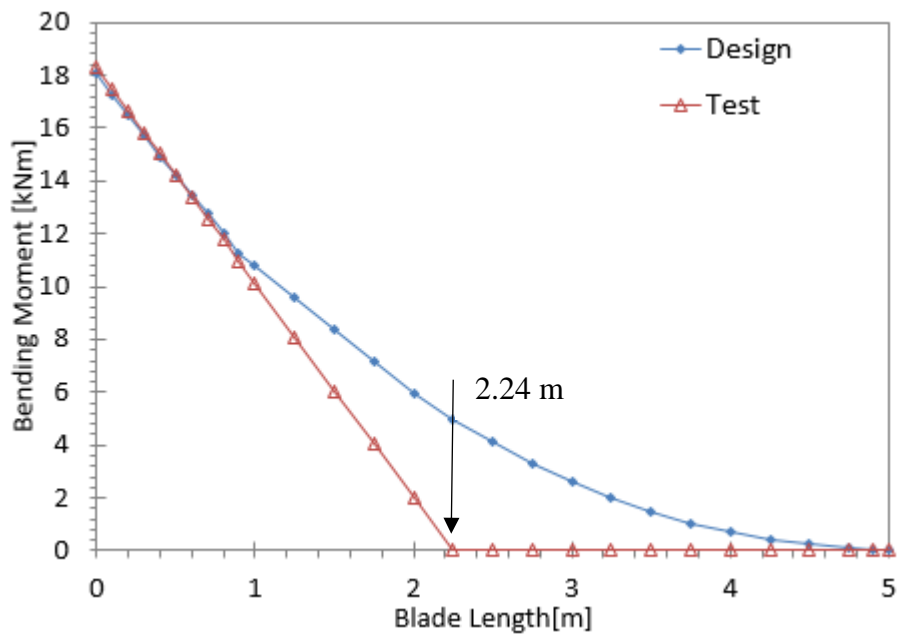


Figure 3.22. Moment Distribution of One Saddle Point

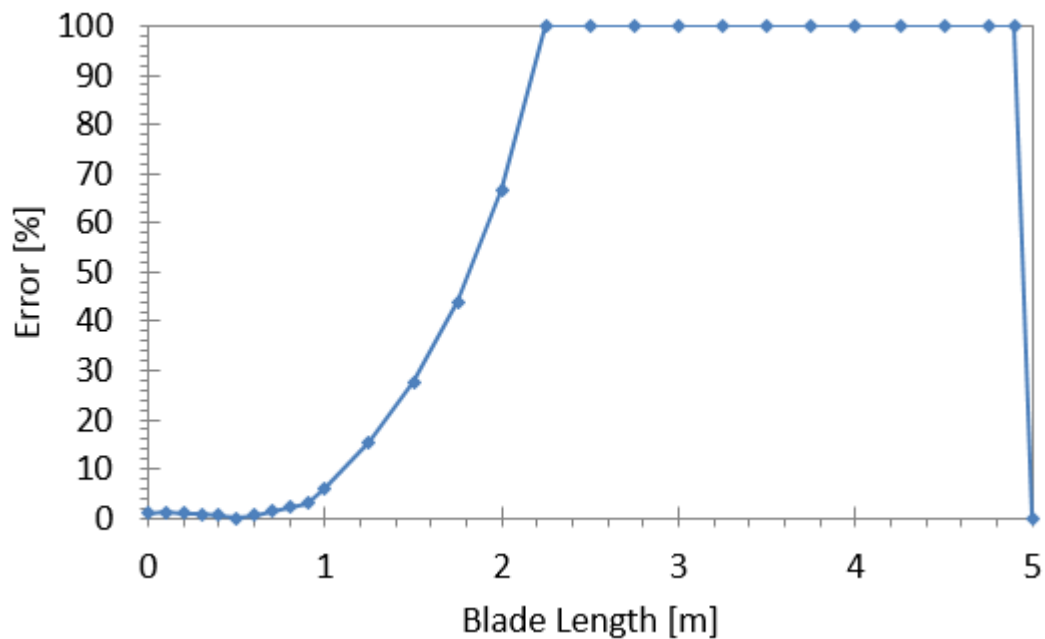


Figure 3.23. Moment Error of One Saddle Point

If the load is applied to the blade at one saddle point, the test moment distribution agrees with the design moment at a distance of 1 meter to the root. Above 1 meter, the moment moves away from design case and the moment error goes to 100% after 2 meters. It can be easily seen how two saddle points improve moment distributions, compared to one saddle point.

Thus, the more realistic loading can be obtained by using two saddle points. Since multiple point method gives the best moment distributions along the blade, in order to design test rig, locations and corresponding loads to be applied obtained in Table 3.2 is used. It should also be noted that the more saddle point used, the more realistic moment distribution are obtained [23]. For the 5-meter length blade, two saddle points are found to be sufficient for loading. Usage of more than two saddle points is not necessary because it would be more expensive and require more time to construct a test setup.

3.6. Discussions

For the calculations of load to be applied to the blade, two cases with different objective function are compared to each other. In the first case, the objective function was the sum of absolute values of the moment error between design moments and moments due to applied saddle loads at each section. In the second case, the objective function was the sum of absolute values of moment differences between design moments and moments due to applied saddle loads at each section. It is aimed to minimize these objective functions in calculations. These cases are used to converge to design moments by using objective functions. After studying both objective functions, we recommend the objective function used in the second case because this approach presents better convergence to the design moment.

As presented in design loads, design moments are decreasing along radial position. Moment values are close to zero near the blade tip as shown in Figure 3.5, where the design moment reaches zero at the tip. In the test case, there are no loads between the tip saddle and the blade tip so that the test moment is zero. For this reason, the sectional moment error between design and test loads at the section between the tip saddle and the blade tip are seen to reach 100%. Since the moment loads at these corresponding sections are small, these errors should not play an important role in the accuracy assessment of the test load calculation.

In testing, loads are applied through two saddle points. The moment to be applied with two saddles can be simulated through finite element analysis of the blade to show how close this approach to the design moment for comparison. With this simulation, comparison can be made between the test case and design case. Also, it is known that the more saddle points give closer approximation to design moment but when errors between design and test case at each section are considered, it can be said that the two saddle points are sufficient to represent moments for this 5-meters blade. In order to show differences between two saddle points and three saddle points, finite element analysis for each cases can be performed.

CHAPTER 4

DESIGN OF TEST SETUP

4.1. Test Rig Design

Full scale test system contains test specimen, support structures, loading interface parts, hydraulic actuators, load cells and data acquisition systems. Test rig design can be conducted with or without whiffletree systems. In this design, a test rig is carried out without a whiffletree system.

The blade will be held by dummy hub and fixed to the reaction wall. Appropriate interfaces will be designed in accordance with locations by imitating the surface of the blade. Hydraulic actuators will be placed to locations identified before under the blade. The concept design sketch of the test rig is shown in Figure 4.1.

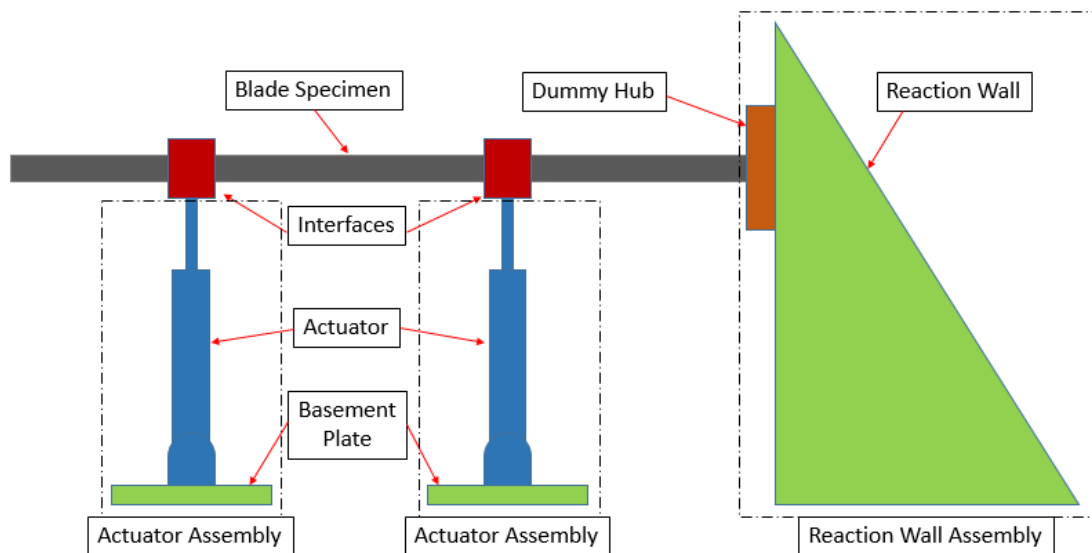


Figure 4.1. Concept Design of the Test Rig

The test rig structure design is conducted with CATIA V5R22. This design mainly consists of load introduction parts, dummy hub design and support structure design. General view of the test rig design is shown in Figure 4.2. This test rig is established on 6.5 m X 1.5 m in the RÜZGEM building.

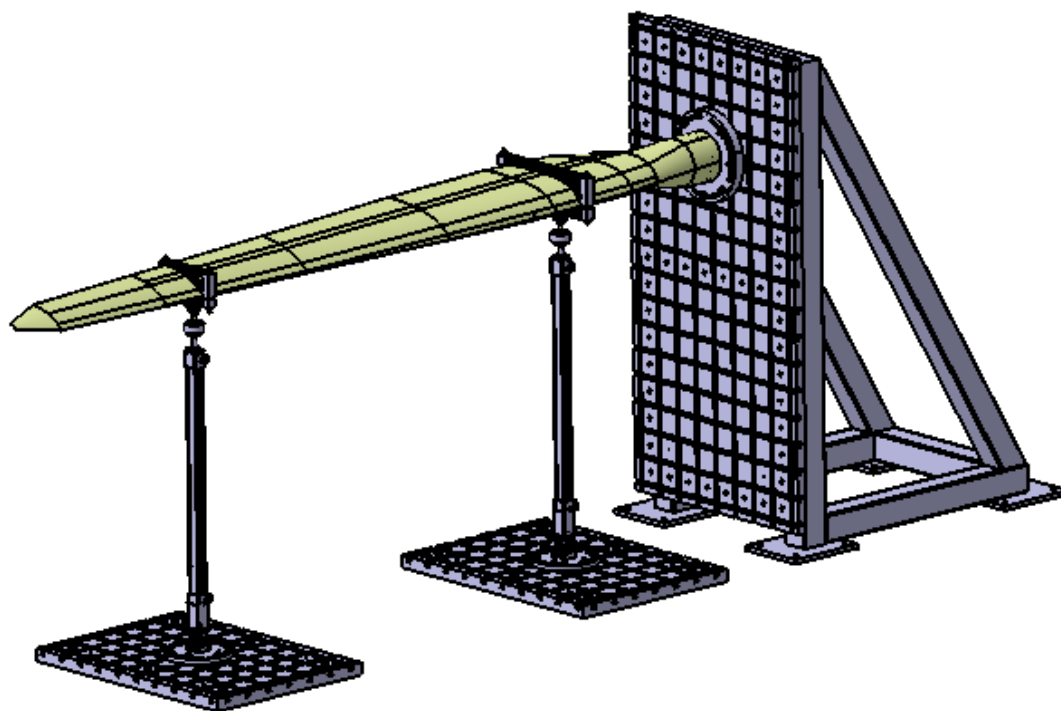


Figure 4.2. General view of the test rig

4.1.1. Dummy Hub and Loading Interfaces Design

Dummy hub is designed to fix the blade root to the reaction wall. The blade root is mounted to a dummy hub with 12 M16x1.5 bolts. The existing blade's root is presented in Figure 4.3 and threaded holes can be seen in this figure. The dummy hub plate designed and assembly of the blade root to the dummy hub plate are shown in Figure 4.4. 12 counterbored holes are drilled on the dummy hub plate to fix the blade. The grade of bolts suggested to use in connection to the hub is stated as 8.8. In this

design, bolts with 12.9 grade, which has much more strength, are used. This dummy hub plate has 3 elongated cylindrical holes (slots) to fix the blade and dummy hub assembly to main reaction wall. These slots diameter is selected as 17.5 mm to mount assembly with M16 bolts located at 220 mm radius of this plate. The outer diameter of the plate is 510 mm. This plate is considered to be made of steel and weighs approximately 80 kg. It should be noted that this dummy hub is specific for this 5-meter RÜZGEM blade.

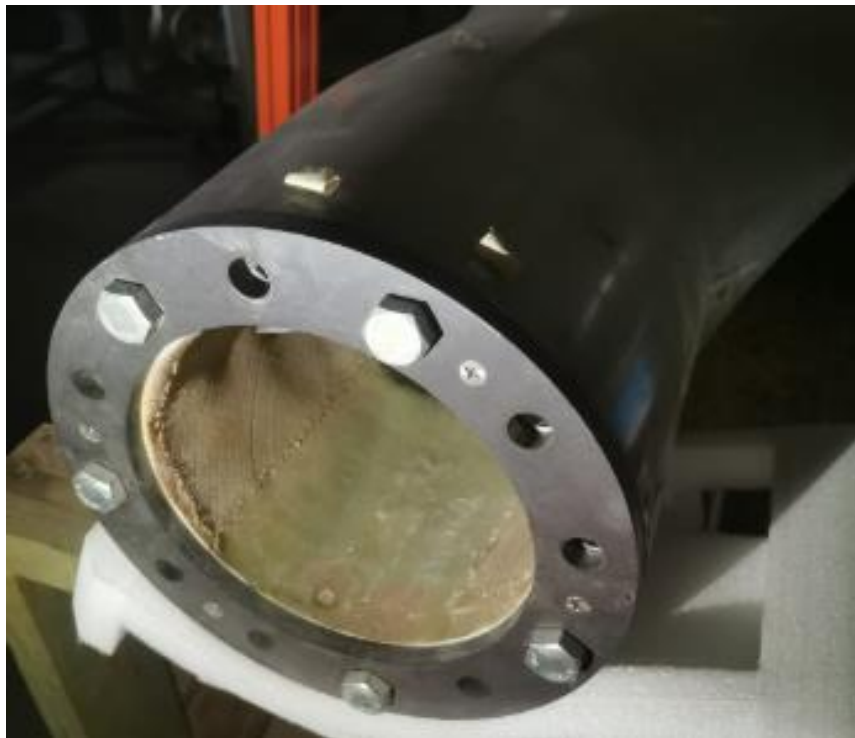


Figure 4.3. Existing Blade's Root Detail

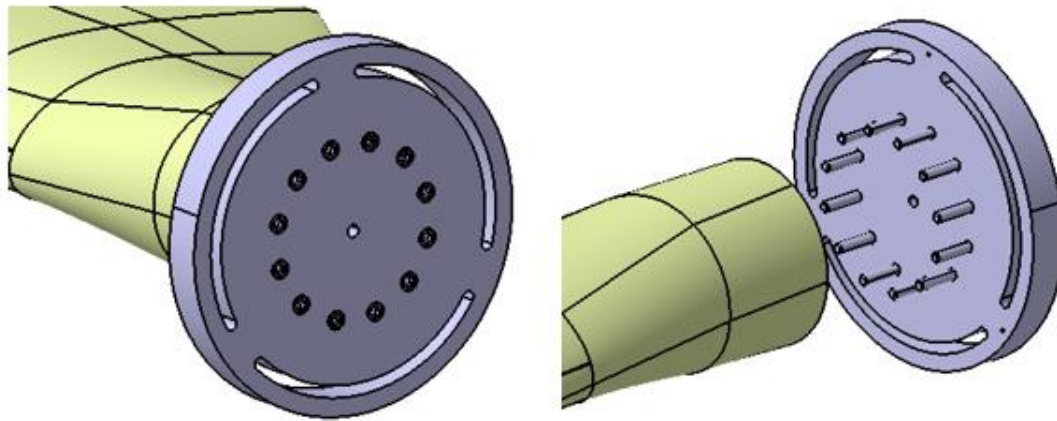


Figure 4.4. Dummy Hub Plate and Assembly

It has been decided that the load introduction is performed with two saddles in the previous chapter. These saddles are designed such that they imitate corresponding sections. Both two saddles designed are shown in Figure 4.5 and Figure 4.6, respectively. Width of saddles are specified as 48 mm, and load application points, which are located at 1.05 m and 3.72 m from the root, are remained in mid-plane of the saddles. Each saddle component is composed of two parts, upper and lower. By dividing into two, assembly of these saddles will be comfortable. Moreover, there are 5 mm offset where saddles match surfaces of blade. A rubber will be stuck to these gaps to prevent any local damage on the blade while mounting and during testing. Shore 35A with 5 mm thickness will be used as a rubber. The upper and lower part of the saddle are connected to each other with M16 threaded rods at trailing and leading edges. At these edges, there are 10 mm gaps where threaded rods located. These gaps provide fitting of upper and lower parts thoroughly. In order to make these parts lighter, sides of the saddles are carved and holes are drilled by keeping matching surfaces the same. In addition, surfaces of the bottom of the lower part and top of the upper part are kept flat and parallel to ground in order to mount clevis and to measure angle while assembling. Moreover, four holes with 10.7 mm diameter are drilled in lower part of the saddles to create a clevis connection. The clevis to be designed is located in feathering axis in order to prevent any torsional loads on the blade while

testing. Saddles are thought to be made of aluminum. An alternative saddle structure can also be made of wood, but in this design, aluminum is preferred in order to make design a simple. Root and tip saddles have approximately 5.5 kg and 3.5 kg, respectively.

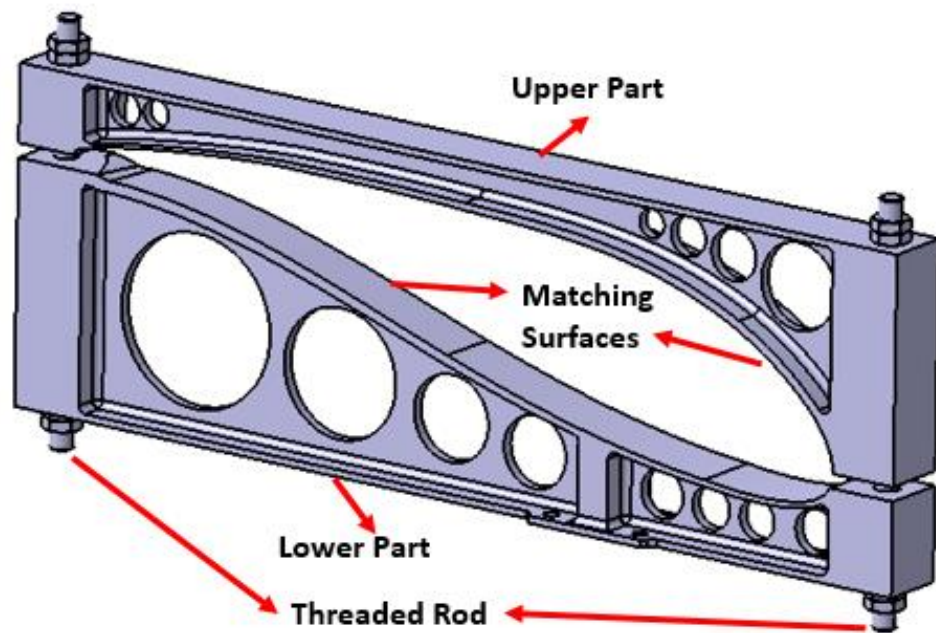


Figure 4.5. Saddle near the Root

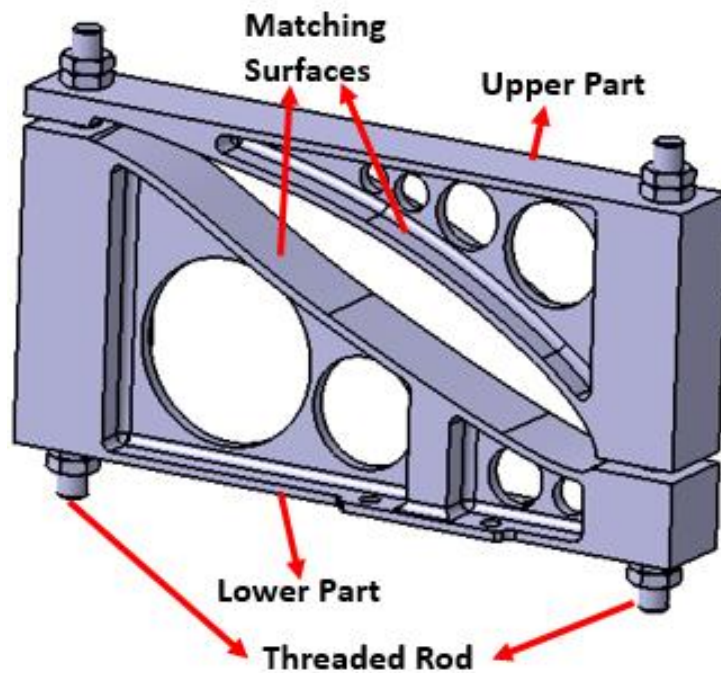


Figure 4.6. Saddle near the Tip

Desired loads are to be applied to the blade saddles by using hydraulic actuators. At the end of the hydraulic actuator, a rod end with spherical bearing should be placed and this rod end that allows three axis-rotation is connected to saddles by means of the clevis assembly. In order to decide clevis interface dimensions, the rod end should be selected at first. The aim of the usage of the rod end with spherical bearing is to transfer load directly coming from the hydraulic actuator without a moment.

According to load calculation, the maximum load, which is encountered in this static test, is 4492 N. In order to select a suitable rod end for this test; safety factor should be chosen at least 3. For the selection of the rod end, INA FAG catalog is investigated, and by taking into account further testing, GIR17-UK model is selected. The specification of this rod end is presented in Figure 4.7. This rod end has a 56500 N basic static load rating [32]. With this selection, further static tests will cover loadings

till 18 kN by considering the safety factor is 3. This rod end can also be used for fatigue tests. The basic dynamic rate is 22500 N.

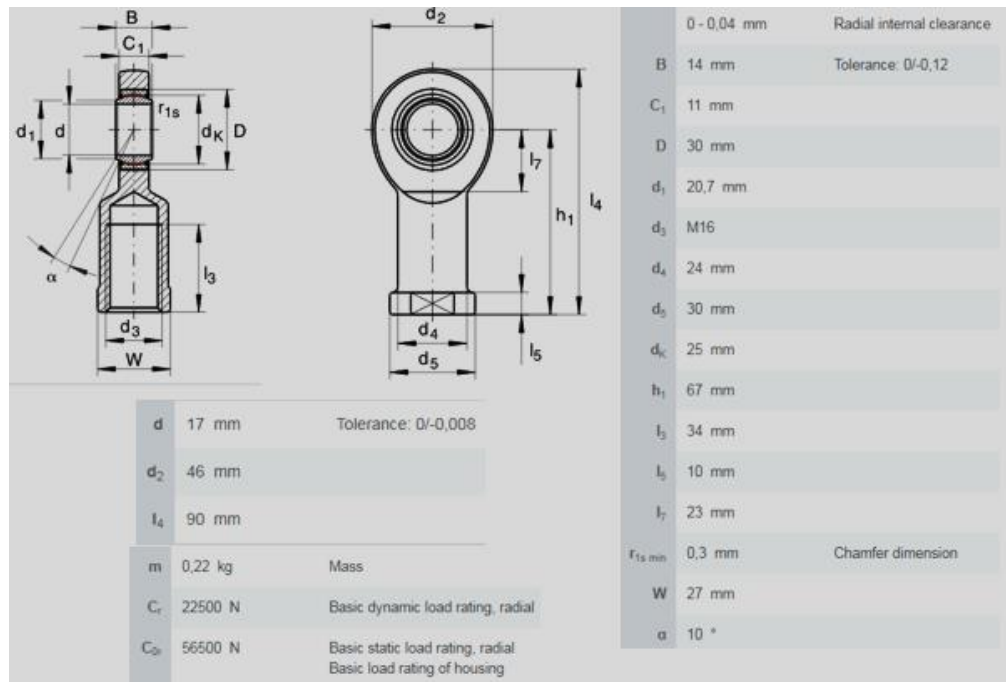


Figure 4.7. INA FAG GIR17-UK Specifications [32]

In the lower part of saddles, clevis connection holes were already allocated. By using rod end interface dimensions, clevis, bushings and pin parts are designed. The cross section of this clevis assembly is illustrated in Figure 4.8 and 3D model of these assembly is shown in Figure 4.9. In order to give more rotation angle in clevis during testing, a flange bushing and a plain bushing are designed to clamp spherical bearing. It should also be stated that the center of spherical bearing is placed in line of feathering axis so that the loading does not create any torsional loading. Only flapwise loading will be seen with this placement. Since the clevis holes are allocated in the lower part of the saddle with four holes, the same pattern is projected to the clevis. With this pattern, clevis is attached to saddle with 4 M10 bolts. These M10 bolts are

tightened to 70 Nm torque. While assembling rod end to the clevis, a pin is tightened with hand torque. All of these apparatus are planned to be made of steel.

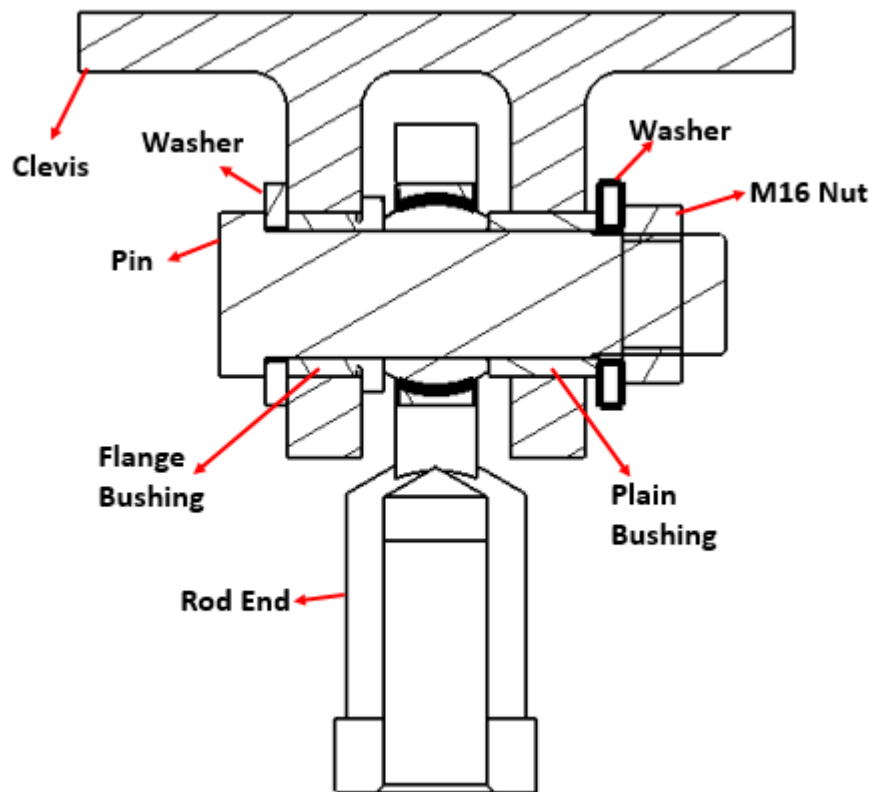


Figure 4.8. Cross Section of Clevis and Rod End Assembly

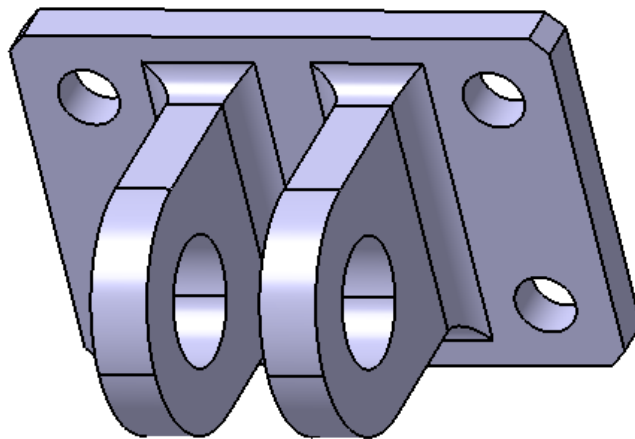


Figure 4.9. 3D Model of the Clevis

Clevises used in both saddles have the same geometry. Clevises attached to the root and tip saddles with a specimen are shown in Figure 4.10 and Figure 4.11, respectively.

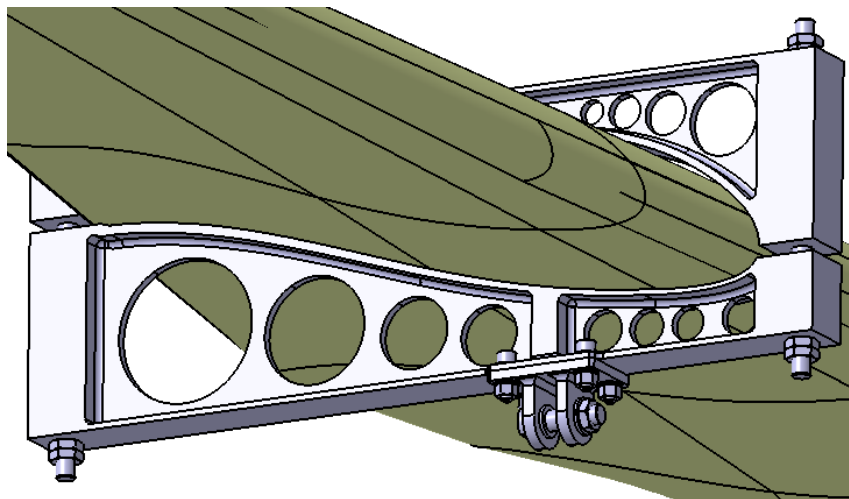


Figure 4.10. Clevis Attached to the Root Saddle

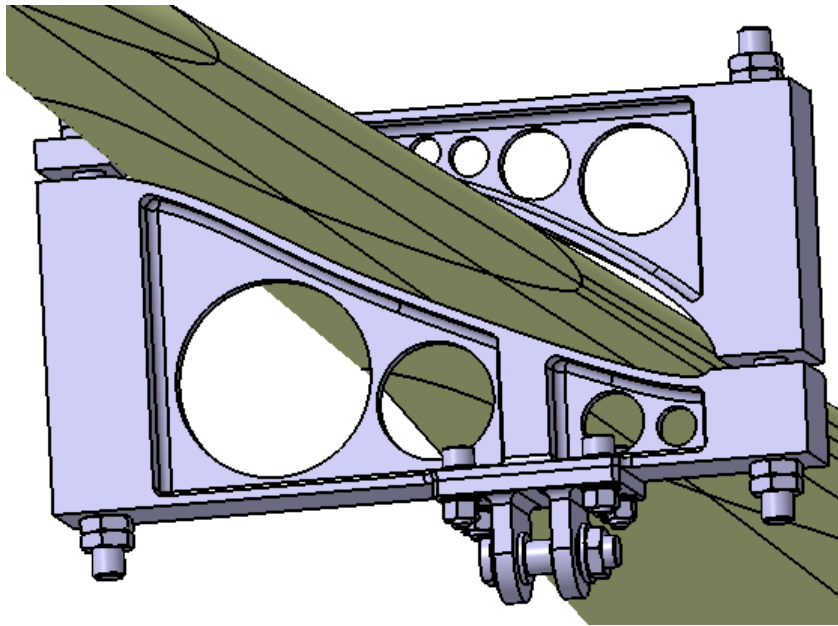


Figure 4.11. Clevis Attached to the Tip Saddle

4.1.2. Load Cell and Hydraulic Actuator Selection

In the static test, required loads are to be applied to saddles via hydraulic actuators. In order to control and measure how much loads applied to the specimen, load cells are necessary. Load cells in the marketplace were investigated, and it was decided that the most reliable and suitable load cell for this test setup is Interface 1000 Series Fatigue Rated Load Cell. The capacity of load cells to be used is determined as 12.5 kN that covers these static loads and further tests. The specification of this load cell is given in Figure 4.12 [33].

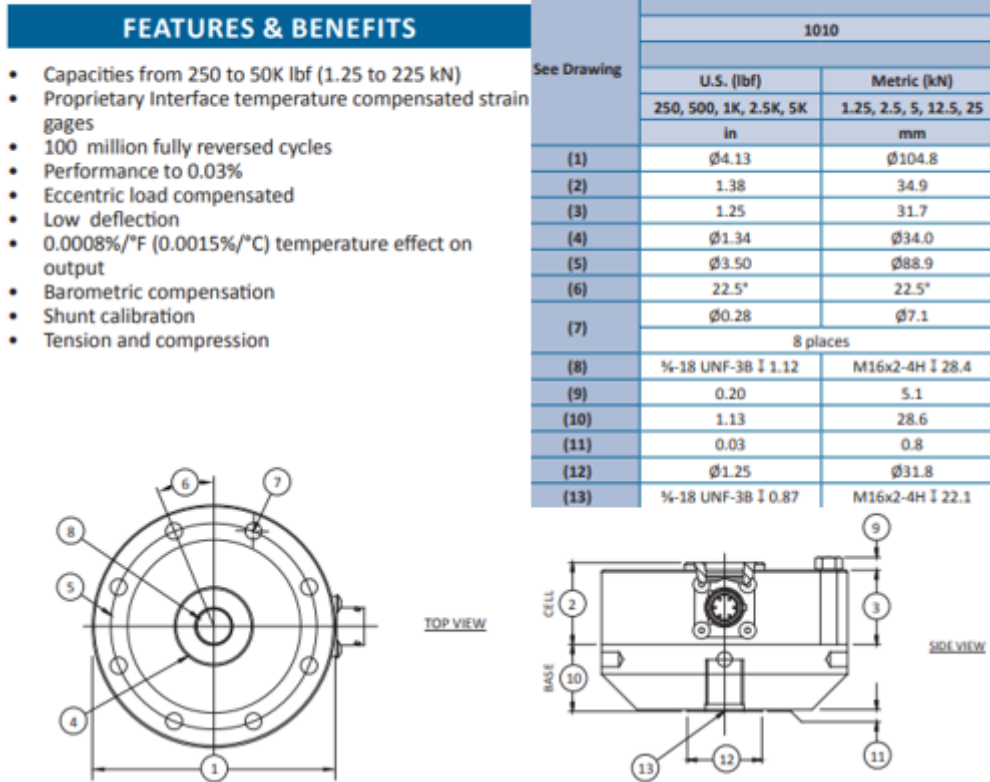
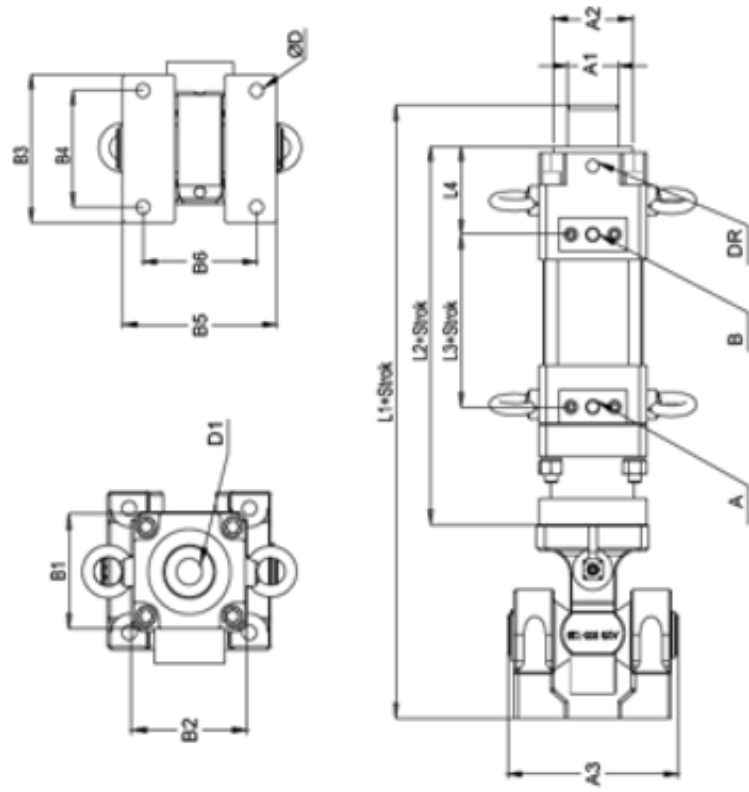


Figure 4.12. Interface Load Cell Specifications [33]

The force transferred to the specimen is conducted with a hydraulic actuator. For this reason, local suppliers are searched to provide hydraulic actuators. RotaTeknik Company has been found in İstanbul as a local supplier, and product of RotaTeknik is used for this testing infrastructure because of reliability and good after-sale support. Custom stroke length is available in order to meet requirements. A tip deflection of this blade according to linear static analysis under extreme ultimate loads is stated as 0.503 m, as presented in Figure 3.2 [29]. By taking into account this information and further tests which will be performed in METUWIND, 1.25 m stroke length is determined. The specification of the hydraulic actuator provided by this company is presented in Figure 4.13. Swivel base having a spherical bearing that allows three-axis

rotation, is used as a hydraulic actuator base in order to give rotation freedom to the actuator. The model of the hydraulic actuator and its assembly, which will be used in testing, are shown in Figure 4.14 [34]. For this static test, the stroke position of actuators will be determined 20 mm for the root actuator and 35 mm for the tip actuator by considering that actuators will push the specimen.



Silindir Model No	EklemYer Bağlantı Model No	Çekme Kuvveti	Basma Kuvveti	Piston ve Mil Çapı (mm)	Çekme Alanı (cm ²)	Basma Alanı (cm ²)					
		(kN)	(kN)								
RTS-11/26 ...-V-X-SB-X	RMSB-30	10	25	40 X 30	5,50	12,56					
L1	L2	L3	L4	A1	A2	A3	B1	B2	B3	B4	B5
(mm)	(mm)	(mm)	(mm)	(mm)	(mm)	(mm)	(mm)	(mm)	(mm)	(mm)	(mm)
474,0	310,0	83,0	74,0	30,0	50,0	105,0	70,0	85,0	86,0	63,6	94,0
B6	D1	∅D	A	B	DR	AÇIRLIK (kg) (Strok 0 mm)		AÇIRLIK (kg) (Her 100 mm strok için)			
(mm)		(mm)				18		1,8			
63,6	M16x2-32	11,0w	G 1/2" -14	G 1/2" -14	G 3/8" -19	18		1,8			

Figure 4.13. RotaTeknik Hydraulic Actuator Specifications [34]

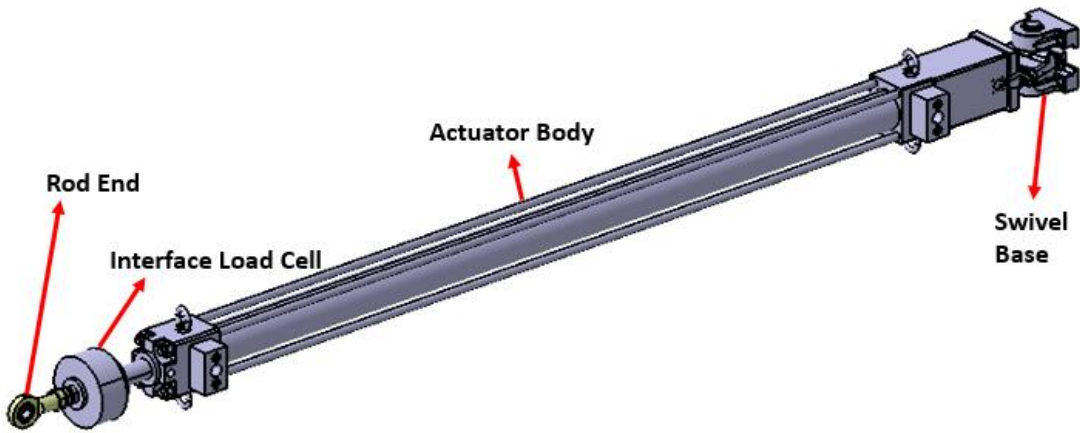


Figure 4.14. Actuator Assembly

While assembling rod end – load cell – actuator to each other, M16 threaded rods are used. Threaded rods are made from steel. Detailed view of this connection is given in Figure 4.15. In this figure, it is seen how actuator assembly is mounted to the clevis.

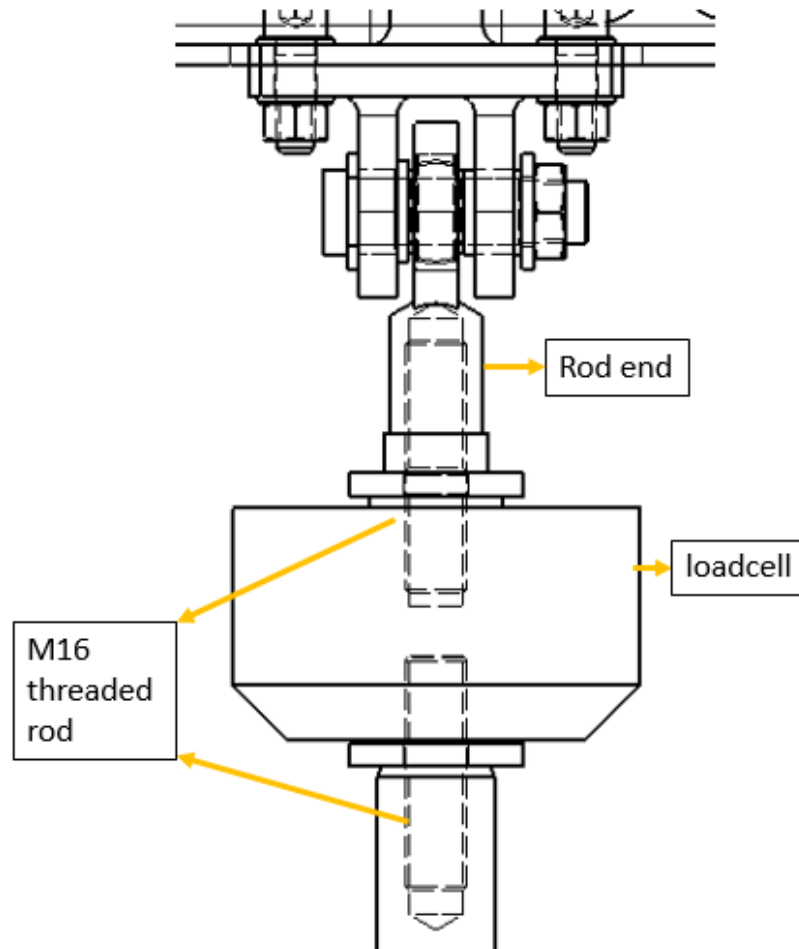
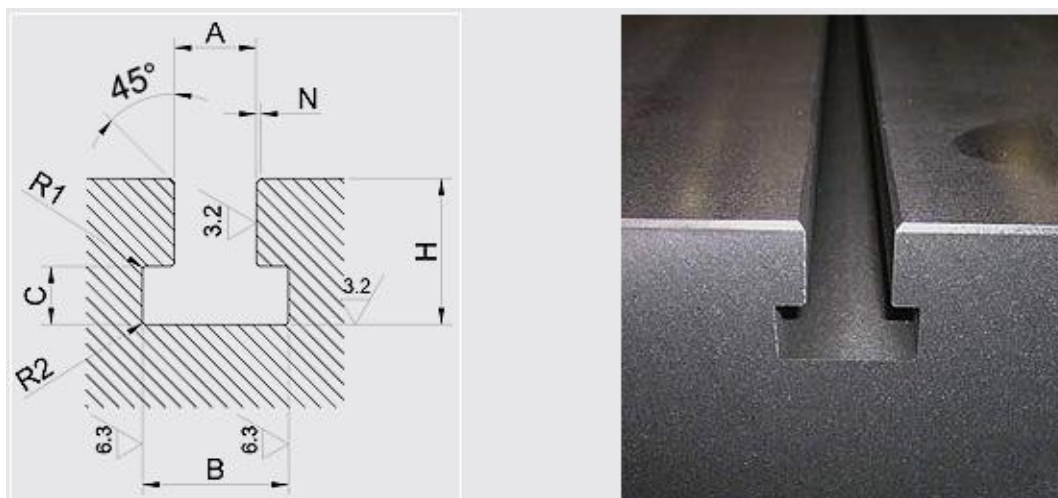


Figure 4.15. Connection of Actuator – Load Cell – Rod End

4.1.3. Support Structure Design

The support structure contains two parts for this test fixture. These are the main reaction wall and ground supports underneath each hydraulic actuator. The design is carried out to fix the blade from the root via a dummy hub plate to the main reaction wall and to fix the hydraulic actuator to the ground. In order to mount the dummy hub plate and the hydraulic actuator to corresponding parts, it is decided to have T channels, which allow mounting bolts any locations in channels. The distance between T channels is determined 150 mm in both the main reaction wall and the ground plate. With the help of T channel design, any details can be mounted to any location on the

surface, and so, these designed details can be used for further testing as a modular structure. This T channel is designed under DIN650 standards given in Figure 4.16 [35]. The design of the T-Slot channel is conducted to have M16 bolts mounting due to reliable and widespread used. Moreover, T nuts that will be used in these slots and how these T nuts provide connection is shown in Figure 4.17 [36]. T nuts have a DIN 508 standard.



A	B		C		H		N	R1	R2	T
		toll.		toll.	max.	min.				
5	10	+1 0	3	+0,5 0	10	8	1	0,6	1	0,5
6	11	+1,5 0	5	+1 0	13	11				
8	14,5		7		18	15				
10	16	+2 0	7	21	17					
12	19		8	25	20					
14	23		9	28	23					
18	30		12	+2 0	36	30	1,6	1,6		
22	37	+3 0	16	0	45	38	1	2,5	1	
28	46	+4 0	20		56	48				
36	56		0	25	+3 0	71	61	2,5	1,6	4
42	68	32		85	74					
48	80	+5 0		36	+4 0	95	84			
54	90	0	40	0	106	94	2	6		

Figure 4.16. T-Slot Specification [35]

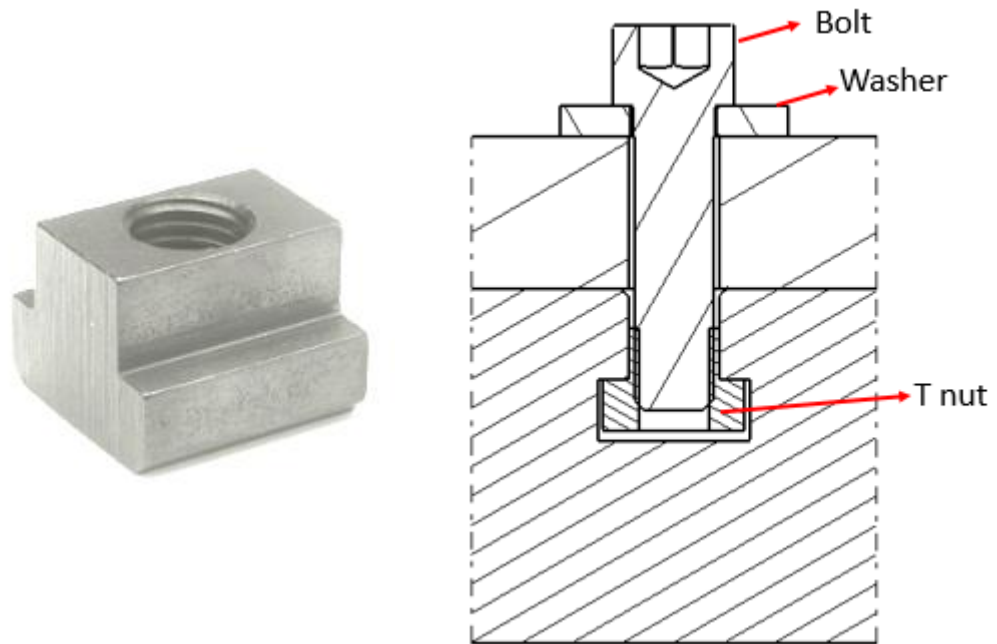


Figure 4.17. DIN 508 T Nut [36] and Assembly of T Nut in T Slot Channel

The main reaction wall is basically composed of two parts. The first is a wall plate which has T slots to mount any dummy hub plate. The second is a wall support. Wall support is made up of 160mm X 160mm welded box profile and allows this structure to attach ground. The reaction wall plate is mounted to weldment assembly through 52 M16 bolts. This welding assembly and reaction wall plate are considered to be made of steel. General dimensions of the reaction wall assembly are given in Figure 4.18 and Figure 4.19. Attaching to ground is provided with 16 M30 anchor. The product of Hilti HAS-U 8.8 will be used to anchor. This anchor is provided in Figure 4.20, and a schematic of how to mount is presented in Figure 4.21. The anchor nut is tightened with 50% of yield strength that gives approximately 1000 Nm torque while mounting to the ground.

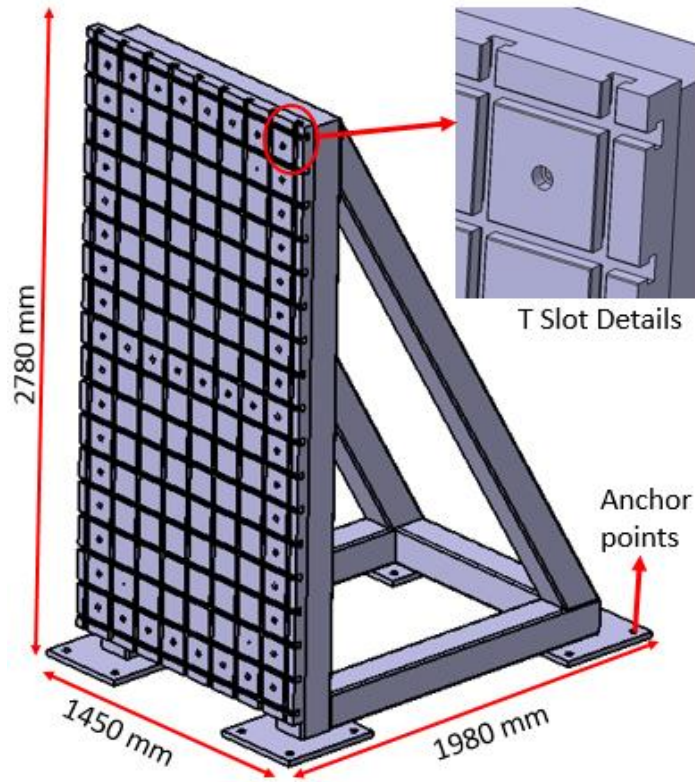


Figure 4.18. General Dimensions of Main Reaction Wall

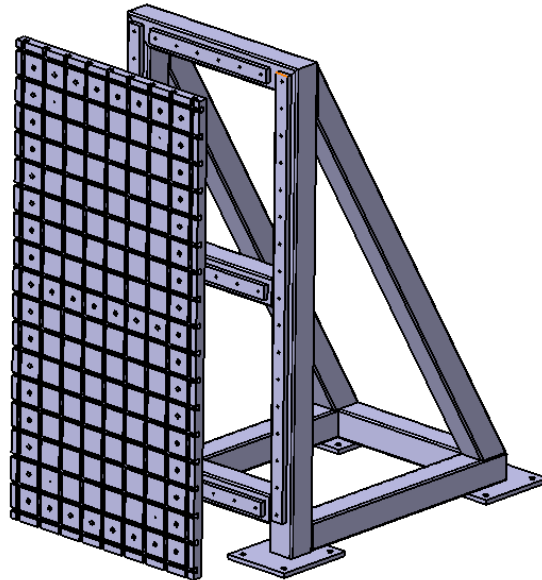


Figure 4.19. Reaction Wall Plate and Weldment Assembly



Figure 4.20. Hilti HAS-U 8.8 Anchor [37]

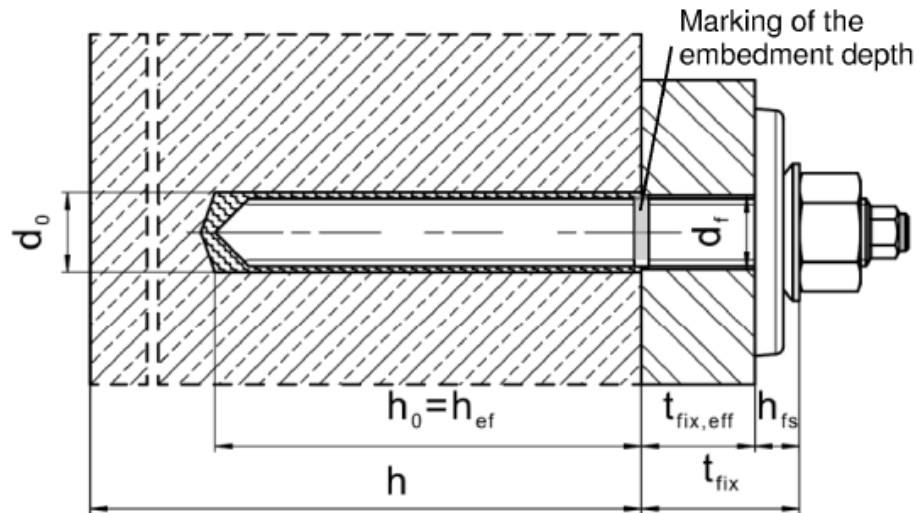


Figure 4.21. Assembly of Hilti HAS-U 8.8 Anchor [38]

Hydraulic actuators will be mounted to the ground support and actuate loads to the blade. The ground support plate is designed to place under each actuator, which will be mount. This ground plate designed is illustrated in Figure 4.22. For each actuator, one ground plate is used. General dimensions of this plate are 1450 mm X 1050 mm X 70 mm. This plate has also DIN650 T channel.

It should be noted that this ground plate and main reaction wall plate are not specific for this test, and any location on the surface can be used for holding detail parts. Moreover, this main reaction wall and ground plate can also be used for further testing. If further tests require more actuators for flapwise loading, the same assembly can be created by using this ground plate and actuator assembly. By simply designing the saddle interfaces, new actuator assembly for loading can be provided. Like main reaction wall assembly, this ground plate is also assembled to the ground by using Hilti HAS-U 8.8 M30 anchor. The ground plate is made up of steel and weighs about 700 kg. In order to make logistics easier, four M20 lifting holes are drilled. This holes are used while lifting and carrying.

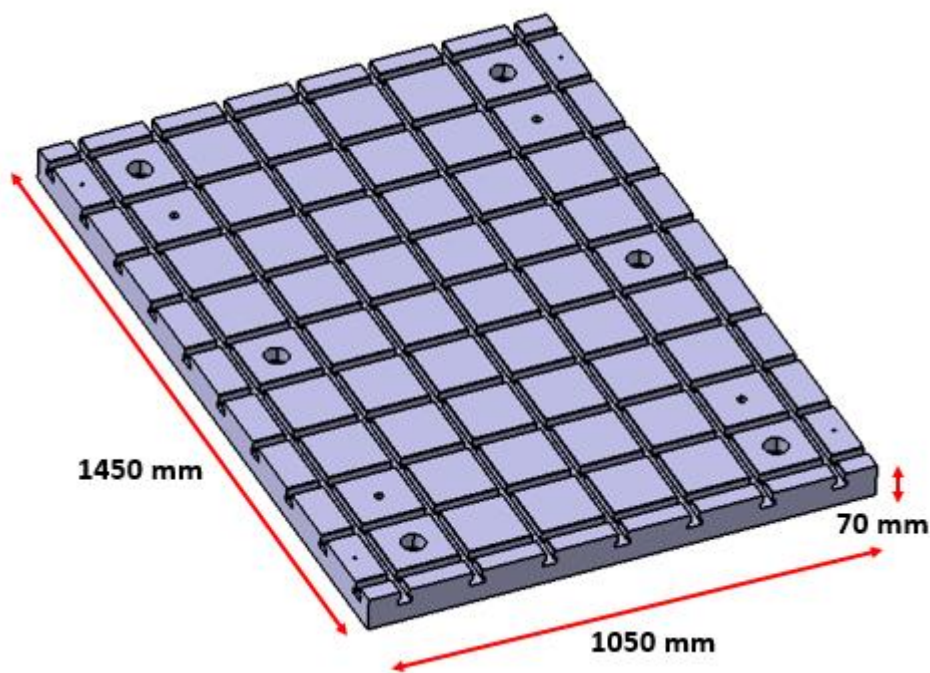


Figure 4.22. Actuator Ground Plate

The actuator is attached to the ground plate by using a circular plate between the actuator and ground plate. The actuator is mounted to the circular plate with four M10

bolts, and this circular plate is assembled to the ground plate via M16 bolts in elongated holes encircled actuator. This assembly representation is given in Figure 4.23. The circular plate is specific for this actuator connection to the ground plate. Also, it should be noted that this actuator circular plate is made of steel.

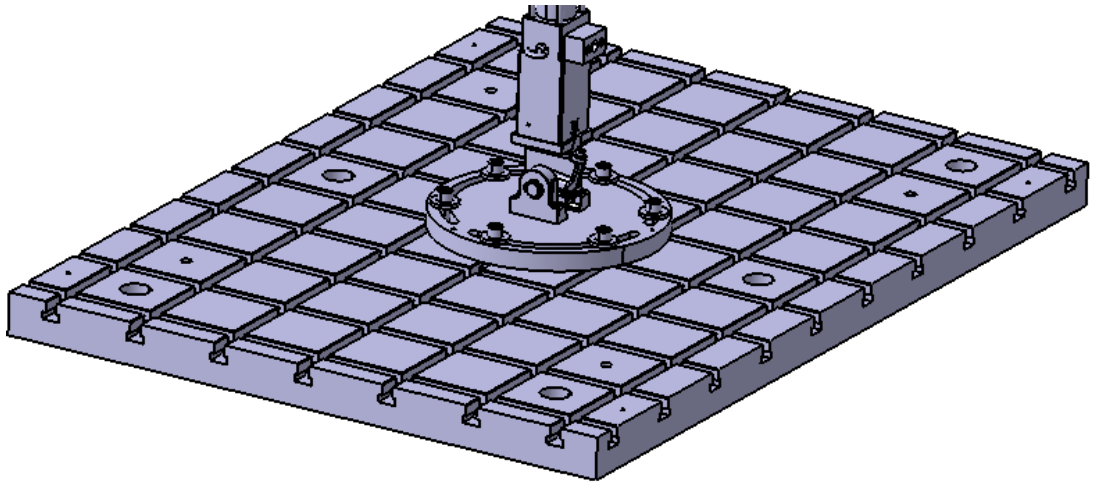


Figure 4.23. Assembly of the Actuator to the Ground Plate

The reaction wall, the actuator ground support, the dummy hub plate, and actuator circular plate are mounted to an exact location by using OTP holes. OTP is optical tooling point that helps to measure the location of details and provide to place detail parts at their exact locations. For this process, at least 3 OTP having 6 mm sensitive dimensions are drilled on the surface of the detail parts, and laser tracking tool is used to mount detail parts at exact locations. Example OTP is shown in Figure 4.24. Saddles have not optical tooling points. They are mounted by measuring locations from the root. After that, inclinometer is used to check angle (parallelism to the ground).

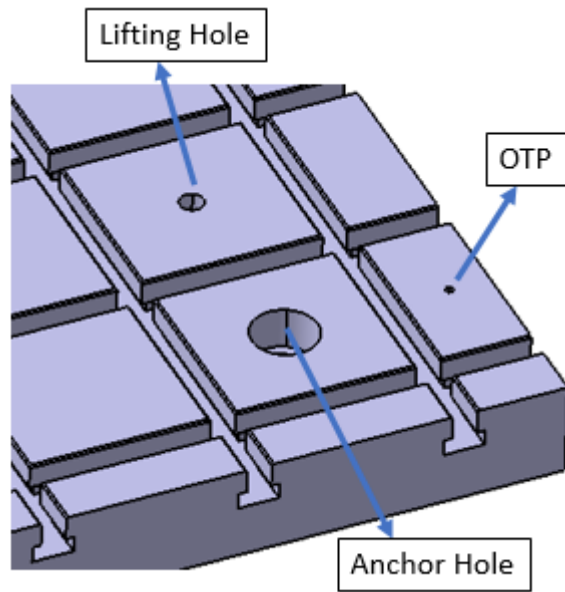


Figure 4.24. Holes on the Plate

The blade specimen is located 2130 mm above the ground. It is mounted with the help of OTP located on the dummy hub. Due to gravitational force, the blade deflects and these deflections are eliminated via hydraulic actuator while mounting by measuring the angle of the upper surface of saddles. In other words, the upper surface of saddles is brought parallel to the ground. At final position, load cells are adjusted to zero in order to start testing. When all of these components are assembled, the final test fixture is revealed, as shown in Figure 4.2.

Final position at 100% loading of the blade and actuators are also studied to show the change in actuators and the blade. In this position, effect of change in angle and change in displacement are shown in Figure 4.25. In order to be more conservative, blade deflection are considered to be a linear. Blade deflection angle at the maximum loading is calculated as 5.77° . Corresponding change in displacement of the root and tip actuators are measured as 106 mm and 374 mm respectively. And also, angle change in the root and tip actuators are also measured 0.15° and 0.46° . With these angles, z component of the maximum loads to be applied are also calculated by;

$$F_{z1} = 4492 \text{ N} \times \sin(0.15) = 11.8 \text{ N} \quad (4-1)$$

$$F_{z2} = 3648 \text{ N} \times \sin(0.46) = 29.2 \text{ N} \quad (4-2)$$

where F_{z1} is the z component of the root actuator and F_{z2} is the z component of the tip actuator. As seen from (4-1) and (4-2), z components are small and they can be neglected.

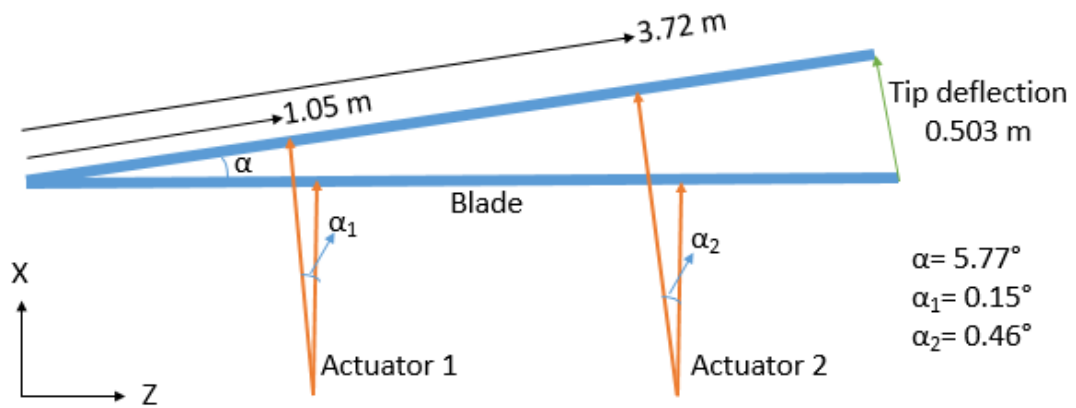


Figure 4.25. Final Position of the Blade at 100% Loading

4.2. Architecture of the Test System

The test is to be carried out by means of hydraulic actuators, test control and test measurement systems that allow control and monitoring of test performance. The test setup architecture is drawn in Figure 4.26.

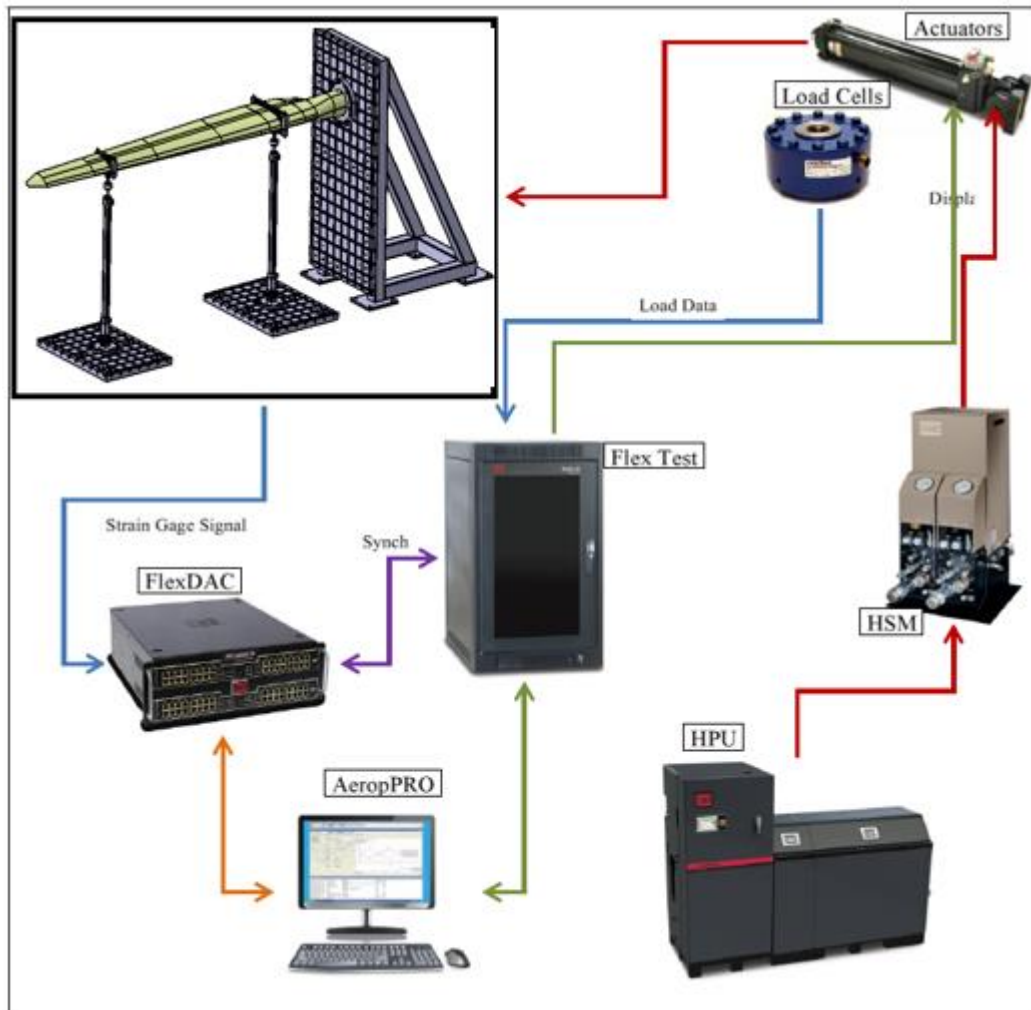


Figure 4.26. Architecture of the Test System

HPU is a hydraulic pump unit which provides needed hydraulic oil to the actuators. HPU is used as a reservoir of hydraulic system. This pump unit sends a hydraulic oil to the hydraulic service manifold (HSM) that regulates this oil before entrance to hydraulic actuators. Since the loss of oil pressure can occur while transferring of oil, HSM is necessary for regular oil flow. HSM provides regulated hydraulic oil with constant pressure. There is a servo valve on the actuators for input. Servo valve is a mechanism which adjusts the direction in which the piston goes. Servo valve on the actuator is controlled by the controller. Controller commands servo valves with

feedback obtained in load cells. Load cells give voltage output to controller and according to this output, controller runs the servo valves. This command and feedback are not only performed by voltage output but also it can be conducted by displacement output obtained in displacement sensors of hydraulic actuators. In order to control the controller, a software is needed. In this software, the test process is introduced concerning test steps, data acquisition frequency, limits of test. If data from the sensors such as strain gauge, displacement transducers, inclinometers are wanted to collect, they are performed by data acquisition system. This data acquisition system is used to measure and record these data. Also, data acquisition system is also connected to the control system computer, which has a software, for synchronizing.

Cost of all equipments required and manufacturing cost of test rig are stated in Appendix.

CHAPTER 5

ANALYSIS OF THE TEST SYSTEM

5.1. Structural Analysis

Having completed the design of the test rig, structural analysis is performed in accordance with our methodology. In order to guarantee that the test rig would not fail during testing, all details used in the test rig shall be analyzed with possible loads in the test rig and it shall be shown that reserve factor values are sufficient to execute testing.

Linear static analysis of the test rig is performed. Finite element analysis and hand calculations are carried out for detail parts of the test rig. The test rig consists of the support structure, which are the main reaction wall and ground plates, actuator assemblies, saddles and load introduction detail parts. Firstly, materials of detail parts are determined. Then, loads to be encountered in testing are evaluated and boundary conditions are given. The loads applied by hydraulic actuators are simulated. According to the detail parts geometry, FEM models are created and solved. Also, hand calculations are performed for detail parts such as a clevis, a pin, and bushings.

5.2. Material Selection

Material selection is carried out by considering the intended purpose of the details parts, stock size, the material strength, the mass and cost-effectiveness.

The main reaction wall's welding assembly and plates consisting of DIN650 T channel are manufactured from St52-3 structural steel due to high strength as structural steel, stock size and widespread use.

Dummy hub plate and the circular plate underneath actuators are manufactured from AISI 4140 steel plate. Actuator assembly consists of two threaded rods between actuator – load cell and load cell – rod end. Also, they are manufactured from AISI 4140 steel. Connection to the saddle is provided by the clevis, bushings and the pin. The clevis and bushings are also made of AISI 4140 steel. This material has high strength and good machinability. Generally, pins have the lowest RF value, so, high strength steel TOOLOX44 is used for pins.

Saddles providing load introduction to the blade is made of aluminum in order to make it lighter. Al2024 T351 is chosen due to cost-effectiveness, and availability in the marketplace.

For the connection, fasteners are used. Standard carbon steel bolts that have 12.9 grade are preferred. In order to assemble support structure to the ground, Hilti HAS-U anchors that have 8.8 grade are used.

The welding to be implemented for assembly is not clear in industry. For this reason, the worst welding, which is E60xx, is chosen to use the worst allowable data in calculation and welding is evaluated with this data.

5.3. Load Data

The loads affecting the details parts are evaluated and which loads are used for every detail part is presented. The static test is to be carried out with two actuators. Actuator assemblies consist of the ground plate, the actuator base circular plate, threaded rods, the rod end, the clevis and the pin. The static load applied from hydraulic actuators are stated as 4492 and 3648 N for root and tip saddles, respectively, in Chapter 3. Since the actuator assemblies have same detail parts, the analysis is conducted by the highest load of 4492 N for the parts in these actuator assemblies. In this way, maximum stress are calculated for these detail parts used in actuator assemblies. For the reaction wall assembly, sectional shear and moment at the root are used as 8140 N

and 18.09 kNm. Bolt loads are obtained from finite element analysis and analyses of the Hilti anchor rods are performed according to properties given in Hilti Datasheet and bolt loads taken from finite element analysis.

5.4. Material, Fastener and Allowable Data

Allowable values of the materials that are used in the test rig structure are listed in Table 5.1. Tables contain tensile yield strength, shear yield strength, elastic modulus and Poisson's ratio. It should be noted that yield strength values are used for test rig detail parts analysis. Ultimate values should not be used. For this reason, ultimate strength values are not placed in these tables.

Table 5.1. *Material Allowable Values [39], [40]*

<i>Material</i>	<i>F_{ty} [MPa]</i>	<i>F_{sy} [MPa]</i>	<i>E [MPa]</i>	<i>γ</i>
AISI 4140 Water Quenched from 845 °C and Tempered at 540 °C	986	591.6	205000	0.29
St52-3	345	207	211000	0.30
Al2024 T351	469	283	73100	0.33
E60xx	345	207	-	-

Allowable values of the fastener materials that are used in the test rig structure are listed in Table 5.2.

Table 5.2. *Fastener Material Allowable Values [40], [41]*

<i>Fastener Material</i>	<i>F_{ty} [MPa]</i>	<i>F_{sy} [MPa]</i>	<i>E [MPa]</i>	<i>γ</i>
TOOLOX 44	1350	810	205000	0.30

Table 5.2 Fastener Material Allowable Values [40], [41] (cont'd)

Carbon Steel Grade 12.9	1100	660	205000	0.29
Carbon Steel Grade 8.8	640	384	205000	0.29

Different calculation methods are used for the analysis of different components. Calculation methods are given in detail in the strength analysis part of a related component. In general, calculation methods given in [41] and [42] are used for the static analysis of the structure.

5.5. Finite Element Model (FEM) Description

Main reaction wall, ground plate, dummy hub plate, circular plate and saddles are modeled by HEX8, QUAD4, TET10, and RBE3 elements with deformable body feature in MSC PATRAN. All of the details used finite element method are modeled with solid elements. Loads are modelled by RBE3 elements.

The actuator circular plate is modelled by HEX8 and RBE3 elements with deformable body feature in MSC PATRAN. The actuator contains swivel base and this base contains spherical bearing that allows rotation in 3-axes. The actuator loads are distributed from the spherical bearing with the help of RBE3 elements. Finite element model is held from the base of this plate. The total number of elements is 82579. Although this plate is used in both two actuators, one FEM analysis is performed by highest load due to both circular plates have the same geometry, properties and boundary conditions. A sketch of the load and boundary conditions and FEM of the actuator circular plate are found in Figure 5.1.

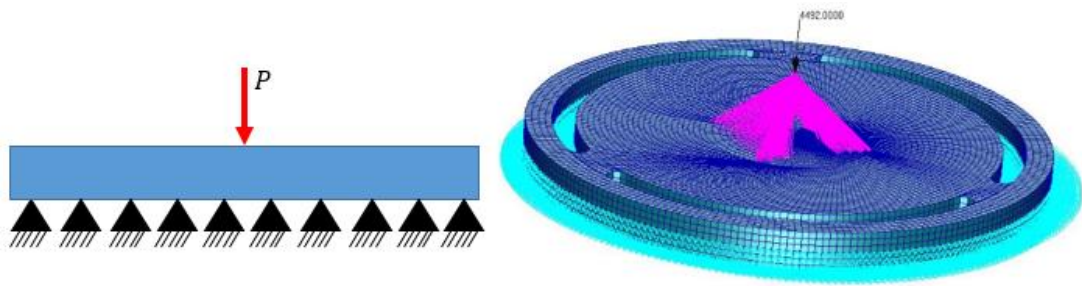


Figure 5.1. Sketch of Load and Boundary Conditions (left), FEM of Actuator Circular Plate (right)

The ground plate which contains DIN650 T slot channels is modelled by HEX8 and RBE3 elements with deformable body feature in MSC PATRAN. The actuator loads are applied at the same point in actuator circular plate. The finite element model is held from the 6 bolt holes that used to mount to the ground. The total number of elements is 434286. The finite element model of ground plate with load and boundary conditions is found in Figure 5.2. Note that the load applied is in-plane at the center of the plate.

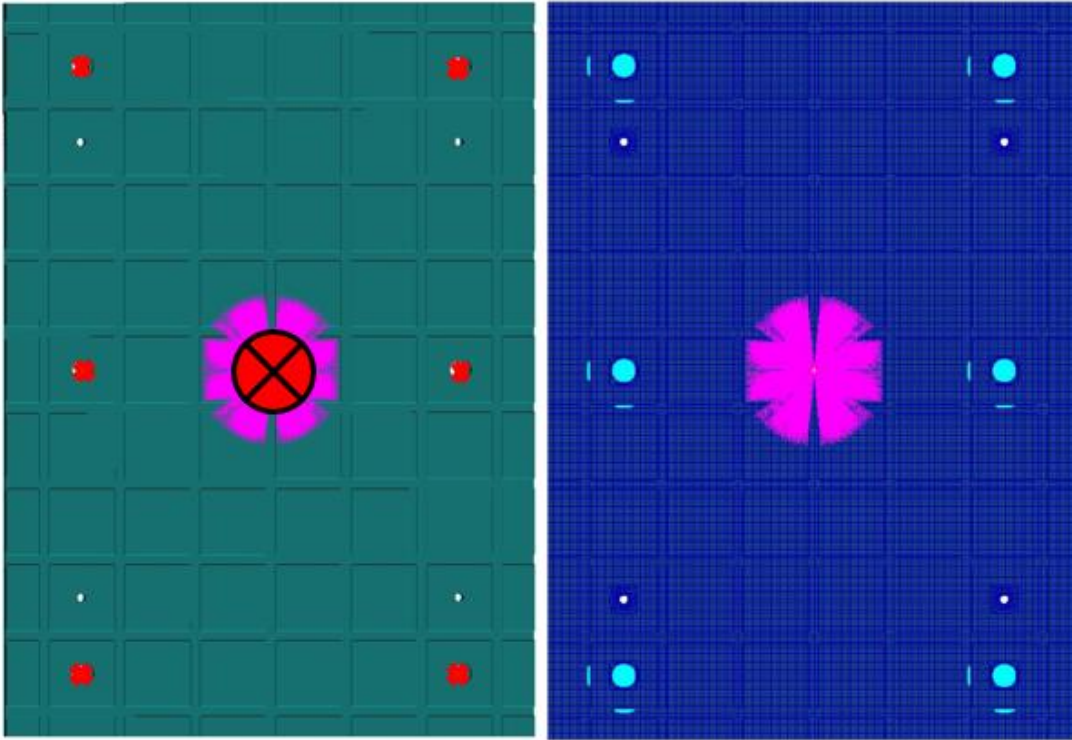


Figure 5.2. Load and Boundary Conditions of the Ground Plate (left), Finite Element Model of the Ground Plate (right)

Saddles are modelled by QUAD4 and RBE3 elements with deformable body feature in MSC PATRAN. The actuator load is distributed to the lower part of saddles from the center of the spherical bearing of the rod end with the help of RBE3 elements. The finite element model is held from the surface where imitate the blade. It should be noted that lower parts of the root and the tip saddle are modelled only. Upper part of saddles is used to hold the saddle fixed. The finite element model of saddle details with load and boundary conditions are found in Figure 5.3 and Figure 5.4, respectively. The lower part of the root saddle has 84310 elements while the tip saddle lower part has 56333 elements.

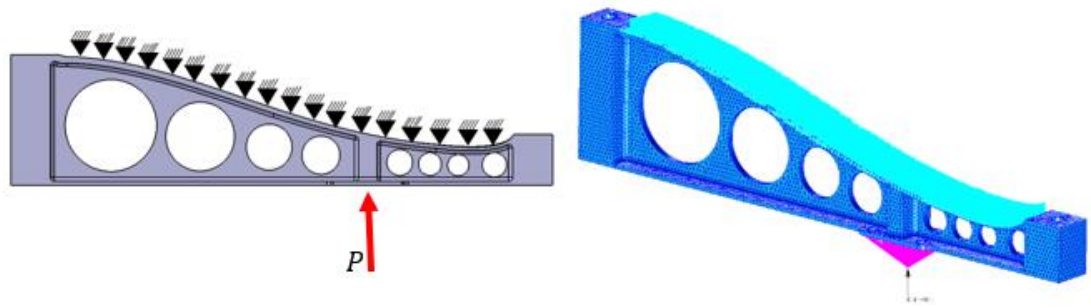


Figure 5.3. FE Model of the Lower Part of the Root Saddle

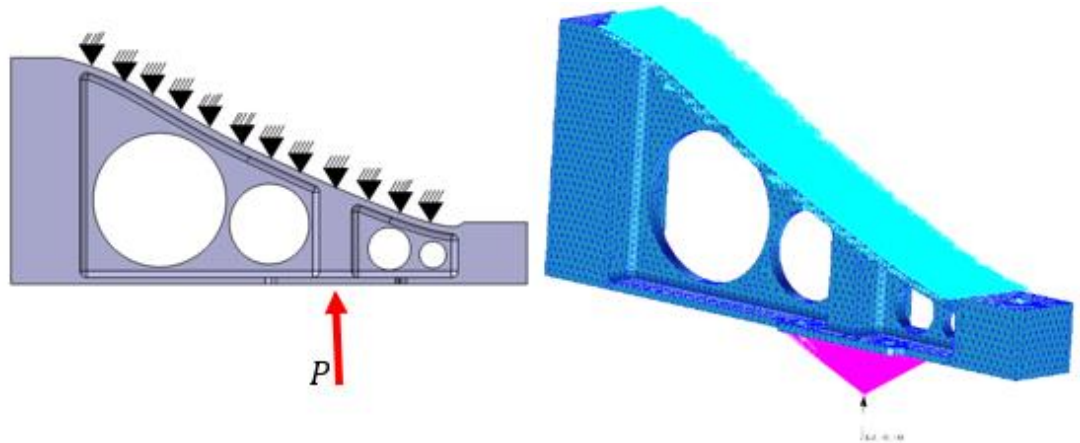


Figure 5.4. FE Model of the Lower Part of the Tip Saddle

The dummy hub plate is modelled by HEX8 elements. The shear load and the moment at the blade root are applied as a load condition. The finite element model is held from five bolt locations that that used to mount to the reaction wall plate. In test case, the dummy hub plate will be held at least seven bolts. In order to be more conservative, only five bolt holes are used in analysis. The total number of the dummy hub plate elements is 19464. Load and boundary conditions, and finite element model of the dummy hub plate is shown in Figure 5.5.

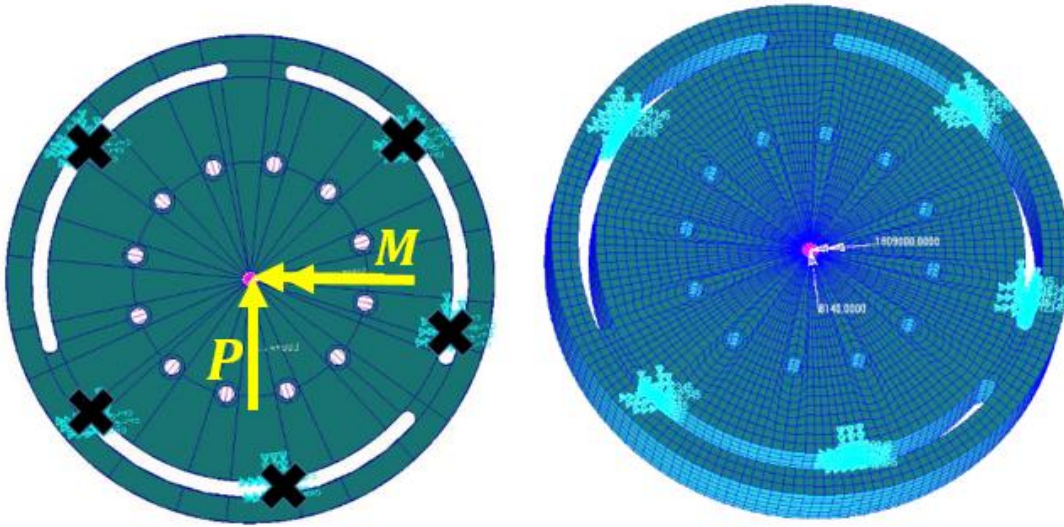


Figure 5.5. Load and Boundary Conditions (left), FE Model of the Dummy Hub Plate (right)

The reaction wall plate with T channel is modelled by HEX8 and RBE3 elements in MSC PATRAN. The load and moment at the root of the blade are distributed to this plate through RBE3. FEM is held from 52 M16 bolt holes providing connection to the weldment assembly of the reaction wall. The total number of elements is 200804. The finite element model of the reaction wall plate with load and boundary conditions is shown in Figure 5.6.

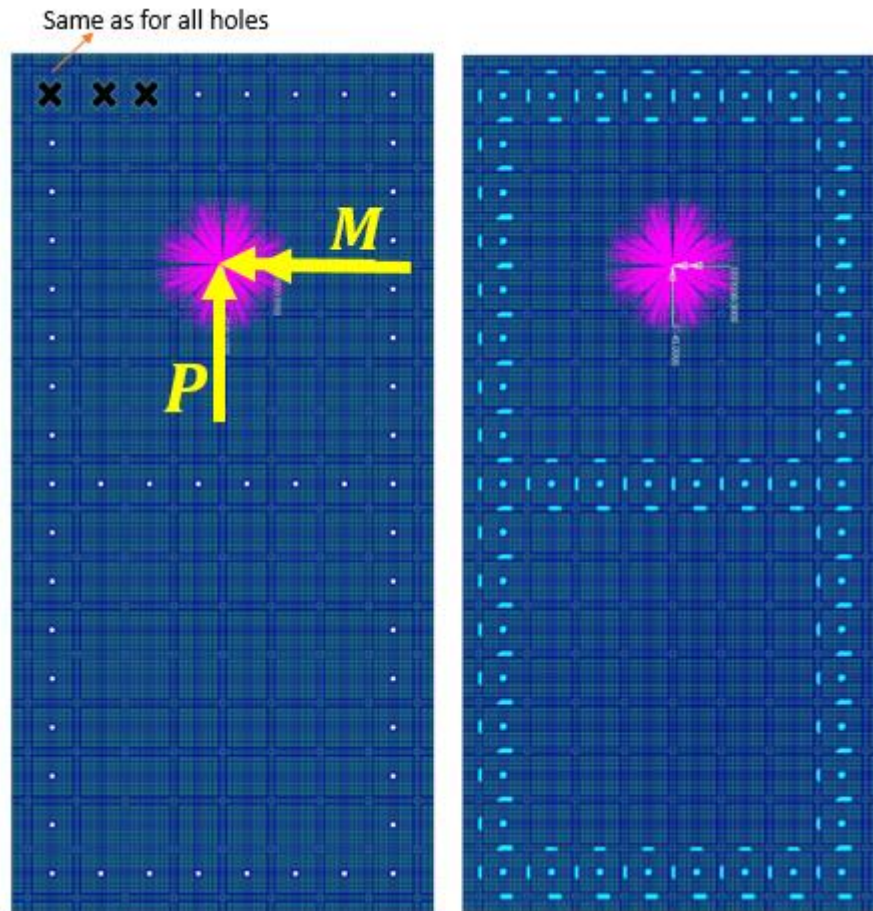


Figure 5.6. FE Model of the Reaction Wall Plate

The reaction wall weldment assembly is modelled by TET10 and RBE3 elements in MSC PATRAN. The load and moment at the root of the blade are distributed to where reaction wall plate mounted through RBE3. The finite element model is held from 16 M30 bolts holes providing connection to the ground. The total number of elements is 831786. The finite element model of the reaction wall weldment assembly with load conditions is shown in Figure 5.7 and the detailed finite element model and boundary conditions are shown in Figure 5.8.

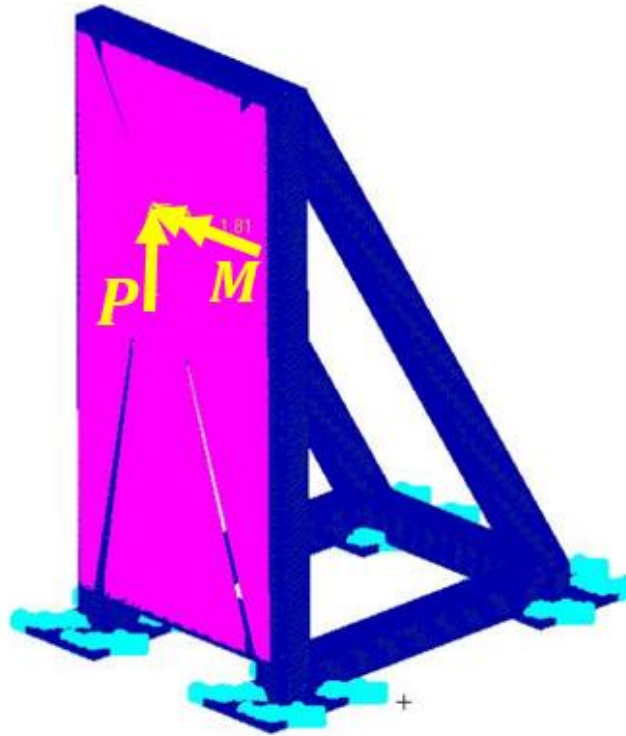


Figure 5.7. FE Model and Load Condition of Reaction Wall Weldment Assembly

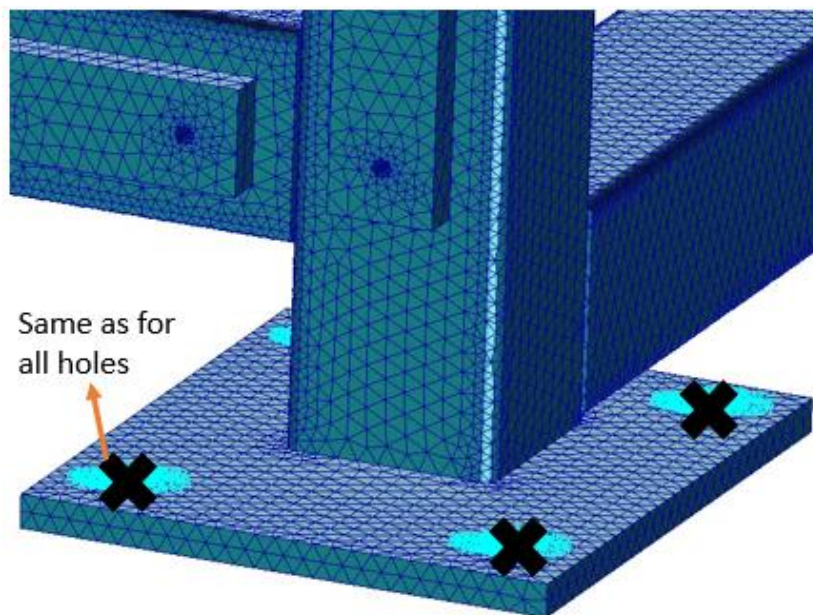


Figure 5.8. Boundary Condition and Detailed FE Model of Reaction Wall Weldment Assembly

5.6. Strength Analysis

Strength analysis is performed by finite element method and hand calculation. Instead of material ultimate strength values, material yield strength values are used to be more conservative in the strength analysis of test rig detail parts. During testing, test rig detail parts shall not fail before the test specimen. So, high reserve factor criteria using yield strength values in analysis are asked for. RF values are calculated for each detail parts by performing strength analysis.

Unless otherwise specified, RF values for support structure shall be greater than 6.0 by using material yield strength values because support structure have to resist extreme loads during testing and it shall not fail before specimen failure [26].

Total displacement results for the ground plate taken from MSC NASTRAN can be seen in Figure 5.9. Maximum deformation value of 0.0105 mm occurs at the center of the ground plate under 4492 N compressive load. Maximum Von-Mises stress results for the ground plate under 4492 N compressive load case is shown in Figure 5.10. Maximum Von-Mises stress value is 7.72 MPa giving an RF value of 44.7, which is much higher than our minimum reserve factor criterion.

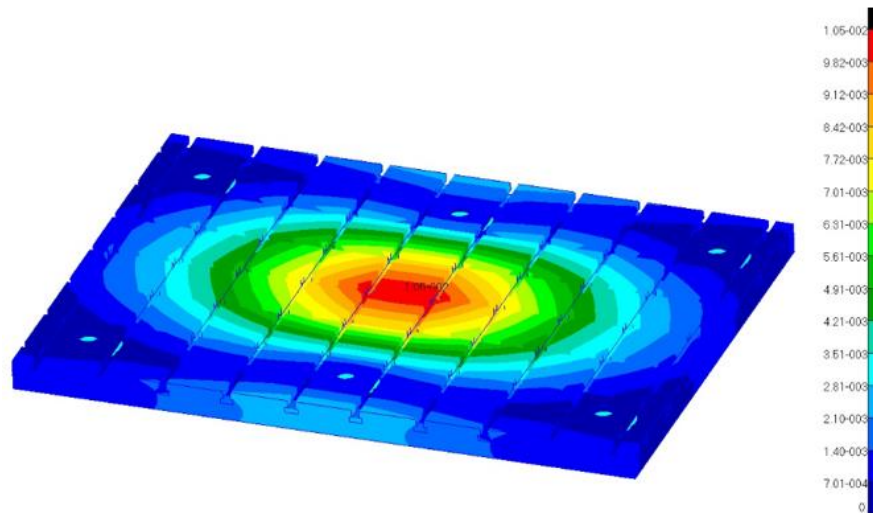


Figure 5.9. Displacement Contours of the Ground Plate [mm]

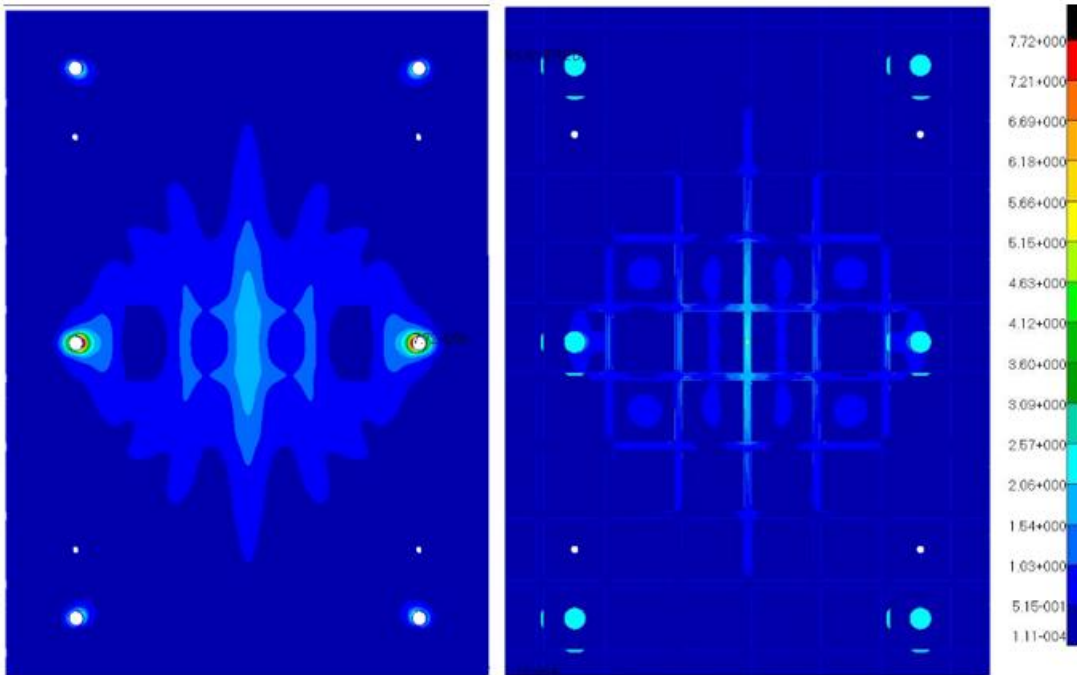


Figure 5.10. Von-Mises Stress Contours of the Ground Plate (left:back, right:front) [MPa]

Total displacement results for actuator base circular plate taken from MSC NASTRAN can be seen in Figure 5.11. Maximum deformation value of 0.00163 mm occurs at the bolt hole edge under 4492 N compressive load. Maximum Von-Mises stress results for the ground plate under 4492 N compressive load case is shown in Figure 5.12. Maximum Von-Mises stress value is 3.76 MPa giving an RF value of 262, which is much higher than our minimum reserve factor criterion.

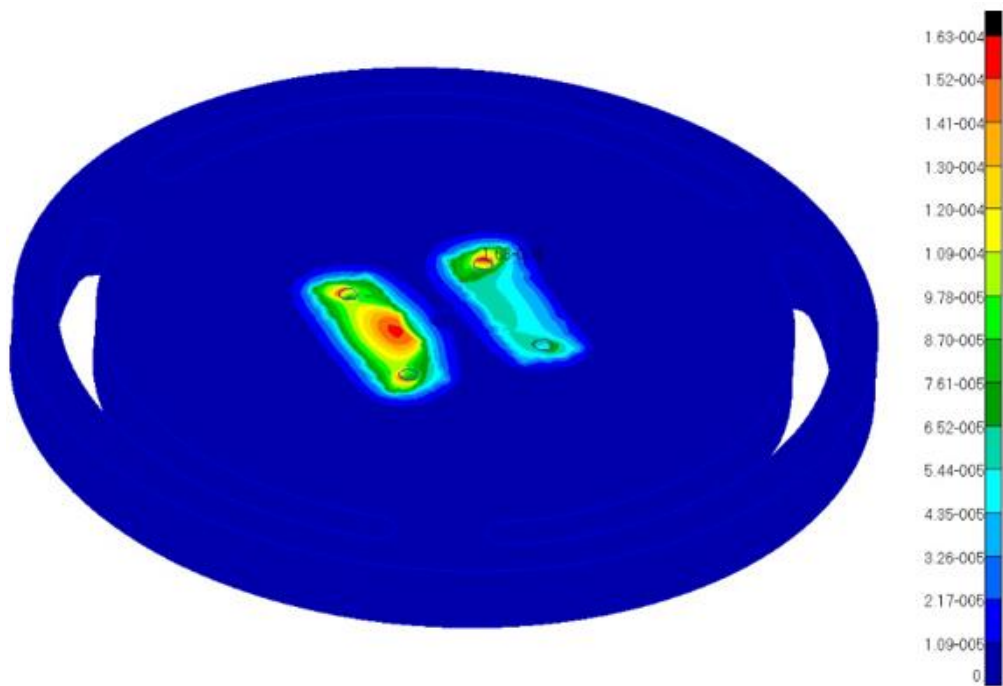


Figure 5.11. Displacement Contours of the Actuator Circular Plate [mm]

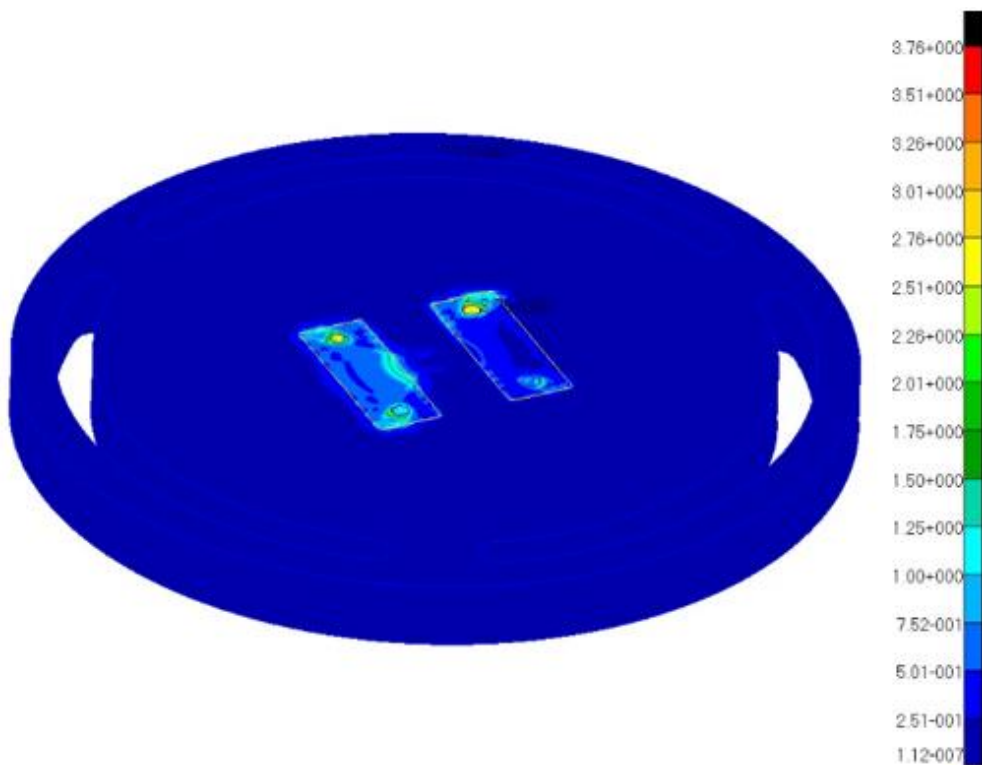


Figure 5.12. Von-Mises Stress Contours of the Actuator Circular Plate [MPa]

Total displacement results for root saddle lower part taken from MSC NASTRAN can be seen in Figure 5.13. Maximum deformation value of 0.0336 mm occurs at bolt edges where clevis mounted under 4492 N compressive load. Maximum Von-Mises stress results for the ground plate under 4492 N compressive load case is shown in Figure 5.14. Maximum Von-Mises stress value is 3.30 MPa giving an RF value of 142, which is much higher than our minimum reserve factor criterion.

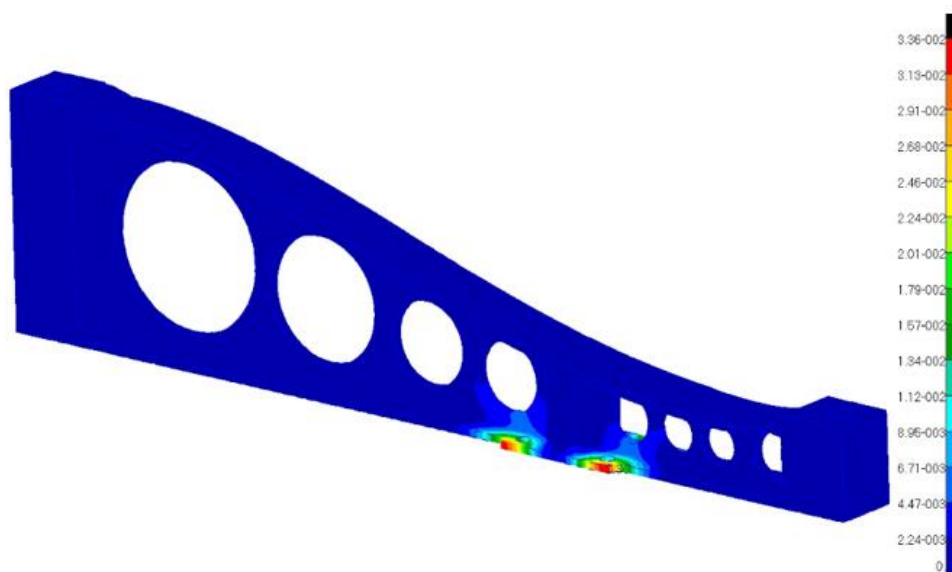


Figure 5.13. Displacement Contours of the Root Saddle of Lower Part [mm]

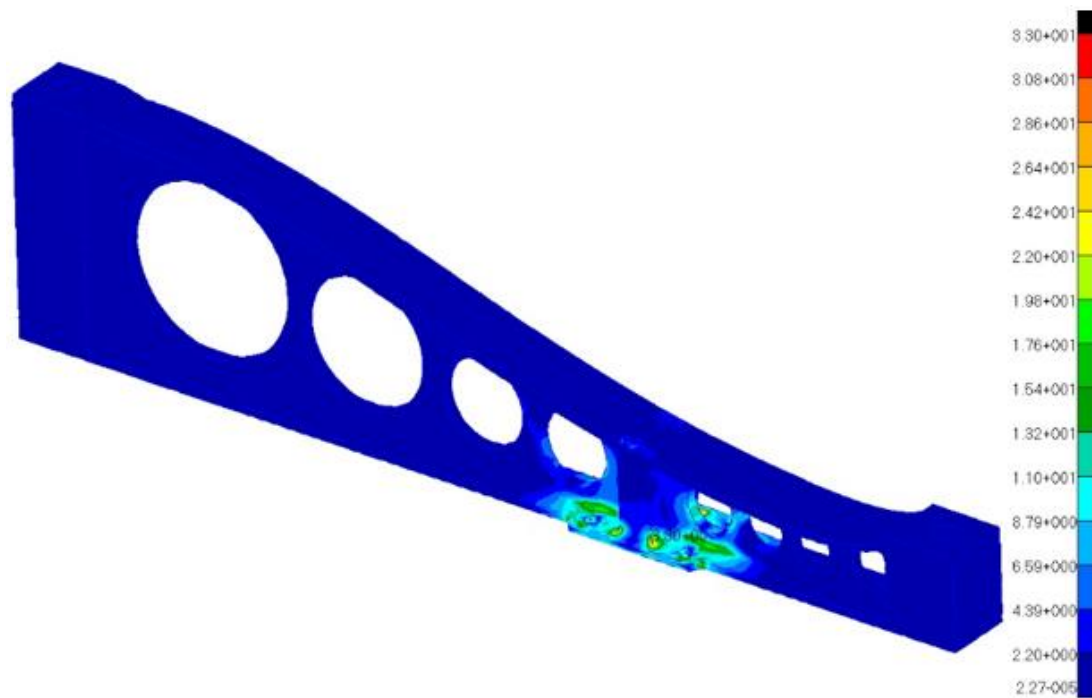


Figure 5.14. Von-Mises Stress Contours of Root Saddle of Lower Part [MPa]

Total displacement results for root saddle lower part taken from MSC NASTRAN can be seen in Figure 5.15. Maximum deformation value of 0.0253 mm occurs at edge of bolt holes where clevis mounted under 3648 N compressive load. Maximum Von-Mises stress results for the ground plate under 4492 N compressive load case is shown in Figure 5.16. Maximum Von-Mises stress value is 1.27 MPa giving an RF value of 369, which is much higher than our minimum reserve factor criterion.

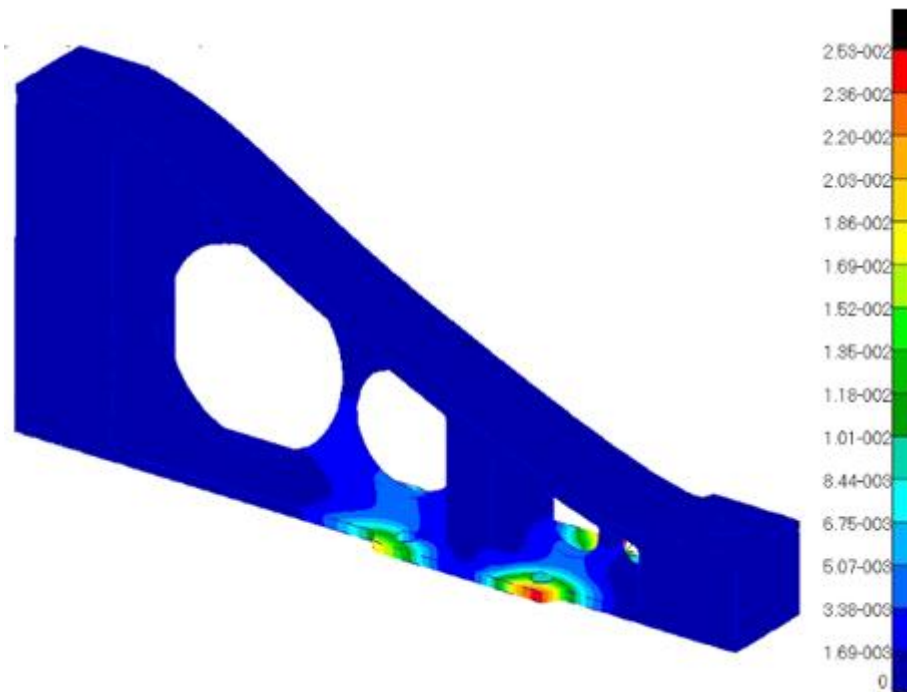


Figure 5.15. Displacement Contours of Tip Saddle of Lower Part [mm]

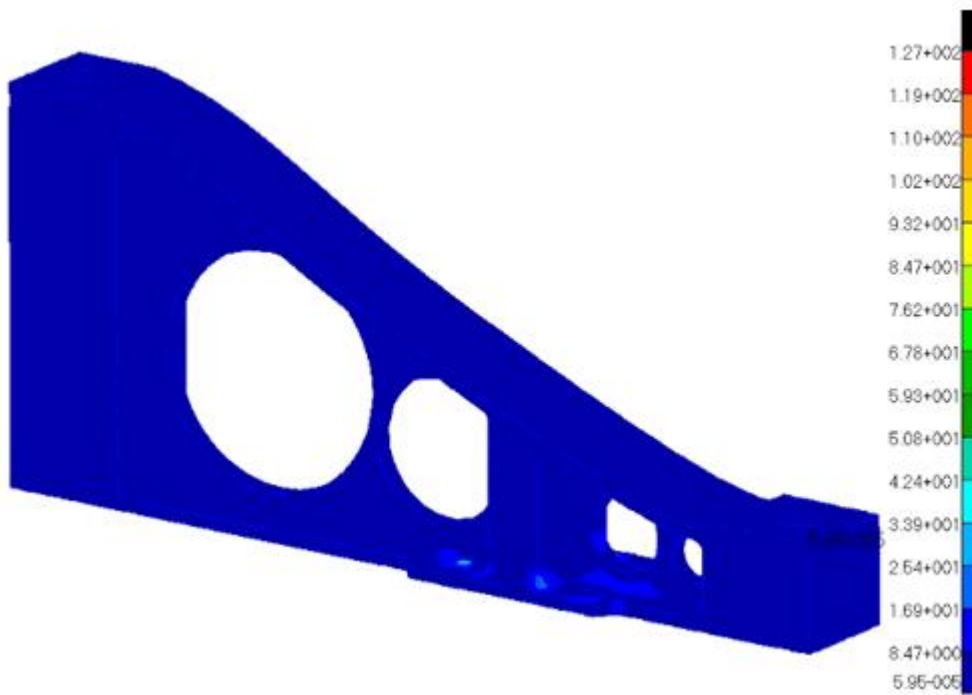


Figure 5.16. Von-Mises Stress Contours of Tip Saddle of Lower Part [MPa]

Total displacement results for dummy hub plate taken from MSC NASTRAN can be seen in Figure 5.17. Maximum deformation value of 0.00118 mm occurs at upper counterbored bolt holes under 8140 N shear load and 18.09 kNm moment at the root. Maximum Von-Mises stress results for the dummy hub plate with loading 8140 N and 18.09 kNm is shown in Figure 5.18. Maximum Von-Mises stress value is 4.58 MPa giving an RF value of 215, which is much higher than our minimum reserve factor criterion.

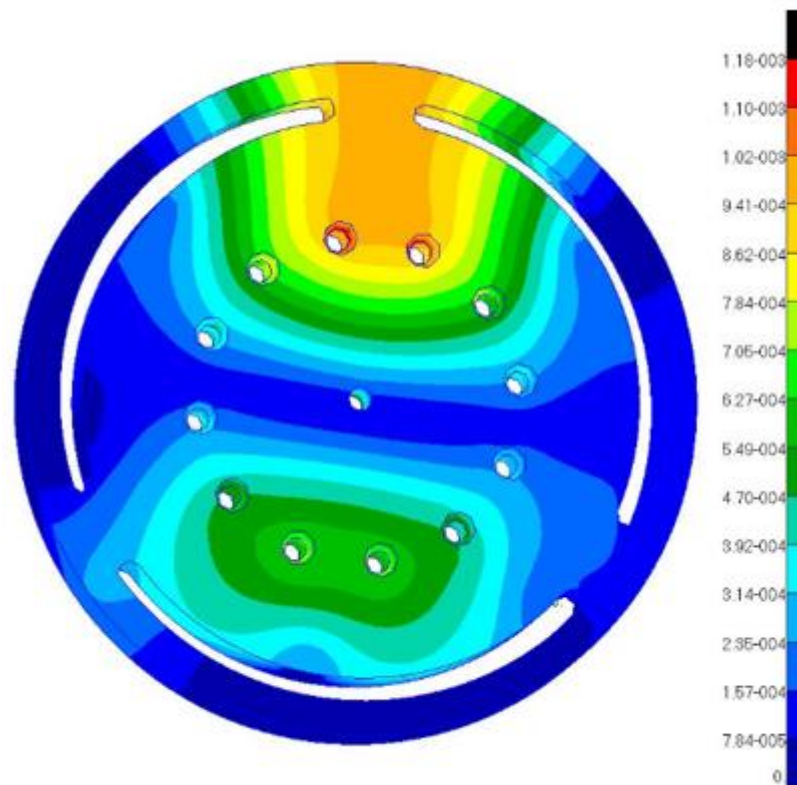


Figure 5.17. Displacement Contours of Dummy Hub Plate [mm]

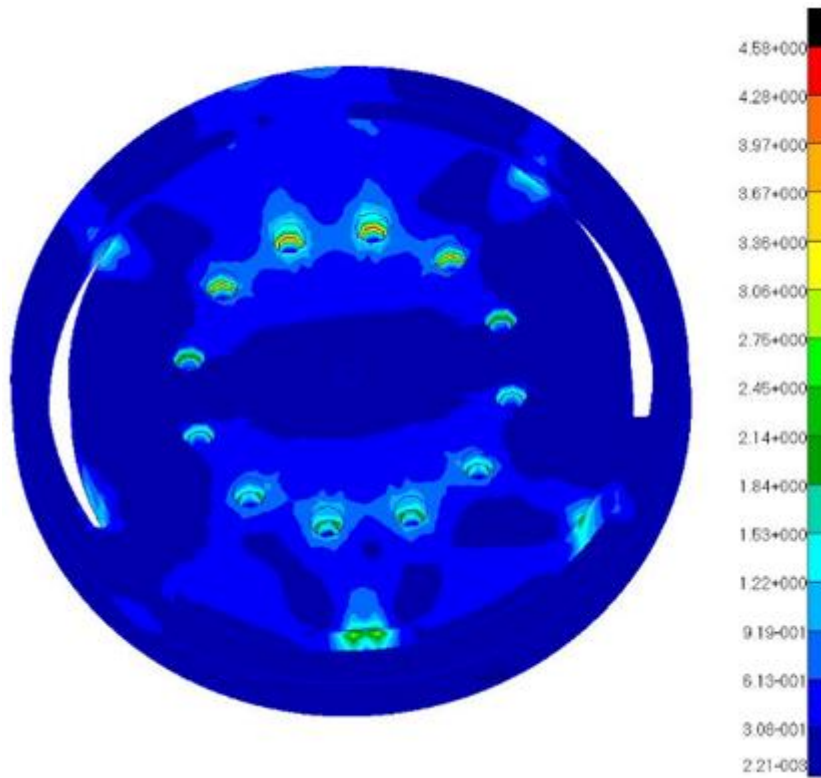


Figure 5.18. Von-Mises Stress Contours of Dummy Hub Plate [MPa]

Total displacement results for reaction wall plate taken from MSC NASTRAN can be seen in Figure 5.19. Maximum deformation value of 0.00918 mm occurs at surface where dummy hub touches with 8140 N shear load and 18.09 kNm moment at the root. Maximum Von-Mises stress results for the reaction wall's T channel plate with loading 8140 N and 18.09 kNm is shown in Figure 5.20. Maximum Von-Mises stress value is 3.47 MPa giving an RF value of 99.4, which is much higher than our minimum reserve factor criterion.

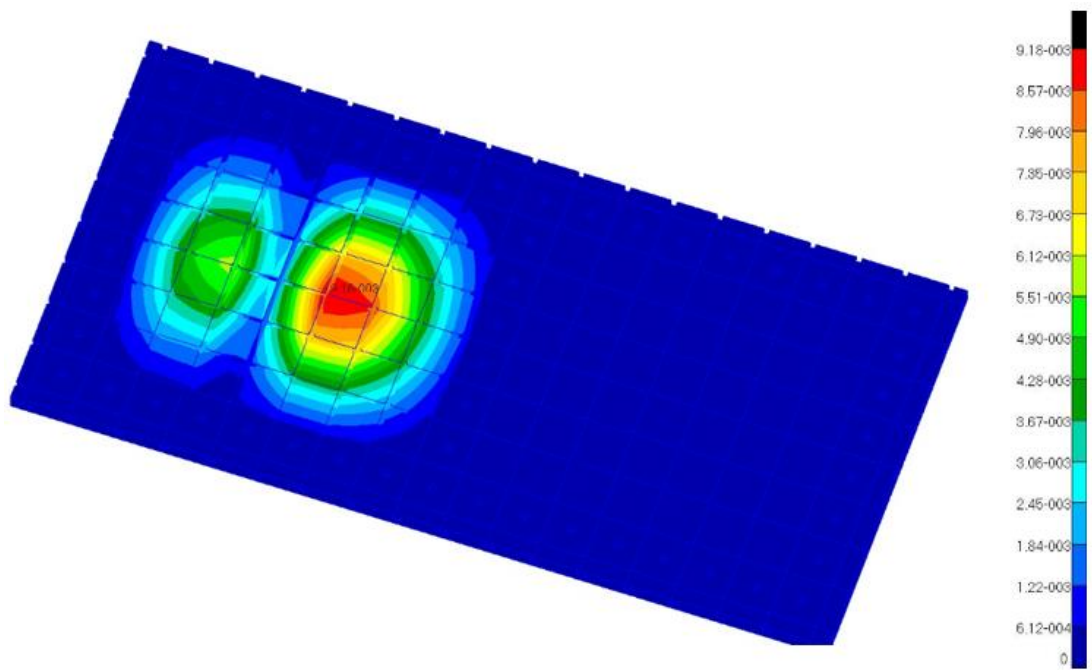


Figure 5.19. Displacement Contours of Reaction Wall Plate [mm]

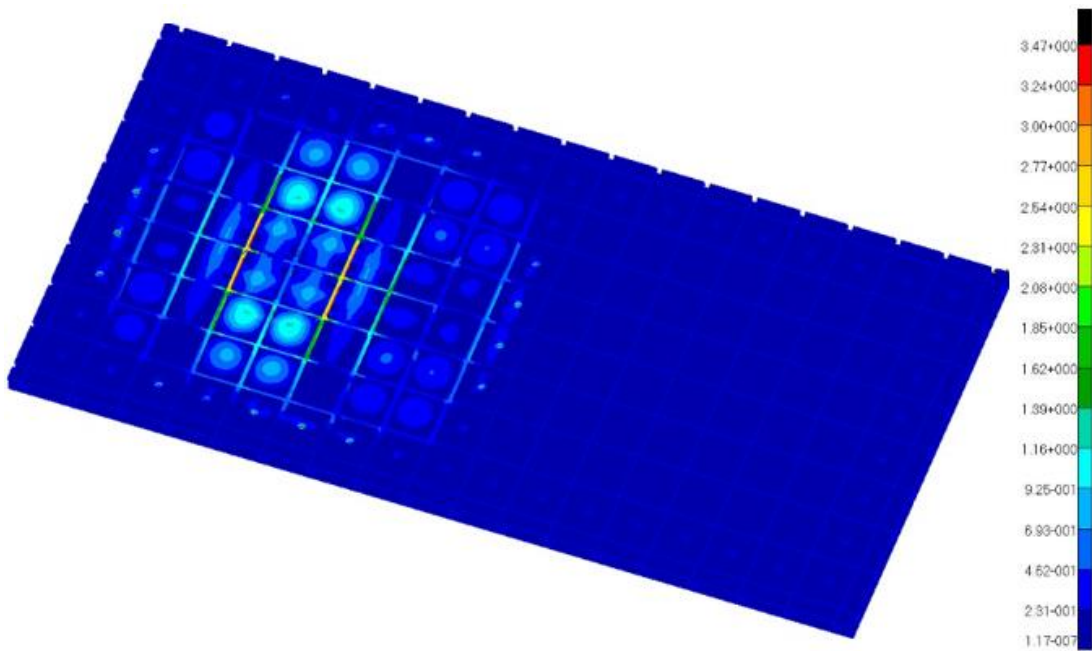


Figure 5.20. Von-Mises Stress Contours of Reaction Wall Plate [MPa]

Total displacement results for reaction wall weldment assembly taken from MSC NASTRAN can be seen in Figure 5.21. Maximum deformation value of 0.0584 mm occurs at upper box profile beam with 8140 N shear load and 18.09 kNm moment at the root. Maximum Von-Mises stress results for the reaction wall weldment assembly occurs at bolt holes used to mount assembly to the ground with loading 8140 N and 18.09 kNm is shown in Figure 5.22. Detail view of maximum Von-Mises stress is found in Figure 5.23. Maximum Von-Mises stress value is 15.5 MPa giving an RF value of 22.3, which is much higher than our minimum reserve factor criterion.

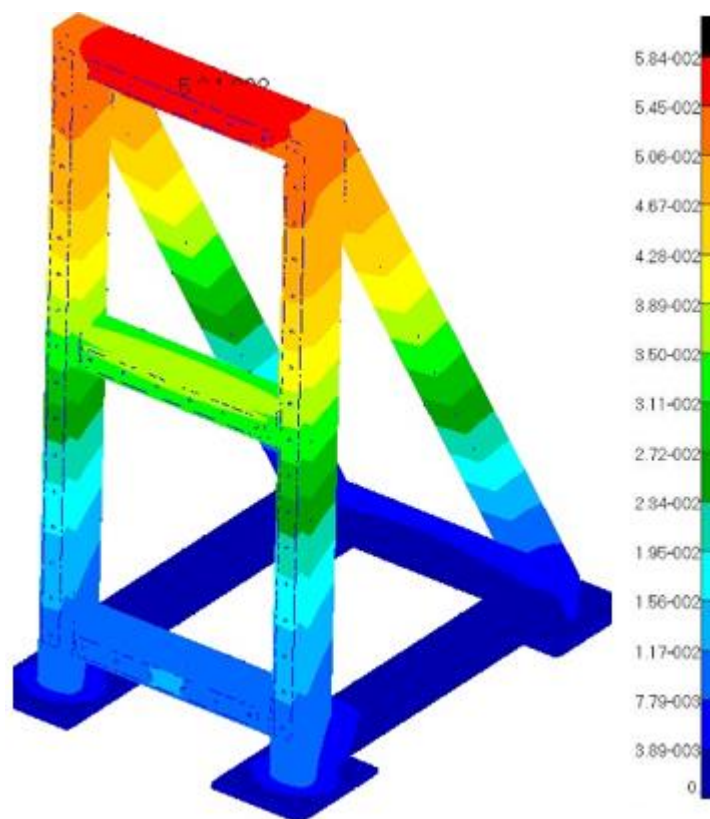


Figure 5.21. Displacement Contours of Reaction Wall Weldment Assembly [mm]

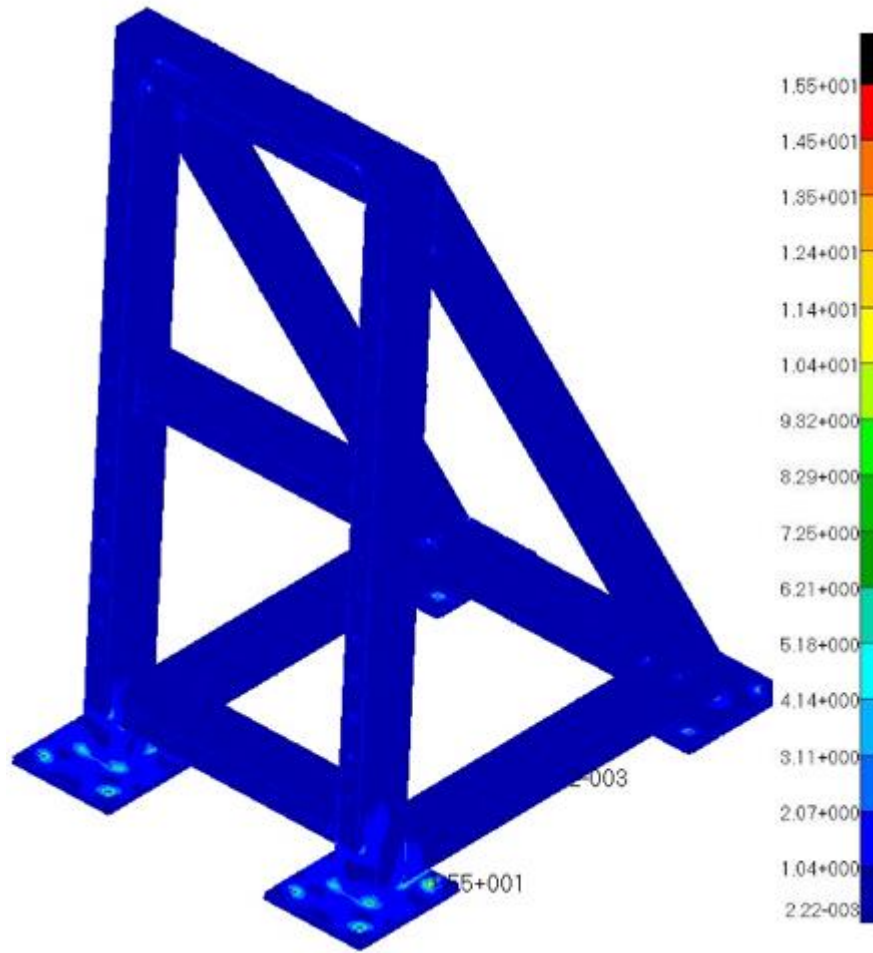


Figure 5.22. Von-Mises Stress Contours of Reaction Wall Weldment Assembly [MPa]

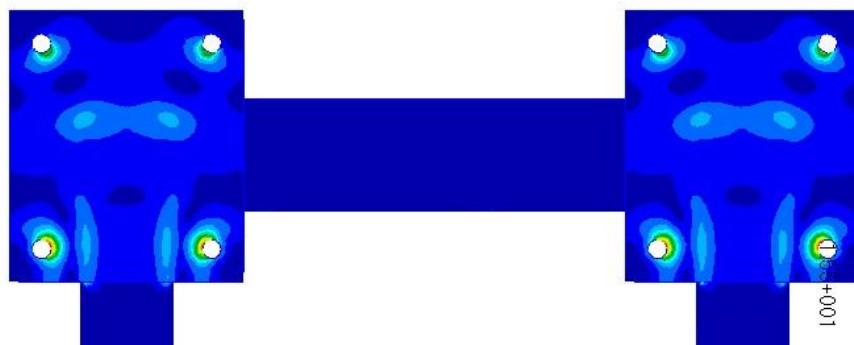


Figure 5.23. Detail View of Von-Mises Stress of Reaction Wall Weldment Assembly [MPa]

To investigate welding, which connects box profile beams to each other, finite element model of the reaction wall weldment assembly is cleared and only welded spots are kept. When these spots are evaluated, maximum Von-Mises stress is found to be 15.5 MPa which gives us RF value of 22.3. Von-Mises stress contours is shown in Figure 5.24.

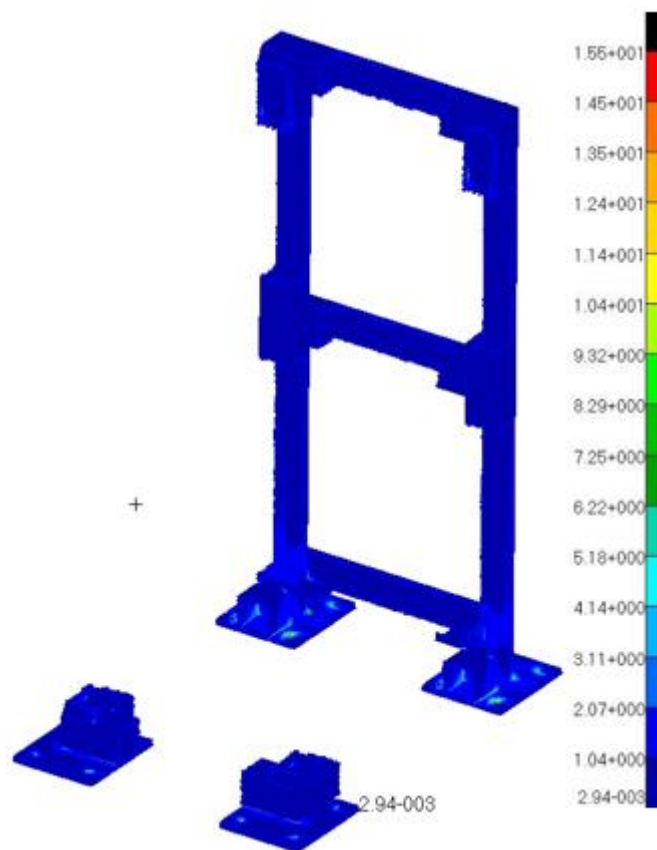


Figure 5.24. Von-Mises Stress Contours of Welding

Threaded rods used for connection between actuator – load cell and load cell – rod end is analyzed with hand calculation. M16 threaded rod is used and it has 60 mm length. Thread stripping analysis for the threaded rod is conducted as explained below.

First, the shear area for internal thread is calculated as follows [43],

$$A_n = \pi n L_e D_{s_{min}} \left(\frac{1}{2n} + 0.57735(D_{s_{min}} - E_{n_{max}}) \right) \quad (5-1)$$

where A_n is the shear area of the internal thread,

n is the number of threads per mm which is 0.5 mm,

L_e is fastener thread engagement which is 22 mm,

$D_{s_{min}}$ is minimum major diameter of external thread,

$E_{n_{max}}$ is maximum pitch diameter of internal thread.

According to Figure 5.25 and the equations given in (5-1), variables of this equation are calculated from,

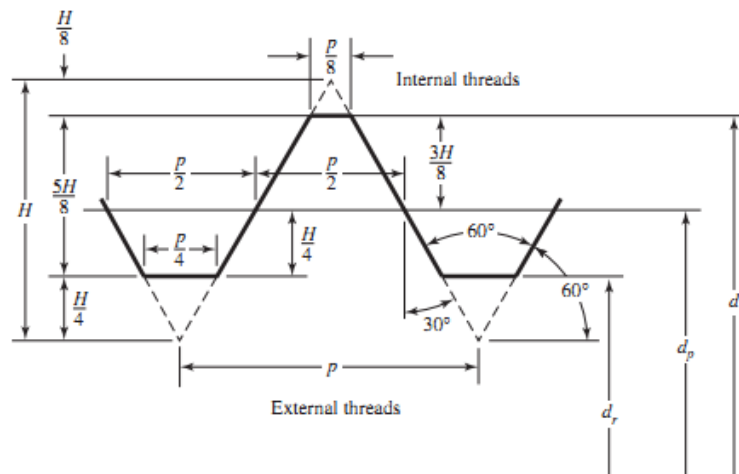


Figure 5.25. Basic Profile for Metric Thread [41]

$$D_{s_{min}} = d \quad (5-2)$$

$$E_{n_{max}} = d - 0.649519p \quad (5-3)$$

where d is the major diameter and p is the pitch which is 2 mm for M16.

In our calculation,

$$D_{s_{min}} = 16 \text{ mm} \quad (5-4)$$

$$E_{n_{max}} = 16 - 0.649519 \times 2 = 14.70 \text{ mm} \quad (5-5)$$

$$A_n = \pi(0,5)(22)(16) \left(\frac{1}{2(0,5)} + 0.57735(16 - 14.70) \right) = 967.12 \text{ mm}^2 \quad (5-6)$$

$$\tau_{int} = \frac{F}{A_s} = \frac{4492}{967.12} = 4.64 \text{ MPa} \quad (5-7)$$

$$RF_{int} = \frac{F_{sy}}{\tau_{int}} = \frac{591.6}{4.64} = 127.5 \quad (5-8)$$

where F_{sy} is the shear yield strength of the threaded stud, 591.6 MPa. It is found that threaded rod has much higher RF value than our minimum reserve factor criterion.

Clevis strength analysis is carried out according to [42] by using yield strength values of the materials to eliminate the effects of the plastic deformation on the test results,

and this analysis explained in detail below. General basic dimensions of clevis is given in Figure 5.26.

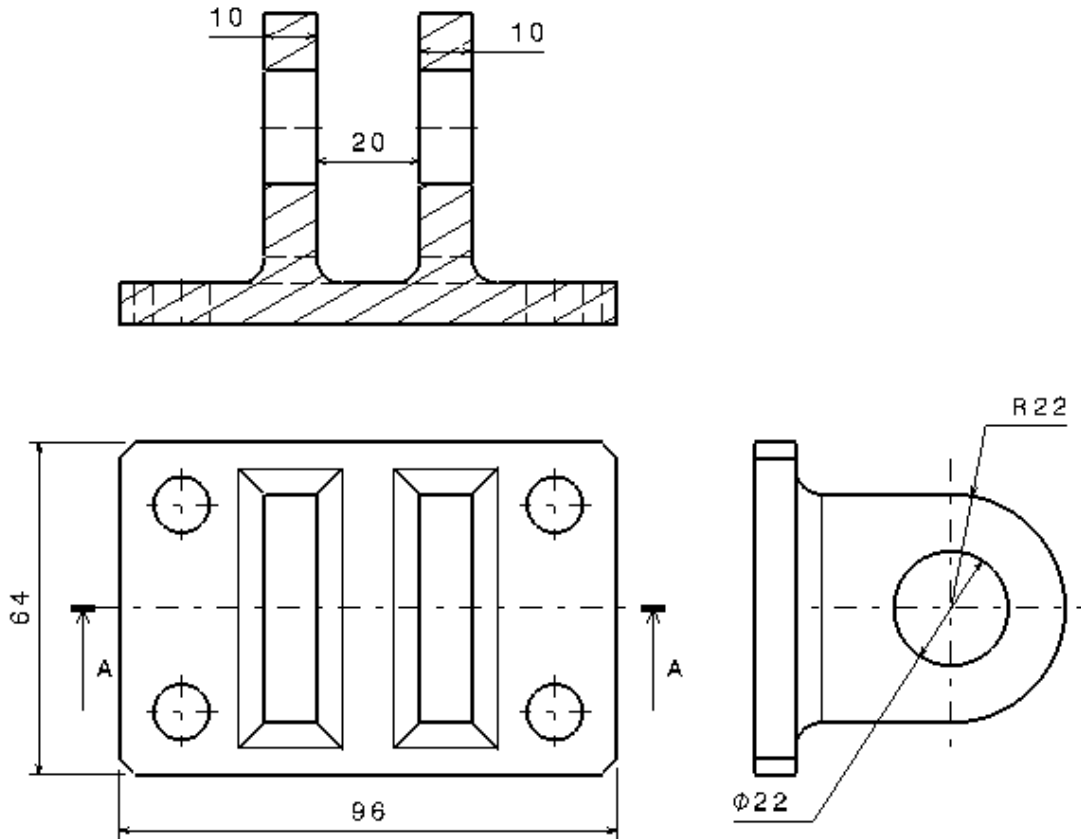


Figure 5.26. General Basic Dimensions of the Clevis

First, the shear-bearing failure analysis is performed by the equation of

$$P_{bru} = k_{br} F_{tux} A_{br} \quad (5-9)$$

where F_{tux} is the ultimate tensile stress in x-direction,

A_{br} is projected bearing area,

and k_{br} is the shear bearing efficiency factor from Figure 5.27.

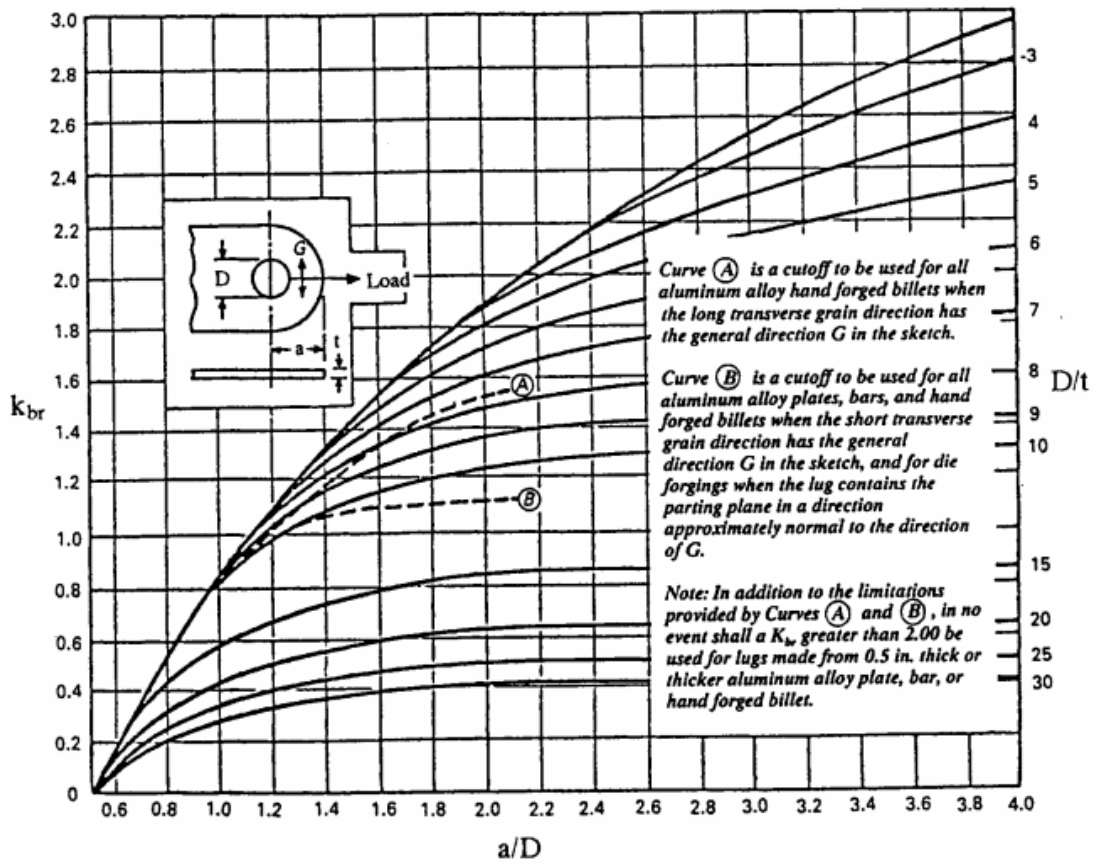


Figure 5.27. Shear-Bearing Efficiency Factor [42]

To define k_{br} value, a/D and D/t ratios are calculated,

$$\frac{a}{D} = \frac{22}{22} = 1 \quad (5-10)$$

$$\frac{D}{t} = \frac{22}{10} = 2.20 \quad (5-11)$$

According to a/D and D/t ratios, k_{br} is found from Figure 5.27 as 1.

Projected bearing area is calculated as,

$$A_{br} = Dt = 20 \times 10 = 220 \text{ mm}^2 \quad (5-12)$$

Then,

$$P_{bru} = (1)(986)(220) = 216.920 \text{ N} \quad (5-13)$$

$$RF_{bru} = \frac{P_{bru}}{\lambda F} = \frac{216920}{1.15(4492)} = 41.99 \quad (5-14)$$

where λ is fitting factor, taken as 1.15 according to [42] and F is the applied force. Shear bearing failure analysis gives us RF value of 41.99 which is much higher than our minimum RF value criterion.

Tension failure analysis of the clevis is also done according to [42],

$$P_{tu} = k_t F_{tux} A_t \quad (5-15)$$

where F_{tux} is the ultimate tensile stress in x-direction,

A_t is minimum net section area for tension,

k_t is net tension efficiency factor from Figure 5.28.

To define k_t value, W/D ratio is calculated as,

$$\frac{W}{D} = \frac{44}{22} = 2 \quad (5-16)$$

According to W/D ratio, k_t is found from Figure 5.28 as 0.969.

Minimum net section area for tension is calculated as,

$$A_t = (W - D)t = (44 - 22)10 = 220 \text{ mm}^2 \quad (5-17)$$

Then,

$$P_{tu} = (0.969)(986)(220) = 210195.48 \text{ N} \quad (5-18)$$

$$RF_{tu} = \frac{P_{tu}}{\lambda F} = \frac{210195.48}{1.15(4492)} = 40.69 \quad (5-19)$$

where λ is fitting factor, taken as 1.15 according to [42], and F is the applied force.

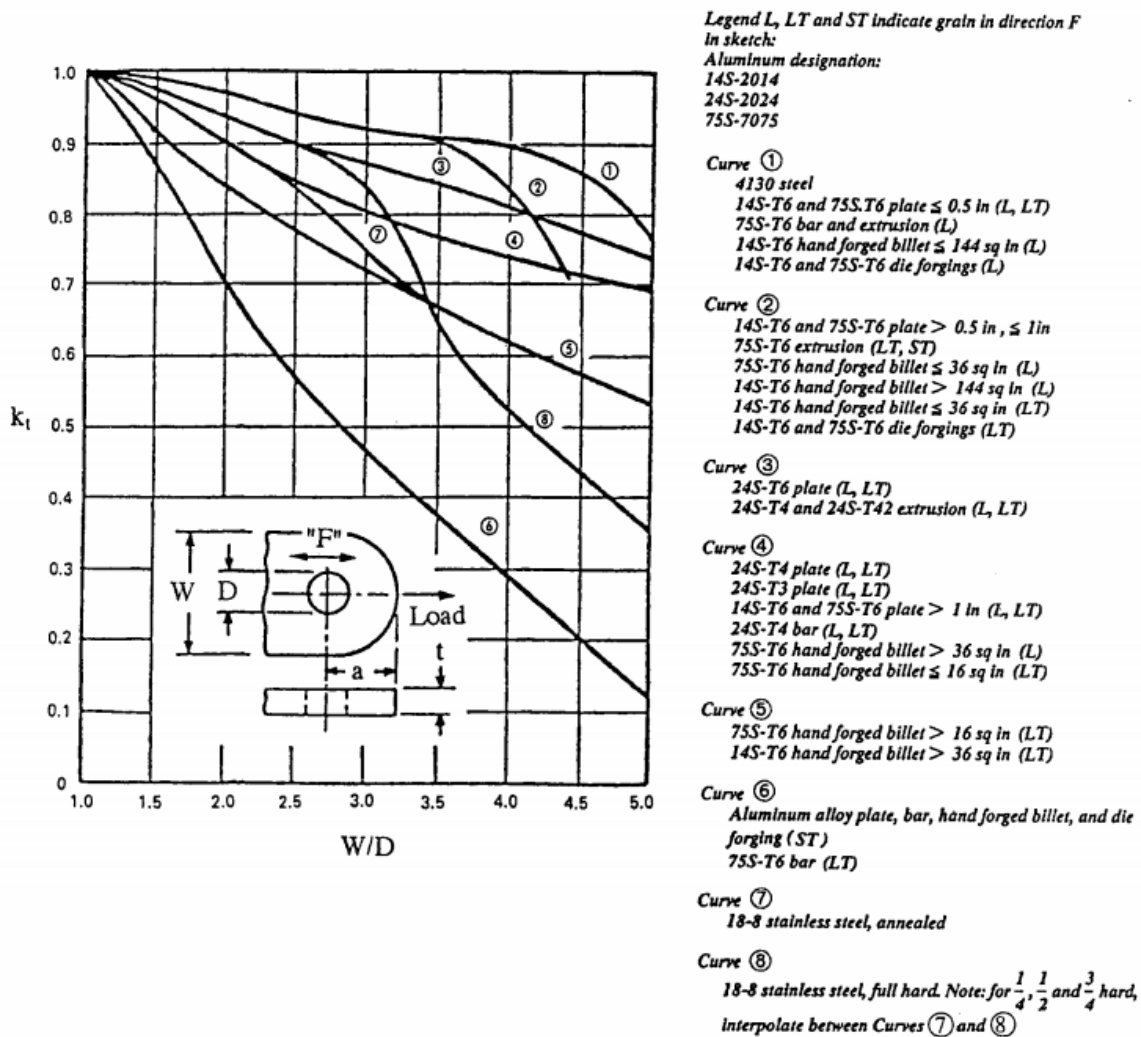


Figure 5.28. Lug Efficiency Factor for Tension [42]

Yield bushing failure analysis is performed according to [42]. Since the appropriate compression yield strength value for clevis could not found, compression yield strength value of the lug material is assumed equal to the tensile yield strength value of the lug material. Yield bushing failure analysis of the clevis is conducted by,

$$P_{bry} = 1.85F_{cy}A_{brb} \quad (5-20)$$

where P_{bry} is bushing yield bearing load,

F_{cy} is compression yield stress of bushing material, 986 MPa,

and A_{brb} is the smaller of the bearing areas of bushing on pin or bushing on lug.

Bearing area of bushing on pin is calculated as follows,

$$A_{brb} = D_p t \quad (5-21)$$

where D_p is diameter of the pin and t is the thickness of clevis.

$$A_{brb} = 17 \times 13 = 221 \text{ mm}^2 \quad (5-22)$$

Then,

$$P_{bry} = 1.85(986)221 = 403126,1 \text{ N} \quad (5-23)$$

$$RF_{bry} = \frac{P_{bry}}{\lambda F} = \frac{403126,1}{(1.15)4492} = 78.04 \quad (5-24)$$

Tensile strength of the surface of the clevis where we provide connection to the saddles is also performed by using the simple stress equation as explained below,

$$\sigma = \frac{F}{A_t} = \frac{F}{Wt - 4\pi r^2} \quad (5-25)$$

where F is the applied force,

A_t is minimum net section area for tension,

W is the width of the clevis,

t is the thickness of the clevis,

r is the radius of the threaded stud hole.

$$\sigma = \frac{4492}{96 \times 64 - \pi(10,7)^2} = 0.78 \text{ MPa} \quad (5-26)$$

$$RF = \frac{F_{tux}}{\sigma} = \frac{986}{0,78} = 1264 \quad (5-27)$$

As seen from the above results, clevis has much higher RF value than our minimum RF criterion to perform the test.

Pin strength analyses are also performed according to [42] and the details of it are expressed below.

Pin shear-off failure analyses are done for clevis in double shear by equation of,

$$P_{p,s} = 2F_{su} \left(\frac{\pi D^2}{4} \right) \quad (5-28)$$

where F_{su} is yield shear strength of the pin material, 810 MPa and D is the diameter of pin. The calculation of this equation is given as,

$$P_{p,s} = 2(810) \left(\frac{\pi 17^2}{4} \right) = 367707.71 \text{ N} \quad (5-29)$$

$$RF_{p,s} = \frac{P_{p,s}}{\lambda F} = \frac{367707.71}{(1.15)4492} = 71 \quad (5-30)$$

Pin shear of failure analysis gives us RF value of 71 and this value is much higher than our RF value criterion.

Pin bending failure analysis is calculated as,

$$M = \frac{P}{2}b \quad (5-31)$$

where M is the applied bending moment on the pin,

P is the applied load, and b is the moment arm.

The moment arm is calculated according to below formulation and Figure 5.29 taken from [44]. This arm calculation is defined as,

$$b = \frac{t_1}{2} + \frac{t_2}{4} + g = \frac{10}{2} + \frac{14}{4} + 3 = 11.5 \text{ mm} \quad (5-32)$$

Then, the moment is calculated as,

$$M = \frac{4492}{2}(11,5) = 25829 \text{ Nmm} \quad (5-33)$$

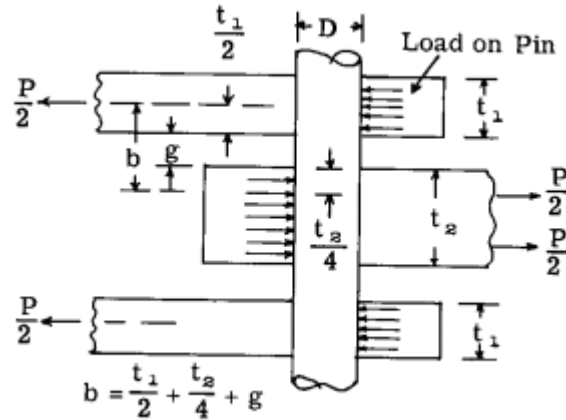


Figure 5.29. Pin Moment Arm for Determination of Bending Moment [44]

RF calculation of pin bending analysis is expressed as,

$$RF_{pb} = \frac{F_{ty}}{\frac{\lambda M \frac{D}{2}}{I_{pin}}} \quad (5-34)$$

where I_{pin} is inertia of pin, which is $\frac{\pi D^4}{64}$. Then RF value of pin bending is found to be

$$RF_{pb} = \frac{1350}{\frac{1.15(25829) \frac{17}{2}}{\frac{\pi(17)^4}{64}}} = 21.92 \quad (5-35)$$

As seen from the above results, pin strength is sufficient to perform the test.

For the fastener analysis, bolt loads are taken from the FE results and maximum bolt loads are given in Table 5.3. Detailed bolt loads are tabulated in Appendix.

Table 5.3. Reaction Wall Assembly Maximum M16 Bolt Loads

Bolt Type	Max Axial Load [N]	Max Radial Load [N]	Preload [N]
M16	399.69	669.78	103088

In a bolted joint, shear force is taken by clamping friction caused by bolt preload [41]. So, if the radial force is lower than the friction force between connecting surfaces, bolts will carry the axial forces only. To check this phenomenon, friction coefficient is taken as 0.2, which is steel-steel with a thick oxide layer friction coefficient. Initial preload value of the M16 bolts with grade 12.9 is shown in Table 5.3. In the light of these variables, friction force is calculated as 20853.2 N. As seen from the Table 5.3, radial force value is lower than the friction value. Therefore, the motion of the bolt in this direction is prevented. So, according to maximum bolt load tabulated, bolts are only checked for their tensile strength due to lower shear loads with respect to the clamping friction force values.

For tensile failure check of the bolts used in the support structure, formulation used in [41] is used. The formula is given as,

$$RF_{tensile} = \frac{F_{ty}A_t - P_i}{CP_{tensile}} \quad (5-36)$$

where F_{ty} is tensile yield strength of the bolt material,

A_t is the tensile load carrying area,

P_i is the initial preload,

C is the stiffness constant of the joint,

$P_{tensile}$ is the applied tensile loading.

Stiffness constant of the joint is calculated from,

$$C = \frac{k_b}{k_b + k_m} \quad (5-37)$$

$$k_b = \frac{(\pi D_{bolt}^2/4)E_{bolt}}{l_d} \quad (5-38)$$

$$k_m = \frac{0.5774\pi E_m d}{2 \ln \left(5 \frac{0.5774l_m + 0.5d}{0.5774l_m + 2.5d} \right)} \quad (5-39)$$

where k_b is the estimated effective stiffness of the bolt,

k_m is the stiffness of the members in the clamped zone,

D_{bolt} is the major-diameter area of fastener,

E_{bolt} is the Young's modulus of bolt,

l_d is length of unthread portion of the grip,

E_m is the Young's modulus of members,

d is the diameter of the bolt,

l_m is total thickness of the connected members.

Calculation details of stiffness constant of the joints of the support structure are found in Table 5.4.

Table 5.4. *Stiffness Constant Calculation Details of Bolts on Support Structure*

Bolt Type	D_{bolt} [mm]	E_{bolt} [MPa]	l_d [mm]	k_b	E_m [MPa]	d [mm]	l_m [mm]	k_m	C
M16	16	205000	30	1177648.45	211000	16	90	2590933.82	0.31

Calculated results and variables of failure check of the M16 bolt on the support structure according to above formulation are tabulated in Table 5.5.

Table 5.5. *Results and Variables of Failure Check of the Bolts on Support Structure*

Bolt Type	F_{ty}[MPa]	A_t [mm²]	RF_{tensile}
M16	940	201.06	697.9

As seen from Table 5.5, RF results of the bolts on the support structure are much higher than our minimum RF value criterion.

For Hilti anchor analysis, 8.8 grade allowable data given in Table 5.1 is used. Anchor loads for the ground plate and the reaction wall assembly are taken from the FE results. All anchor loads are tabulated in Appendix B and C, and maximum bolt load is given in Table 5.6. Based on torque calculation with tightened 50% yield strength value of HAS-U 8.8 anchor, preload is obtained 179388 N [41].

Table 5.6. *M30 Hilti HAS-U 8.8 Maximum Anchor Loads*

Bolt Type	Max Axial Load [N]	Max Radial Load [N]	Preload [N]
M30 Hilti Anchor with grade 8.8	2689.9	1127.3	179388

For these anchors, same calculations performed for M16 bolts are conducted. Friction coefficient is taken as 0.2 to be more conservative. Initial preload value of the M30 grade 8.8 anchors can be found in Table 5.6. In the light of these variables, friction force is calculated as 35877.6 N. As seen from the Table 5.6, radial force value is lower than the friction values. Therefore, the motion of the bolt in this direction is prevented. So, according to bolt load tabulated, bolts are only checked for their tensile strength. Hilti anchor tensile yield strength is given as 640 MPa. Maximum tensile stress of the anchor is calculated with the maximum axial load, and this calculation gives us a minimum RF value of 168.42. As seen from this RF value result, anchors are much higher RF value than our minimum RF value criterion.

The rod end used in test rig is chosen from the INA FAG catalog. Its radial static load rating is stated as 56500 N. According to this value, RF value of the rod end for static testing is found to be 12.57. This RF value is higher than our minimum RF value criterion and sufficient to perform testing.

5.6.1. Reserve Factor Summary

All detail parts used in test rig are analyzed and reserve factor summary of these parts are tabulated in Table 5.7. It is shown that all detail parts used in test rig have satisfying RF values to perform testing.

Table 5.7. Reserve Factor Summary

Part Name	Material	RF Value
Actuator Circular Plate	St52-3	262
Ground Plate	AISI 4140	44.7
Tip Saddle Lower Part	Al2024 T351	369
Root Saddle Lower Part	Al2024 T351	142
Dummy Hub	AISI 4140	215

Reaction Wall's Plate	St52-3	99.4
Reaction Wall's Weldment Assy	St52-3	22.3
Welding	E60xx	22.3
Clevis	AISI 4140	40.69
Pin	TOOLOX44	21.92
Bushing	AISI 4140	78.04
Threaded Rod	AISI 4140	127.5
Rod End	Standard	12.57
M16 Bolts	Grade 12.9	697.9
Hilti HAS-U 8.8 M30	Grade 8.8	168.42

5.7. Fatigue Analysis

In order to show that the test rig can perform fatigue tests, detail parts used in the test rig shall endure more than 10^7 cycles. If maximum Von-Mises stress values of detail parts are lower than endurance strength of materials, detail parts endure more than 10^7 cycles. For the calculation of endurance limit of materials, endurance strength values of materials are calculated as [41],

$$S'_e = \begin{cases} 0.5S_{ut} & S_{ut} \leq 200 \text{ kpsi} (1400 \text{ MPa}) \\ 100 \text{ kpsi} & S_{ut} > 200 \text{ kpsi} \\ 700 \text{ MPa} & S_{ut} > 1400 \text{ MPa} \end{cases} \quad (5-40)$$

According to these formula, endurance strength of materials are calculated and tabulated in Table 5.8. Scatter factor is chosen as 3.3 for these materials [45].

Table 5.8. *Endurance Strength*

Material	<i>Yield Strength [MPa]</i>	<i>Endurance Strength without Scatter Factor [MPa]</i>	<i>Endurance Strength with Scatter Factor [MPa]</i>
AISI 4140	986	493	149.4
St52-3	345	172.5	52.3
Al2024-T351	469	234.5	71
E60xx	345	172.5	52.3
TOOLOX44	1350	675	204.5
Carbon Steel Grade 12.9	1100	550	166.7
Carbon Steel Grade 8.8	640	320	97

Maximum Von-Mises stress of detail parts are calculated in 5.6. When these stress are compared to endurance strength values given in Table 5.8, it is seen that all detail parts endure more than 10^7 cycles.

CHAPTER 6

CONCLUSION

6.1. Summaries and Conclusion

In this thesis, testing fixture is designed that can be used for wind turbine blades from 5 to 9 meters. The testing includes static testing and can be extended for failure and fatigue testing. The RÜZGEM 5 m experimental wind turbine blade designed for METUWIND is tested in this testing fixture. Different test methods for wind turbine blade are mentioned. RÜZGEM Blade to be tested is used to define required load and boundary conditions.

Design of test setup is summarized below:

- Blade loads and boundary conditions (input)
- Deciding test methods (uni-axial, bi-axial etc.)
- Load Calculation
 - o Converting design loads (distributed loads) to concentrated loads
 - o Deciding saddle points and corresponding loads
- Design
 - o Conceptual design
 - o 3D detailed design
 - Dummy hub design
 - Load introduction design
 - Selection of hydraulic actuators, determination of stroke length
 - Selection of load cell
 - Support structure design
- Determination of hydraulic equipment and data acquisition system
- Analysis

- Structural analysis of test fixture
- Cost analysis

Static test is to be carried out as a first step according to this document. Design loads of the blade are summarized and according to these design loads, 2 approaches for static test are compared by using Excel Solver Tool. In this solver, design loads defined in 28 sections are optimized in order to apply these loads in multiple points method – 2 saddle point. In this calculation, saddle point locations and corresponding loads are found.

With these loads and knowledge of boundary conditions, test rig design is carried out. Firstly, load introduction adapters and dummy hub that simulates the root connection of the blade are designed. After that, a load cell and a hydraulic actuator requirement are determined and supplier investigation are conducted. A model of the load cell and the hydraulic actuator decided are inserted to the test rig. By taking into account this static testing and further tests, a support structure which contains the reaction wall and the ground support plate design is performed. In analysis chapter, designed detail parts are analyzed and it is shown that all of detail parts are met requirements. Finally, the cost of test infrastructure to be planned to establish are summarized and estimated total cost are given.

6.2. Future Work

After this study, procurement procedure can be carried out. Test infrastructure equipment can be searched and provided. After manufacturing test rig detail parts, assembly of test setup can start. During assembling, instrumentation of specimen can be performed. In instrumentation process, data measurement system like strain gages are applied and during the testing, linear variable displacement transducers can be used to measure displacement of the blade at any desired region. Also, new measurement techniques can also be tried on this specimen. Having completing assembling, testing process will start with commissioning.

REFERENCES

- [1] J. Manwell, *Wind Energy Explained, Theory Design and Application*, John Wiley & Son, 2010.
- [2] Hahn, B., Durstewitz, M., & Rohrig, K., Reliability of Wind Turbines. In J. Peinke, P. Schaumann, & S. Barth (Eds.), *Wind Energy* (pp. 329–332). Berlin, Heidelberg: Springer Berlin Heidelberg, 2002.
- [3] White, D., *New Method for Dual-Axis Fatigue Testing of Large Wind Turbine Blades Using Resonance Excitation and Spectral Loading*. 10.2172/15007390, 2004.
- [4] Malhotra, P., *Advanced Blade Testing Methods for Wind Turbines*. MS Thesis. University of Massachusetts, Amherst, MA, 2010.
- [5] Lyu, P., *How Do I Compute Lift and Drag?* Retrieved from <https://www.comsol.com/blogs/how-do-i-compute-lift-and-drag/> on July 08, 2019.
- [6] Busmann, H., Kensche, C., Bürkner, F., Sayer, F., & Wiemann, K., *Testing of Rotor Blades*, vol. 30, pp. 5–9, 2007.
- [7] British Standard, *Wind Turbines – Part 22: Conformity Testing and Certification*, IEC 61400-22. Geneva, Switzerland: IEC, 2010.
- [8] British Standard, *Wind Turbines – Part 23: Full-Scale Structural Testing of Rotor Blades*, IEC 61400-23. Geneva, Switzerland: IEC, 2001.
- [9] The National Renewable Energy Laboratory. Retrieved from <https://www.nrel.gov/> on June 21, 2018.

- [10] The Centre for Renewable Energy Sources and Saving. Retrieved from http://www.cres.gr/kape/index_eng.htm on June 21, 2018.
- [11] TU Delft Wind Energy. Retrieved from <https://www.tudelft.nl/lr/organisatie/afdelingen/aerodynamics-wind-energy-flight-performance-and-propulsion/windenergy> on June 21, 2018.
- [12] Technical University of Denmark, Retrieved from <https://www.dtu.dk/english/about> on June 21, 2018.
- [13] Wingerde, A.M., Sayer, F., Putnam, E. “Subcomponent Testing of Rotor Blades.” *Proceedings of the Conference of Wind Energy Science and Technology*, RUZGEM 2013, Ankara, Turkey, 3-4 October 2013.
- [14] Kensche, C. W., Fatigue of composites for wind turbines. *International Journal of Fatigue*, 28 (10 SPEC. ISS.), 1363–1374. <https://doi.org/10.1016/j.ijfatigue.2006.02.040>, 2006.
- [15] P. Malhotra, R.W. Hyers, J.F. Manwell, J.G. McGowan, *A review and design study of blade testing systems for utility-scale wind turbines*, Renewable and Sustainable Energy Reviews, Volume 16, Issue 1, Pages 284-292, 2012.
- [16] Valyou, D. N., Arsenault, T. J., Janoyan, K., Marzocca, P., Post, N., Grappasonni, C., Probst, O. *Development and Commissioning of a Small/Mid-Size Wind Turbine Test Facility*, 2015.
- [17] Blade Test Facility, Clarkson University. Retrieved from <https://www.clarkson.edu/btf> on August 8, 2019
- [18] Burkner, F., van Wingerde, A. M., & Busmann, H. G. Testing of rotor blades of wind turbines. In *DEWEK 2008 Ninth German Wind Energy Conference—Book of Abstracts*, p. 75, 2008.
- [19] Bürkner, F., & Wingerde, A. V. *Testing of Rotor Blades*. 8th International Conference on Structural Dynamics, 2011.

- [20] Sundaresan, M. J., Schulz, M. J., & Ghoshal, A. *Structural Health Monitoring Static Test Of A Wind Turbine Blade Subcontract Report NREL*. SR-500-28719. Colorado. 2002.
- [21] Yang, J., Peng, C., Xiao, J., Zeng, J., Xing, S., Jin, J., Deng, H. Structural Investigation Of Composite Wind Turbine Blade Considering Structural Collapse In Full-Scale Static Tests, *Composite Structures*, Volume 97, pp. 15-29, ISSN 0263-8223. 2013.
- [22] Yeniceli, S. C., *Design Optimization of Whiffletree Systems for Wind Turbine*, MS Thesis. Middle East Technical University, Ankara, Turkey, 2014.
- [23] Yeniceli, S. C., Kayran, A., "Design optimization of a whiffletree system for static testing of a wind turbine blade", *Conference on Wind Energy Science and Technology RUZGEM 2013*, Ankara, Turkey, 2013.
- [24] Limon, A.U., Ulu, Y., Çöker, D., *Döner Kiriş Benzeri Havacılık Yapılarının Yapısal Testi İçin Eyleyici Yükü Hesaplama Algoritması ve Çok Eksenli Test ile Doğrulanması*, Ulusal Havacılık ve Uzay Konferansı, Kocaeli, Turkey, 2016.
- [25] Limon, A.U., Ulu, Y., Çöker, D., *Actuator Load Calculation Algorithm for a Multiaxial Test System of a Rotating Beam like Aerostructure*. Asian-Australian Rotorcraft Forum, Jeju Island, Korea, 2018.
- [26] Limon, A.U., *Actuator Load Calculation Tool For A Multiaxial Test System Of A Rotating Beam Like Aerostructure*, MS Thesis, Middle East Technical University, Ankara, Turkey, 2018.
- [27] MTS Systems Corporation. Wind Turbine Blade Testing Solutions. In MTS Systems Corporation. Retrieved from http://www.mts.com/cs/groups/public/documents/library/dev_005130.pdf on May 05, 2017.

- [28] Pechlivanoglou, G., Weinzierl, G. *Aerodynamic and Aeroelastic Design Report of METUWIND Small Rotor Blade*, SmartBlade GmbH, unpublished, 2013.
- [29] T. P. Philippidis and G. A. Roukis, "*Structure Design Report of METUWIND Small Rotor Blade*," Confidential Interim Report, unpublished, 2013.
- [30] Ozyildiz, M. *Finite Element Modelling of a Composite Wind Turbine Blade with Fully-Bonded and Partically Unbonded Trailing Edge*. MS Thesis. Middle East Technical University, Ankara, Turkey. 2018.
- [31] Beer, Ferdinand P. *Mechanics of Materials*. New York: McGraw-Hill Higher Education, 2009.
- [32] INA FAG GIR17-UK. Retrieved from https://medias.schaeffler.com/medias/en!hp.ec.br.pr/GIR..-UK*GIR17-UK on December 14, 2018.
- [33] Interface Force Measurement System Inc. 1000 Fatigue Rated Load Cell. Scottsdale, USA. Retrieved from <https://www.interfaceforce.com/products/load-cells/1000-high-capacity-fatigue-rated-low-profile-load-cell/> on December 15, 2018.
- [34] RotaTeknik Test Ekipmanları Katalogu, RotaTeknik Inc., 2019.
- [35] T-Slot Dimensions According to DIN650. Retrieved from <https://www.fabchipcnc.com/floor-plates-new> on January 22, 2019.
- [36] DIN 508 T-Nuts. Retrieved from <https://www.elesa.com/en/elesab2bstoreoc/Machine-elements--T-Nuts--DIN508> on January 24, 2019.
- [37] Photo of Hilti HAS-U 8.8. Retrieved from https://www.hilti.com.tr/c/CLS_FASTENER_7135/CLS_ANCHOR_RODS_ELEMENTS-7135/r9864251 on February 14, 2019.

- [38] European Technical Assessment ETA-11/0493, Hilti Hit Hy-200 A, Injection Mortar, 2019.
- [39] ASM International Handbook Committee. *ASM Handbook*. 2nd Edition, Nondestructive Evaluation and Quality Control. Metals Park, Ohio. ASM International, 1989.
- [40] Material Allowable Data. Retrieved from <http://www.matweb.com> Online Materials Database, on March 21, 2019.
- [41] Shigley, J.E., Mischke, C.R. *Mechanical Engineering Design*. 5th ed. Blacklick, OH: McGraw-Hill College, 1989.
- [42] Niu, C. *Airframe Stress Analysis and Sizing*. Conmilit Press; Technical Book Co., 2011.
- [43] Federal Standard. FED-STD-H28A. *Screw-Thread Standards for Federal Services*. 1994.
- [44] Bruhn, E.F. *Analysis and Design of Flight Vehicle Structures*. Cincinnati, OH: Tri-State Offset Company, 1973.
- [45] Limon, A.U., *Personal Communication*, August 13, 2019.

APPENDIX

A. Extreme Loads Including Safety Factor

Extreme loads at blade radius $R = 0.00\text{m}$

	LC_{index}	γ_F	F_x [kN]	F_y [kN]	F_z [kN]	F_{res} [kN]	M_x [kNm]	M_y [kNm]	M_z [kNm]	M_{res} [kNm]
$F_{x,min}$	1	1.35	-7.25	0.72	-1.31	7.29	-1.23	-16.88	-0.13	16.88
$F_{x,max}$	2	1.35	8.14	-1.07	-1.30	8.21	1.69	18.09	-0.18	18.09
$F_{y,min}$	3	1.35	0.86	-5.32	-0.33	5.39	12.08	1.85	0.02	12.22
$F_{y,max}$	4	1.35	-6.76	2.44	-1.17	7.18	-4.04	-15.26	-0.17	15.79
$F_{z,min}$	2	1.35	7.99	-1.06	-1.31	8.06	1.67	17.82	-0.18	17.96
$F_{z,max}$	5	1.35	0.59	-1.21	27.00	1.35	2.82	1.98	-0.02	3.46
$F_{res,max}$	2	1.35	8.14	-1.07	-1.30	8.21	1.69	18.09	-0.19	18.09
$M_{x,min}$	4	1.35	-6.76	2.44	-1.17	7.18	-4.04	-15.26	-0.17	15.79
$M_{x,max}$	3	1.35	0.86	-5.32	-0.33	5.39	12.08	1.85	0.02	12.22
$M_{y,min}$	1	1.35	-7.25	0.72	-1.31	7.29	-1.23	-16.88	-0.13	16.88
$M_{y,max}$	2	1.35	8.14	-1.07	-1.29	8.21	1.69	18.09	-0.18	18.09
$M_{z,min}$	7	1.35	5.56	-1.69	10.98	5.82	4.87	15.79	-0.35	16.47
$M_{z,max}$	8	1.35	-0.24	-5.01	-0.28	5.02	11.54	-0.62	0.08	11.57
$M_{res,max}$	2	1.35	8.13	-1.07	-1.30	8.21	1.69	18.09	-0.19	18.09

Extreme loads at blade radius $R = 0.10\text{m}$

	LC_{index}	γ_F	F_x [kN]	F_y [kN]	F_z [kN]	F_{res} [kN]	M_x [kNm]	M_y [kNm]	M_z [kNm]	M_{res} [kNm]
$F_{x,min}$	1	1.35	-7.14	0.72	-1.25	7.18	-1.16	-16.19	-0.12	16.21
$F_{x,max}$	2	1.35	8.03	-1.06	-1.24	8.09	1.57	17.24	-0.18	17.36
$F_{y,min}$	3	1.35	0.86	-5.19	-0.31	5.27	11.56	1.77	0.02	11.70
$F_{y,max}$	4	1.35	-6.69	2.37	-1.12	7.09	-3.81	-14.60	-0.16	15.12
$F_{z,min}$	2	1.35	7.89	-1.06	-1.25	7.95	1.57	16.97	-0.18	17.11
$F_{z,max}$	5	1.35	0.61	-1.19	26.60	1.34	2.70	1.92	-0.02	3.31
$F_{res,max}$	2	1.35	8.03	-1.06	-1.24	8.09	1.59	17.24	-0.18	17.36
$M_{x,min}$	4	1.35	-6.69	2.37	-1.12	7.09	-3.81	-14.60	-0.16	15.12
$M_{x,max}$	3	1.35	0.86	-5.19	-0.31	5.27	11.56	1.77	0.02	11.70
$M_{y,min}$	1	1.35	-7.14	0.72	-1.25	7.18	-1.16	-16.19	-0.12	16.21
$M_{y,max}$	2	1.35	8.02	-1.06	-1.24	8.09	1.57	17.24	-0.18	17.36
$M_{z,min}$	7	1.35	5.55	-1.69	10.82	5.80	4.71	15.22	-0.34	15.87
$M_{z,max}$	8	1.35	-0.24	-4.89	-0.27	4.90	11.07	-0.59	0.08	11.08
$M_{res,max}$	2	1.35	8.02	-1.06	-1.24	8.09	1.59	17.24	-0.18	17.36

Extreme loads at blade radius $R = 0.20\text{m}$

	LC_{index}	γF	F_x [kN]	F_y [kN]	F_z [kN]	F_{res} [kN]	M_x [kNm]	M_y [kNm]	M_z [kNm]	M_{res} [kNm]
$F_{x,min}$	1	1.35	-7.02	0.71	-1.21	7.06	-1.09	-15.45	-0.12	15.51
$F_{x,max}$	2	1.35	7.90	-1.06	-1.20	7.97	1.47	16.47	-0.18	16.55
$F_{y,min}$	3	1.35	0.85	-5.09	-0.29	5.16	11.06	1.69	0.02	11.19
$F_{y,max}$	4	1.35	-6.61	2.28	-1.07	6.99	-3.58	-13.94	-0.16	14.41
$F_{z,min}$	2	1.35	7.77	-1.05	-1.21	7.84	1.47	16.20	-0.17	16.34
$F_{z,max}$	5	1.35	0.62	-1.18	26.14	1.33	2.59	1.86	-0.02	3.18
$F_{res,max}$	2	1.35	7.90	-1.06	-1.20	7.97	1.48	16.47	-0.18	16.55
$M_{x,min}$	4	1.35	-6.61	2.28	-1.07	6.99	-3.58	-13.94	-0.16	14.41
$M_{x,max}$	3	1.35	0.85	-5.09	-0.29	5.16	11.06	1.69	0.02	11.19
$M_{y,min}$	1	1.35	-7.02	0.71	-1.21	7.06	-1.09	-15.45	-0.12	15.51
$M_{y,max}$	2	1.35	7.89	-1.06	-1.19	7.97	1.47	16.47	-0.18	16.55
$M_{z,min}$	7	1.35	5.53	-1.70	10.66	5.78	4.54	14.68	-0.34	15.29
$M_{z,max}$	8	1.35	-0.23	-4.78	-0.25	4.79	10.59	-0.57	0.07	10.61
$M_{res,max}$	2	1.35	7.89	-1.06	-1.20	7.97	1.48	16.47	-0.18	16.55

Extreme loads at blade radius $R = 0.30\text{m}$

	LC_{index}	γF	F_x [kN]	F_y [kN]	F_z [kN]	F_{res} [kN]	M_x [kNm]	M_y [kNm]	M_z [kNm]	M_{res} [kNm]
$F_{x,min}$	1	1.35	-6.90	0.71	-1.16	6.93	-1.02	-14.72	-0.11	14.82
$F_{x,max}$	2	1.35	7.77	-1.05	-1.15	7.84	1.37	15.70	-0.17	15.74
$F_{y,min}$	3	1.35	0.85	-4.98	-0.27	5.05	10.55	1.60	0.02	10.68
$F_{y,max}$	4	1.35	-6.53	2.19	-1.03	6.88	-3.36	-13.27	-0.16	13.70
$F_{z,min}$	2	1.35	7.65	-1.04	-1.16	7.72	1.36	15.43	-0.17	15.57
$F_{z,max}$	5	1.35	0.63	-1.16	25.68	1.32	2.47	1.80	-0.02	3.05
$F_{res,max}$	2	1.35	7.77	-1.05	-1.15	7.84	1.37	15.70	-0.17	15.74
$M_{x,min}$	4	1.35	-6.53	2.19	-1.03	6.88	-3.36	-13.27	-0.16	13.70
$M_{x,max}$	3	1.35	0.85	-4.98	-0.27	5.05	10.55	1.60	0.02	10.68
$M_{y,min}$	1	1.35	-6.90	0.71	-1.16	6.93	-1.02	-14.72	-0.11	14.82
$M_{y,max}$	2	1.35	7.77	-1.05	-1.15	7.84	1.37	15.70	-0.17	15.74
$M_{z,min}$	7	1.35	5.51	-1.71	10.50	5.77	4.37	14.14	-0.33	14.71
$M_{z,max}$	8	1.35	-0.23	-4.68	-0.24	4.69	10.11	-0.55	0.07	10.13
$M_{res,max}$	2	1.35	7.77	-1.05	-1.15	7.84	1.37	15.70	-0.17	15.74

Extreme loads at blade radius $R = 0.40\text{m}$

	LC_{index}	γ_F	F_x [kN]	F_y [kN]	F_z [kN]	F_{res} [kN]	M_x [kNm]	M_y [kNm]	M_z [kNm]	M_{res} [kNm]
$F_{x,min}$	1	1.35	-6.78	0.70	-1.11	6.81	-0.95	-14.00	-0.11	14.13
$F_{x,max}$	2	1.35	7.64	-1.04	-1.11	7.71	1.26	14.93	-0.16	14.93
$F_{y,min}$	3	1.35	0.84	-4.88	-0.26	4.95	10.05	1.52	0.02	10.17
$F_{y,max}$	4	1.35	-6.44	2.10	-0.98	6.76	-3.13	-12.61	-0.15	13.00
$F_{z,min}$	2, 14	1.35	7.36	-1.02	-1.12	7.59	1.24	14.37	-0.16	14.80
$F_{z,max}$	5	1.35	0.65	-1.15	25.21	1.32	2.36	1.74	-0.02	2.92
$F_{res,max}$	2	1.35	7.64	-1.04	-1.11	7.71	1.27	14.93	-0.16	14.93
$M_{x,min}$	4	1.35	-6.44	2.10	-0.98	6.76	-3.13	-12.61	-0.15	13.00
$M_{x,max}$	3	1.35	0.84	-4.88	-0.26	4.95	10.05	1.52	0.02	10.17
$M_{y,min}$	1	1.35	-6.78	0.70	-1.11	6.81	-0.95	-14.00	-0.11	14.13
$M_{y,max}$	2	1.35	7.64	-1.04	-1.11	7.71	1.26	14.93	-0.16	14.93
$M_{z,min}$	7	1.35	5.49	-1.71	10.34	5.75	4.20	13.60	-0.33	14.14
$M_{z,max}$	8	1.35	-0.23	-4.57	-0.22	4.58	9.64	-0.52	0.07	9.66
$M_{res,max}$	2, 7	1.35	7.62	-1.05	-0.97	7.69	1.30	14.93	-0.17	14.94

Extreme loads at blade radius $R = 0.50\text{m}$

	LC_{index}	γ_F	F_x [kN]	F_y [kN]	F_z [kN]	F_{res} [kN]	M_x [kNm]	M_y [kNm]	M_z [kNm]	M_{res} [kNm]
$F_{x,min}$	1	1.35	-6.62	0.67	-1.08	6.65	-0.89	-13.37	-0.11	13.48
$F_{x,max}$	2	1.35	7.44	-0.99	-1.07	7.50	1.17	14.21	-0.16	14.21
$F_{y,min}$	3	1.35	0.82	-4.77	-0.24	4.84	9.59	1.44	0.02	9.70
$F_{y,max}$	4	1.35	-6.27	1.99	-0.95	6.58	-2.95	-12.00	-0.15	12.36
$F_{z,min}$	2, 14	1.35	4.75	-0.71	-1.08	7.26	0.87	9.42	-0.15	14.01
$F_{z,max}$	5	1.35	0.66	-1.12	24.74	1.30	2.26	1.74	-0.02	2.85
$F_{res,max}$	2	1.35	7.44	-0.99	-1.07	7.50	1.17	14.21	-0.16	14.21
$M_{x,min}$	4	1.35	-6.27	1.99	-0.95	6.58	-2.95	-12.00	-0.15	12.36
$M_{x,max}$	3	1.35	0.82	-4.77	-0.24	4.84	9.59	1.44	0.02	9.70
$M_{y,min}$	1	1.35	-6.62	0.67	-1.08	6.65	-0.89	-13.37	-0.11	13.48
$M_{y,max}$	2	1.35	7.44	-0.99	-1.07	7.50	1.17	14.21	-0.16	14.21
$M_{z,min}$	7	1.35	5.44	-1.70	10.16	5.70	4.03	13.04	-0.32	13.57
$M_{z,max}$	8	1.35	-0.22	-4.47	-0.21	4.48	9.20	-0.50	0.07	9.23
$M_{res,max}$	2, 7	1.35	7.16	-1.15	1.07	7.26	1.66	14.14	-0.19	14.23

Extreme loads at blade radius $R = 0.60\text{m}$

	LC_{index}	γF	F_x [kN]	F_y [kN]	F_z [kN]	F_{res} [kN]	M_x [kNm]	M_y [kNm]	M_z [kNm]	M_{res} [kNm]
$F_{x,min}$	1	1.35	-6.46	0.64	-1.05	6.49	-0.82	-12.74	-0.10	12.83
$F_{x,max}$	2	1.35	7.23	-0.94	-1.04	7.29	1.07	13.48	-0.15	13.49
$F_{y,min}$	3	1.35	0.80	-4.66	-0.23	4.73	9.12	1.36	0.02	9.23
$F_{y,max}$	4	1.35	-6.11	1.89	-0.92	6.39	-2.77	-11.39	-0.14	11.72
$F_{z,min}$	2, 14	1.35	2.14	-0.40	-1.05	6.94	0.51	4.46	-0.13	13.23
$F_{z,max}$	5	1.35	0.68	-1.09	24.27	1.29	2.17	1.73	-0.02	2.78
$F_{res,max}$	2	1.35	7.23	-0.94	-1.04	7.29	1.07	13.48	-0.15	13.49
$M_{x,min}$	4	1.35	-6.11	1.89	-0.92	6.39	-2.77	-11.39	-0.14	11.72
$M_{x,max}$	3	1.35	0.80	-4.66	-0.23	4.73	9.12	1.36	0.02	9.23
$M_{y,min}$	1	1.35	-6.46	0.65	-1.05	6.49	-0.82	-12.74	-0.10	12.83
$M_{y,max}$	2	1.35	7.23	-0.94	-1.04	7.29	1.07	13.48	-0.15	13.49
$M_{z,min}$	7	1.35	5.39	-1.69	9.99	5.65	3.85	12.49	-0.31	13.01
$M_{z,max}$	8	1.35	-0.22	-4.38	-0.20	4.38	8.77	-0.48	0.07	8.79
$M_{res,max}$	2, 7	1.35	6.69	-1.25	3.10	6.83	2.02	13.35	-0.21	13.53

Extreme loads at blade radius $R = 0.70\text{m}$

	LC_{index}	γF	F_x [kN]	F_y [kN]	F_z [kN]	F_{res} [kN]	M_x [kNm]	M_y [kNm]	M_z [kNm]	M_{res} [kNm]
$F_{x,min}$	1	1.35	-6.30	0.62	-1.01	6.33	-0.75	-12.11	-0.10	12.18
$F_{x,max}$	2	1.35	7.03	-0.89	-1.01	7.08	0.98	12.75	-0.14	12.76
$F_{y,min}$	3	1.35	0.78	-4.56	-0.22	4.62	8.66	1.27	0.01	8.76
$F_{y,max}$	4	1.35	-5.94	1.78	-0.89	6.20	-2.58	-10.78	-0.14	11.09
$F_{z,min}$	2, 14	1.35	-0.47	-0.09	-1.02	6.61	0.14	-0.49	-0.12	12.45
$F_{z,max}$	5	1.35	0.70	-1.06	23.80	1.27	2.08	1.73	-0.02	2.70
$F_{res,max}$	2	1.35	7.03	-0.89	-1.01	7.08	0.98	12.75	-0.14	12.76
$M_{x,min}$	4	1.35	-5.94	1.78	-0.89	6.20	-2.58	-10.78	-0.14	11.09
$M_{x,max}$	3	1.35	0.78	-4.56	-0.22	4.62	8.66	1.27	0.01	8.76
$M_{y,min}$	1	1.35	-6.30	0.62	-1.01	6.33	-0.76	-12.12	-0.10	12.18
$M_{y,max}$	2	1.35	7.03	-0.89	-1.01	7.08	0.98	12.75	-0.14	12.76
$M_{z,min}$	7	1.35	5.34	-1.68	9.81	5.60	3.68	11.94	-0.30	12.45
$M_{z,max}$	8	1.35	-0.22	-4.28	-0.19	4.28	8.34	-0.46	0.06	8.36
$M_{res,max}$	2, 7	1.35	6.23	-1.34	5.13	6.39	2.37	12.56	-0.24	12.82

Extreme loads at blade radius $R = 0.80\text{m}$

	LC_{index}	γ_F	F_x [kN]	F_y [kN]	F_z [kN]	F_{res} [kN]	M_x [kNm]	M_y [kNm]	M_z [kNm]	M_{res} [kNm]
$F_{x,min}$	1	1.35	-6.14	0.59	-0.98	6.17	-0.69	-11.48	-0.09	11.53
$F_{x,max}$	2	1.35	6.82	-0.84	-0.97	6.87	0.88	12.02	-0.14	12.04
$F_{y,min}$	3	1.35	0.76	-4.45	-0.21	4.51	8.20	1.19	0.01	8.29
$F_{y,max}$	4	1.35	-5.77	1.68	-0.85	6.01	-2.40	-10.16	-0.13	10.45
$F_{z,min}$	2, 14	1.35	-3.09	0.22	-0.98	6.28	-0.22	-5.44	-0.10	11.67
$F_{z,max}$	5	1.35	0.71	-1.03	23.33	1.26	1.99	1.72	-0.03	2.63
$F_{res,max}$	2	1.35	6.82	-0.84	-0.97	6.87	0.88	12.02	-0.14	12.04
$M_{x,min}$	4	1.35	-5.77	1.68	-0.85	6.01	-2.40	-10.16	-0.13	10.45
$M_{x,max}$	3	1.35	0.76	-4.45	-0.21	4.51	8.20	1.19	0.01	8.29
$M_{y,min}$	1	1.35	-6.14	0.59	-0.98	6.17	-0.69	-11.49	-0.09	11.53
$M_{y,max}$	2	1.35	6.82	-0.84	-0.97	6.87	0.88	12.02	-0.14	12.04
$M_{z,min}$	7	1.35	5.29	-1.67	9.63	5.55	3.51	11.38	-0.30	11.89
$M_{z,max}$	8	1.35	-0.21	-4.18	-0.18	4.18	7.91	-0.43	0.06	7.92
$M_{res,max}$	2, 7	1.35	5.77	-1.44	7.17	5.96	2.73	11.77	-0.26	12.12

Extreme loads at blade radius $R = 0.90\text{m}$

	LC_{index}	γ_F	F_x [kN]	F_y [kN]	F_z [kN]	F_{res} [kN]	M_x [kNm]	M_y [kNm]	M_z [kNm]	M_{res} [kNm]
$F_{x,min}$	1	1.35	-5.98	0.56	-0.94	6.01	-0.62	-10.85	-0.09	10.88
$F_{x,max}$	2	1.35	6.62	-0.80	-0.94	6.66	0.78	11.29	-0.13	11.32
$F_{y,min}$	3	1.35	0.75	-4.34	-0.20	4.40	7.73	1.11	0.01	7.81
$F_{y,max}$	4	1.35	-5.60	1.57	-0.82	5.82	-2.22	-9.55	-0.13	9.81
$F_{z,min}$	2, 14	1.35	-5.70	0.52	-0.95	5.95	-0.58	-10.39	-0.09	10.89
$F_{z,max}$	5	1.35	0.73	-1.01	22.85	1.24	1.90	1.71	-0.03	2.56
$F_{res,max}$	2	1.35	6.62	-0.80	-0.94	6.66	0.78	11.29	-0.13	11.32
$M_{x,min}$	4	1.35	-5.60	1.57	-0.82	5.82	-2.22	-9.55	-0.13	9.81
$M_{x,max}$	3	1.35	0.75	-4.34	-0.20	4.40	7.73	1.11	0.01	7.81
$M_{y,min}$	1	1.35	-5.98	0.56	-0.95	6.01	-0.63	-10.86	-0.09	10.88
$M_{y,max}$	2	1.35	6.62	-0.80	-0.94	6.66	0.79	11.29	-0.13	11.32
$M_{z,min}$	7	1.35	5.24	-1.66	9.45	5.50	3.34	10.83	-0.29	11.33
$M_{z,max}$	8	1.35	-0.21	-4.08	-0.17	4.09	7.47	-0.41	0.06	7.49
$M_{res,max}$	2, 7	1.35	5.30	-1.53	9.20	5.53	3.09	10.99	-0.28	11.41

Extreme loads at blade radius $R = 1.00\text{m}$

	LC_{index}	γ_F	F_x [kN]	F_y [kN]	F_z [kN]	F_{res} [kN]	M_x [kNm]	M_y [kNm]	M_z [kNm]	M_{res} [kNm]
$F_{x,min}$	1	1.35	-5.80	0.53	-0.91	5.83	-0.58	-10.35	-0.08	10.38
$F_{x,max}$	2	1.35	6.40	-0.75	-0.90	6.44	0.73	10.75	-0.12	10.78
$F_{y,min}$	3	1.35	0.72	-4.21	-0.19	4.27	7.37	1.05	0.01	7.45
$F_{y,max}$	4	1.35	-5.42	1.51	-0.79	5.62	-2.10	-9.10	-0.12	9.34
$F_{z,min}$	14	1.35	-5.75	0.52	-0.91	5.77	-0.58	-10.35	-0.08	10.38
$F_{z,max}$	5	1.35	0.74	-0.98	22.24	1.23	1.82	1.69	-0.03	2.49
$F_{res,max}$	2	1.35	6.40	-0.75	-0.90	6.44	0.73	10.75	-0.12	10.78
$M_{x,min}$	4, 17	1.35	-5.30	1.50	0.44	5.51	-2.10	-8.95	-0.12	9.20
$M_{x,max}$	3, 18	1.35	0.70	-4.21	-0.12	4.26	7.37	1.04	0.01	7.45
$M_{y,min}$	1, 14	1.35	-5.80	0.53	-0.91	5.83	-0.59	-10.36	-0.08	10.38
$M_{y,max}$	2, 7	1.35	6.38	-0.81	-0.35	6.43	0.83	10.79	-0.13	10.83
$M_{z,min}$	7	1.35	5.13	-1.62	9.20	5.38	3.19	10.37	-0.27	10.85
$M_{z,max}$	8	1.35	-0.20	-3.97	-0.16	3.97	7.13	-0.39	0.06	7.14
$M_{res,max}$	7	1.35	5.15	-1.50	9.14	5.38	2.99	10.50	-0.27	10.92

Extreme loads at blade radius $R = 1.25\text{m}$

	LC_{index}	γ_F	F_x [kN]	F_y [kN]	F_z [kN]	F_{res} [kN]	M_x [kNm]	M_y [kNm]	M_z [kNm]	M_{res} [kNm]
$F_{x,min}$	1	1.35	-5.36	0.46	-0.81	5.38	-0.49	-9.12	-0.07	9.15
$F_{x,max}$	2	1.35	5.85	-0.64	-0.80	5.88	0.61	9.44	-0.10	9.46
$F_{y,min}$	3	1.35	0.64	-3.89	-0.17	3.94	6.48	0.91	0.01	6.55
$F_{y,max}$	4	1.35	-4.95	1.34	-0.70	5.13	-1.82	-7.99	-0.10	8.20
$F_{z,min}$	14	1.35	-5.31	0.46	-0.82	5.33	-0.49	-9.13	-0.07	9.15
$F_{z,max}$	5	1.35	0.74	-0.92	20.66	1.18	1.64	1.63	-0.02	2.32
$F_{res,max}$	2	1.35	5.85	-0.64	-0.80	5.88	0.61	9.44	-0.10	9.46
$M_{x,min}$	4, 17	1.35	-4.53	1.32	3.86	4.72	-1.82	-7.44	-0.09	7.67
$M_{x,max}$	3, 18	1.35	0.59	-3.88	0.07	3.92	6.49	0.88	0.01	6.55
$M_{y,min}$	1, 14	1.35	-5.35	0.46	-0.81	5.38	-0.50	-9.14	-0.07	9.15
$M_{y,max}$	2, 7	1.35	5.79	-0.88	1.25	5.86	0.99	9.58	-0.12	9.66
$M_{z,min}$	7	1.35	4.82	-1.53	8.57	5.06	2.83	9.23	-0.23	9.65
$M_{z,max}$	8	1.35	-0.19	-3.67	-0.14	3.67	6.28	-0.35	0.05	6.29
$M_{res,max}$	7	1.35	4.85	-1.41	8.51	5.06	2.65	9.36	-0.23	9.73

Extreme loads at blade radius $R = 1.50\text{m}$

	LC_{index}	γ_F	F_x [kN]	F_y [kN]	F_z [kN]	F_{res} [kN]	M_x [kNm]	M_y [kNm]	M_z [kNm]	M_{res} [kNm]
$F_{x,min}$	1	1.35	-4.91	0.39	-0.72	4.93	-0.41	-7.90	-0.05	7.92
$F_{x,max}$	2	1.35	5.30	-0.53	-0.71	5.33	0.49	8.12	-0.08	8.14
$F_{y,min}$	3	1.35	0.57	-3.57	-0.15	3.61	5.59	0.77	0.00	5.65
$F_{y,max}$	4	1.35	-4.48	1.17	-0.62	4.64	-1.53	-6.88	-0.08	7.05
$F_{z,min}$	14	1.35	-4.88	0.39	-0.72	4.89	-0.40	-7.91	-0.05	7.93
$F_{z,max}$	5	1.35	0.75	-0.85	19.08	1.14	1.46	1.56	-0.02	2.15
$F_{res,max}$	2	1.35	5.30	-0.53	-0.71	5.33	0.49	8.12	-0.08	8.14
$M_{x,min}$	4, 17	1.35	-3.76	1.14	7.27	3.92	-1.54	-5.94	-0.07	6.15
$M_{x,max}$	3, 18	1.35	0.47	-3.55	0.26	3.57	5.61	0.72	0.00	5.65
$M_{y,min}$	1, 14	1.35	-4.90	0.39	-0.72	4.92	-0.41	-7.92	-0.05	7.93
$M_{y,max}$	2, 7	1.35	5.19	-0.94	2.85	5.29	1.15	8.38	-0.12	8.49
$M_{z,min}$	7	1.35	4.51	-1.43	7.94	4.73	2.47	8.09	-0.19	8.46
$M_{z,max}$	8	1.35	-0.17	-3.38	-0.12	3.38	5.43	-0.30	0.04	5.44
$M_{res,max}$	7	1.35	4.55	-1.31	7.88	4.73	2.30	8.23	-0.19	8.54

Extreme loads at blade radius $R = 1.75\text{m}$

	LC_{index}	γ_F	F_x [kN]	F_y [kN]	F_z [kN]	F_{res} [kN]	M_x [kNm]	M_y [kNm]	M_z [kNm]	M_{res} [kNm]
$F_{x,min}$	1	1.35	-4.46	0.32	-0.62	4.48	-0.32	-6.67	-0.04	6.69
$F_{x,max}$	2	1.35	4.75	-0.42	-0.61	4.77	0.37	6.81	-0.06	6.82
$F_{y,min}$	3	1.35	0.50	-3.24	-0.13	3.28	4.71	0.62	0.00	4.75
$F_{y,max}$	4	1.35	-4.02	1.01	-0.54	4.14	-1.25	-5.77	-0.06	5.91
$F_{z,min}$	14	1.35	-4.44	0.32	-0.63	4.45	-0.31	-6.69	-0.04	6.71
$F_{z,max}$	5	1.35	0.76	-0.79	17.51	1.10	1.28	1.50	-0.02	1.98
$F_{res,max}$	2	1.35	4.75	-0.42	-0.61	4.77	0.37	6.81	-0.06	6.82
$M_{x,min}$	4, 17	1.35	-2.98	0.96	10.69	3.13	-1.26	-4.43	-0.05	4.62
$M_{x,max}$	3, 18	1.35	0.35	-3.21	0.46	3.23	4.73	0.55	0.00	4.76
$M_{y,min}$	1, 14	1.35	-4.45	0.32	-0.62	4.47	-0.31	-6.69	-0.04	6.71
$M_{y,max}$	2, 7	1.35	4.60	-1.00	4.45	4.71	1.30	7.17	-0.11	7.33
$M_{z,min}$	7	1.35	4.21	-1.33	7.31	4.41	2.11	6.95	-0.15	7.26
$M_{z,max}$	8	1.35	-0.16	-3.08	-0.09	3.08	4.59	-0.26	0.03	4.59
$M_{res,max}$	7	1.35	4.24	-1.22	7.25	4.41	1.96	7.09	-0.15	7.35

Extreme loads at blade radius $R = 2.00\text{m}$

	LC_{index}	γ_F	F_x [kN]	F_y [kN]	F_z [kN]	F_{res} [kN]	M_x [kNm]	M_y [kNm]	M_z [kNm]	M_{res} [kNm]
$F_{x,min}$	1	1.35	-4.02	0.25	-0.53	4.03	-0.23	-5.44	-0.02	5.46
$F_{x,max}$	2	1.35	4.20	-0.32	-0.51	4.22	0.25	5.49	-0.03	5.51
$F_{y,min}$	3	1.35	0.43	-2.92	-0.11	2.95	3.82	0.48	-0.00	3.85
$F_{y,max}$	4	1.35	-3.55	0.84	-0.45	3.65	-0.97	-4.66	-0.04	4.76
$F_{z,min}$	14	1.35	-4.00	0.25	-0.53	4.01	-0.22	-5.47	-0.02	5.48
$F_{z,max}$	5	1.35	0.76	-0.73	15.93	1.06	1.10	1.43	-0.02	1.81
$F_{res,max}$	2	1.35	4.20	-0.32	-0.51	4.22	0.25	5.49	-0.03	5.51
$M_{x,min}$	4, 17	1.35	-2.21	0.78	14.11	2.34	-0.98	-2.92	-0.02	3.09
$M_{x,max}$	3, 18	1.35	0.24	-2.88	0.65	2.88	3.84	0.39	-0.00	3.86
$M_{y,min}$	1, 14	1.35	-4.00	0.25	-0.53	4.02	-0.22	-5.47	-0.02	5.48
$M_{y,max}$	2, 7	1.35	4.00	-1.07	6.04	4.14	1.46	5.97	-0.10	6.16
$M_{z,min}$	7	1.35	3.90	-1.23	6.68	4.09	1.75	5.81	-0.11	6.07
$M_{z,max}$	8	1.35	-0.14	-2.79	-0.07	2.79	3.74	-0.21	0.02	3.74
$M_{res,max}$	7	1.35	3.94	-1.12	6.61	4.09	1.61	5.95	-0.11	6.16

Extreme loads at blade radius $R = 2.25\text{m}$

	LC_{index}	γ_F	F_x [kN]	F_y [kN]	F_z [kN]	F_{res} [kN]	M_x [kNm]	M_y [kNm]	M_z [kNm]	M_{res} [kNm]
$F_{x,min}$	1, 14	1.35	-3.59	0.20	-0.45	3.60	-0.17	-4.52	-0.02	4.53
$F_{x,max}$	2, 7	1.35	3.76	-0.44	1.00	3.80	0.41	4.64	-0.03	4.69
$F_{y,min}$	3, 18	1.35	0.29	-2.61	-0.04	2.63	3.15	0.32	-0.00	3.17
$F_{y,max}$	4, 17	1.35	-2.84	0.72	2.83	2.94	-0.79	-3.53	-0.03	3.62
$F_{z,min}$	14	1.35	-3.58	0.20	-0.45	3.59	-0.17	-4.54	-0.02	4.55
$F_{z,max}$	5	1.35	0.71	-0.66	14.39	0.97	0.93	1.24	-0.02	1.56
$F_{res,max}$	2, 7	1.35	3.76	-0.44	1.00	3.80	0.41	4.64	-0.03	4.68
$M_{x,min}$	17	1.35	-1.83	0.67	13.91	1.94	-0.79	-2.21	-0.02	2.35
$M_{x,max}$	18	1.35	0.20	-2.58	0.65	2.58	3.17	0.31	-0.00	3.18
$M_{y,min}$	14	1.35	-3.58	0.20	-0.45	3.59	-0.17	-4.54	-0.02	4.55
$M_{y,max}$	7	1.35	3.60	-1.00	5.99	3.74	1.32	5.00	-0.09	5.18
$M_{z,min}$	7	1.35	3.55	-1.13	6.06	3.73	1.47	4.86	-0.09	5.08
$M_{z,max}$	8	1.35	-0.13	-2.51	-0.06	2.51	3.09	-0.18	0.01	3.09
$M_{res,max}$	7	1.35	3.61	-1.02	5.99	3.75	1.35	5.00	-0.09	5.18

Extreme loads at blade radius $R = 2.50\text{m}$

	LC_{index}	γF	F_x [kN]	F_y [kN]	F_z [kN]	F_{res} [kN]	M_x [kNm]	M_y [kNm]	M_z [kNm]	M_{res} [kNm]
$F_{x,min}$	1, 14	1.35	-3.18	0.15	-0.38	3.18	-0.13	-3.70	-0.01	3.70
$F_{x,max}$	2, 7	1.35	3.35	-0.65	3.01	3.43	0.66	3.95	-0.04	4.04
$F_{y,min}$	3, 18	1.35	0.14	-2.31	0.06	2.32	2.55	0.16	-0.00	2.56
$F_{y,max}$	4, 17	1.35	-2.06	0.61	7.22	2.15	-0.64	-2.39	-0.02	2.48
$F_{z,min}$	14	1.35	-3.18	0.15	-0.38	3.18	-0.13	-3.70	-0.01	3.71
$F_{z,max}$	5	1.35	0.63	-0.59	12.87	0.86	0.77	1.01	-0.01	1.27
$F_{res,max}$	2, 7	1.35	3.35	-0.65	3.01	3.44	0.67	3.95	-0.05	4.03
$M_{x,min}$	17	1.35	-1.57	0.59	12.46	1.68	-0.64	-1.76	-0.01	1.88
$M_{x,max}$	18	1.35	0.19	-2.30	0.59	2.30	2.57	0.27	-0.00	2.58
$M_{y,min}$	14	1.35	-3.18	0.15	-0.38	3.18	-0.13	-3.70	-0.01	3.71
$M_{y,max}$	7	1.35	3.28	-0.90	5.37	3.40	1.08	4.12	-0.07	4.26
$M_{z,min}$	7	1.35	3.19	-1.03	5.43	3.35	1.22	3.98	-0.07	4.16
$M_{z,max}$	8	1.35	-0.12	-2.23	-0.05	2.23	2.50	-0.14	0.01	2.50
$M_{res,max}$	7	1.35	3.28	-0.93	5.37	3.40	1.10	4.12	-0.07	4.27

Extreme loads at blade radius $R = 2.75\text{m}$

	LC_{index}	γF	F_x [kN]	F_y [kN]	F_z [kN]	F_{res} [kN]	M_x [kNm]	M_y [kNm]	M_z [kNm]	M_{res} [kNm]
$F_{x,min}$	14	1.35	-2.77	0.11	-0.31	2.77	-0.09	-2.89	-0.01	2.89
$F_{x,max}$	7	1.35	2.95	-0.82	4.74	3.05	0.86	3.27	-0.05	3.39
$F_{y,min}$	18	1.35	0.02	-2.01	0.15	2.01	1.97	0.02	0.00	1.97
$F_{y,max}$	17	1.35	-1.33	0.51	11.01	1.42	-0.49	-1.33	-0.01	1.43
$F_{z,min}$	14	1.35	-2.77	0.11	-0.31	2.77	-0.09	-2.89	-0.01	2.89
$F_{z,max}$	5	1.35	0.55	-0.53	11.35	0.76	0.61	0.79	-0.01	1.00
$F_{res,max}$	7	1.35	2.95	-0.83	4.76	3.07	0.88	3.27	-0.05	3.37
$M_{x,min}$	17	1.35	-1.33	0.51	11.01	1.42	-0.49	-1.33	-0.01	1.43
$M_{x,max}$	18, 22	1.35	0.17	-2.01	0.50	2.01	1.98	0.22	-0.01	1.99
$M_{y,min}$	14	1.35	-2.77	0.11	-0.31	2.77	-0.09	-2.89	-0.01	2.89
$M_{y,max}$	7, 23	1.35	2.95	-0.80	4.74	3.05	0.84	3.27	-0.05	3.37
$M_{z,min}$	7, 24	1.35	2.82	-0.93	5.03	2.97	0.98	3.12	-0.05	3.26
$M_{z,max}$	8, 25	1.35	-0.16	-1.89	0.38	1.94	1.87	-0.16	0.00	1.92
$M_{res,max}$	7	1.35	2.95	-0.82	4.76	3.05	0.87	3.27	-0.05	3.39

Extreme loads at blade radius $R = 3.00\text{m}$

	LC_{index}	γ_F	F_x [kN]	F_y [kN]	F_z [kN]	F_{res} [kN]	M_x [kNm]	M_y [kNm]	M_z [kNm]	M_{res} [kNm]
$F_{x,min}$	14	1.35	-2.41	0.09	-0.24	2.41	-0.06	-2.29	-0.01	2.29
$F_{x,max}$	7	1.35	2.60	-0.72	4.12	2.69	0.68	2.61	-0.04	2.70
$F_{y,min}$	18	1.35	0.09	-1.74	0.30	1.74	1.53	0.10	-0.00	1.54
$F_{y,max}$	17	1.35	-1.13	0.44	9.54	1.21	-0.38	-1.05	-0.01	1.12
$F_{z,min}$	14	1.35	-2.40	0.09	-0.24	2.40	-0.06	-2.29	-0.01	2.29
$F_{z,max}$	5	1.35	0.50	-0.47	9.83	0.69	0.49	0.66	-0.01	0.83
$F_{res,max}$	7	1.35	2.60	-0.73	4.14	2.70	0.69	2.61	-0.04	2.70
$M_{x,min}$	17	1.35	-1.13	0.44	9.54	1.21	-0.38	-1.05	-0.01	1.12
$M_{x,max}$	18, 22	1.35	0.15	-1.74	0.21	1.74	1.54	0.16	-0.00	1.55
$M_{y,min}$	14	1.35	-2.41	0.09	-0.24	2.41	-0.06	-2.29	-0.01	2.29
$M_{y,max}$	7, 23	1.35	2.59	-0.70	4.12	2.69	0.66	2.61	-0.04	2.69
$M_{z,min}$	7, 24	1.35	2.40	-0.82	6.62	2.53	0.79	2.45	-0.04	2.58
$M_{z,max}$	8, 25	1.35	-0.70	-0.92	4.55	1.53	0.92	-0.61	0.00	1.43
$M_{res,max}$	7	1.35	2.60	-0.72	4.13	2.69	0.68	2.61	-0.04	2.71

Extreme loads at blade radius $R = 3.25\text{m}$

	LC_{index}	γ_F	F_x [kN]	F_y [kN]	F_z [kN]	F_{res} [kN]	M_x [kNm]	M_y [kNm]	M_z [kNm]	M_{res} [kNm]
$F_{x,min}$	14	1.35	-2.05	0.07	-0.18	2.05	-0.04	-1.70	-0.00	1.70
$F_{x,max}$	7	1.35	2.26	-0.62	3.50	2.34	0.50	1.98	-0.02	2.03
$F_{y,min}$	18	1.35	0.16	-1.47	0.42	1.47	1.11	0.16	-0.00	1.12
$F_{y,max}$	17	1.35	-0.93	0.36	8.08	1.00	-0.27	-0.78	-0.00	0.83
$F_{z,min}$	14	1.35	-2.04	0.06	-0.18	2.04	-0.04	-1.70	-0.00	1.70
$F_{z,max}$	5	1.35	0.46	-0.42	8.31	0.62	0.38	0.54	-0.00	0.66
$F_{res,max}$	7	1.35	2.26	-0.62	3.52	2.34	0.51	1.98	-0.02	2.04
$M_{x,min}$	17, 4	1.35	-0.97	0.36	7.74	1.03	-0.27	-0.80	-0.00	0.85
$M_{x,max}$	22	1.35	0.12	-1.47	-0.05	1.47	1.11	0.10	-0.00	1.12
$M_{y,min}$	14	1.35	-2.05	0.07	-0.18	2.05	-0.04	-1.70	-0.00	1.70
$M_{y,max}$	23	1.35	2.24	-0.59	3.50	2.32	0.49	1.98	-0.02	2.03
$M_{z,min}$	24	1.35	1.99	-0.72	7.85	2.11	0.61	1.81	-0.02	1.92
$M_{z,max}$	25	1.35	-1.15	-0.06	8.04	1.15	0.08	-0.97	0.00	0.98
$M_{res,max}$	7, 23	1.35	2.26	-0.61	3.50	2.34	0.50	1.98	-0.02	2.04

Extreme loads at blade radius $R = 3.50\text{m}$

	LC_{index}	γ_F	F_x [kN]	F_y [kN]	F_z [kN]	F_{res} [kN]	M_x [kNm]	M_y [kNm]	M_z [kNm]	M_{res} [kNm]
$F_{x,min}$	14	1.35	-1.72	0.05	-0.14	1.72	-0.03	-1.26	-0.00	1.26
$F_{x,max}$	7	1.35	1.93	-0.51	2.89	1.99	0.36	1.49	-0.01	1.53
$F_{y,min}$	18	1.35	0.13	-1.21	0.34	1.21	0.80	0.12	-0.00	0.81
$F_{y,max}$	17	1.35	-0.77	0.30	6.65	0.83	-0.20	-0.58	-0.00	0.62
$F_{z,min}$	14	1.35	-1.70	0.05	-0.14	1.71	-0.03	-1.26	-0.00	1.26
$F_{z,max}$	5	1.35	0.46	-0.37	6.84	0.59	0.29	0.45	-0.00	0.53
$F_{res,max}$	7	1.35	1.93	-0.51	2.90	1.99	0.37	1.49	-0.01	1.53
$M_{x,min}$	17, 4	1.35	-1.09	0.29	3.53	1.13	-0.20	-0.76	-0.00	0.79
$M_{x,max}$	22	1.35	0.10	-1.20	-0.04	1.21	0.81	0.08	-0.00	0.81
$M_{y,min}$	14	1.35	-1.72	0.05	-0.14	1.72	-0.03	-1.26	-0.00	1.26
$M_{y,max}$	23	1.35	1.92	-0.50	2.89	1.99	0.36	1.49	-0.01	1.53
$M_{z,min}$	24	1.35	1.70	-0.61	6.46	1.80	0.46	1.38	-0.01	1.45
$M_{z,max}$	25	1.35	-0.97	-0.07	6.62	0.97	0.07	-0.73	0.00	0.74
$M_{res,max}$	7, 23	1.35	1.93	-0.51	2.89	1.99	0.36	1.49	-0.01	1.53

Extreme loads at blade radius $R = 3.75\text{m}$

	LC_{index}	γ_F	F_x [kN]	F_y [kN]	F_z [kN]	F_{res} [kN]	M_x [kNm]	M_y [kNm]	M_z [kNm]	M_{res} [kNm]
$F_{x,min}$	14	1.35	-1.39	0.04	-0.09	1.39	-0.02	-0.84	-0.00	0.84
$F_{x,max}$	7, 23	1.35	1.60	-0.40	2.28	1.66	0.23	1.02	-0.01	1.04
$F_{y,min}$	18, 22	1.35	0.11	-0.95	0.24	0.95	0.51	0.08	-0.00	0.52
$F_{y,max}$	17, 4	1.35	-0.64	0.23	5.03	0.68	-0.13	-0.40	-0.00	0.42
$F_{z,min}$	14	1.35	-1.36	0.04	-0.09	1.38	-0.02	-0.83	-0.00	0.83
$F_{z,max}$	5	1.35	0.45	-0.32	5.38	0.55	0.20	0.36	-0.00	0.41
$F_{res,max}$	7	1.35	1.60	-0.41	2.30	1.66	0.24	1.02	-0.01	1.05
$M_{x,min}$	4	1.35	-1.16	0.22	-0.09	1.18	-0.13	-0.70	-0.00	0.71
$M_{x,max}$	22	1.35	0.08	-0.95	-0.03	0.95	0.51	0.05	-0.00	0.52
$M_{y,min}$	14	1.35	-1.39	0.04	-0.09	1.39	-0.02	-0.84	-0.00	0.84
$M_{y,max}$	23, 24	1.35	1.60	-0.40	2.38	1.65	0.24	1.02	-0.01	1.05
$M_{z,min}$	24	1.35	1.41	-0.51	5.08	1.50	0.31	0.96	-0.01	1.01
$M_{z,max}$	25	1.35	-0.79	-0.06	5.21	0.79	0.05	-0.50	0.00	0.51
$M_{res,max}$	23, 24	1.35	1.60	-0.41	2.38	1.65	0.24	1.02	-0.01	1.05

Extreme loads at blade radius $R = 4.00\text{m}$

	LC_{index}	γF	F_x [kN]	F_y [kN]	F_z [kN]	F_{res} [kN]	M_x [kNm]	M_y [kNm]	M_z [kNm]	M_{res} [kNm]
$F_{x,min}$	14	1.35	-1.09	0.03	-0.06	1.09	-0.01	-0.56	-0.00	0.56
$F_{x,max}$	7, 23	1.35	1.29	-0.32	1.70	1.33	0.15	0.69	-0.00	0.70
$F_{y,min}$	18, 22	1.35	0.08	-0.71	0.10	0.71	0.33	0.05	-0.00	0.33
$F_{y,max}$	17, 4	1.35	-0.67	0.17	2.28	0.70	-0.08	-0.33	-0.00	0.34
$F_{z,min}$	14	1.35	-1.07	0.03	-0.06	1.08	-0.01	-0.55	-0.00	0.55
$F_{z,max}$	5	1.35	0.42	-0.26	4.00	0.49	0.13	0.26	-0.00	0.30
$F_{res,max}$	7	1.35	1.29	-0.32	1.71	1.33	0.16	0.69	-0.00	0.70
$M_{x,min}$	4	1.35	-0.91	0.17	-0.06	0.92	-0.08	-0.47	-0.00	0.47
$M_{x,max}$	22	1.35	0.07	-0.71	-0.02	0.71	0.33	0.04	-0.00	0.33
$M_{y,min}$	14	1.35	-1.09	0.03	-0.06	1.09	-0.01	-0.56	-0.00	0.56
$M_{y,max}$	23, 24	1.35	1.26	-0.35	2.54	1.31	0.17	0.69	-0.00	0.71
$M_{z,min}$	24	1.35	1.17	-0.40	3.78	1.24	0.20	0.66	-0.00	0.69
$M_{z,max}$	25	1.35	-0.64	-0.06	3.88	0.64	0.04	-0.34	0.00	0.34
$M_{res,max}$	23, 24	1.35	1.26	-0.35	2.54	1.31	0.17	0.69	-0.00	0.71

Extreme loads at blade radius $R = 4.25\text{m}$

	LC_{index}	γF	F_x [kN]	F_y [kN]	F_z [kN]	F_{res} [kN]	M_x [kNm]	M_y [kNm]	M_z [kNm]	M_{res} [kNm]
$F_{x,min}$	14	1.35	-0.80	0.02	-0.04	0.80	-0.01	-0.30	-0.00	0.30
$F_{x,max}$	23, 24	1.35	0.97	-0.23	1.16	1.00	0.08	0.38	-0.00	0.39
$F_{y,min}$	22, 29	1.35	0.05	-0.48	-0.01	0.48	0.17	0.02	-0.00	0.17
$F_{y,max}$	4	1.35	-0.66	0.12	-0.04	0.67	-0.05	-0.25	-0.00	0.26
$F_{z,min}$	14, 30	1.35	-0.78	0.02	-0.04	0.78	-0.01	-0.30	-0.00	0.30
$F_{z,max}$	5	1.35	0.38	-0.19	2.69	0.43	0.08	0.17	-0.00	0.19
$F_{res,max}$	7, 24	1.35	0.97	-0.23	1.16	1.00	0.08	0.38	-0.00	0.39
$M_{x,min}$	4	1.35	-0.66	0.12	-0.04	0.67	-0.05	-0.25	-0.00	0.26
$M_{x,max}$	22, 29	1.35	0.05	-0.48	-0.01	0.48	0.17	0.02	-0.00	0.17
$M_{y,min}$	14	1.35	-0.80	0.02	-0.04	0.80	-0.01	-0.30	-0.00	0.30
$M_{y,max}$	24	1.35	0.93	-0.28	2.53	0.97	0.11	0.39	-0.00	0.40
$M_{z,min}$	24, 8	1.35	0.91	-0.29	2.53	0.96	0.11	0.38	-0.00	0.40
$M_{z,max}$	25, 24	1.35	-0.47	-0.05	2.61	0.49	0.02	-0.19	0.00	0.19
$M_{res,max}$	24	1.35	0.93	-0.28	2.53	0.97	0.11	0.39	-0.00	0.40

Extreme loads at blade radius $R = 4.50\text{m}$

	LC_{index}	γ_F	F_x [kN]	F_y [kN]	F_z [kN]	F_{res} [kN]	M_x [kNm]	M_y [kNm]	M_z [kNm]	M_{res} [kNm]
$F_{x,min}$	14	1.35	-0.53	0.01	-0.02	0.53	-0.00	-0.19	0.00	0.19
$F_{x,max}$	23, 24	1.35	0.66	-0.15	0.79	0.68	0.05	0.24	-0.00	0.25
$F_{y,min}$	22, 29	1.35	0.04	-0.31	-0.01	0.31	0.10	0.01	-0.00	0.11
$F_{y,max}$	4	1.35	-0.44	0.08	-0.02	0.45	-0.03	-0.16	-0.00	0.16
$F_{z,min}$	14, 30	1.35	-0.47	-0.00	-0.02	0.49	-0.00	-0.18	-0.00	0.18
$F_{z,max}$	5	1.35	0.26	-0.13	1.73	0.29	0.05	0.11	-0.00	0.12
$F_{res,max}$	7, 24	1.35	0.66	-0.16	0.79	0.68	0.05	0.24	-0.00	0.25
$M_{x,min}$	4	1.35	-0.44	0.08	-0.02	0.45	-0.03	-0.16	-0.00	0.16
$M_{x,max}$	22, 29	1.35	0.04	-0.31	-0.01	0.31	0.10	0.01	-0.00	0.11
$M_{y,min}$	14	1.35	-0.53	0.01	-0.02	0.53	-0.00	-0.19	0.00	0.19
$M_{y,max}$	24	1.35	0.63	-0.19	1.63	0.66	0.07	0.24	-0.00	0.25
$M_{z,min}$	24, 8	1.35	0.56	-0.19	1.56	0.61	0.07	0.24	-0.00	0.25
$M_{z,max}$	25, 24	1.35	-0.23	-0.04	1.68	0.36	0.01	-0.11	0.00	0.12
$M_{res,max}$	24	1.35	0.63	-0.19	1.63	0.66	0.07	0.24	-0.00	0.25

Extreme loads at blade radius $R = 4.75\text{m}$

	LC_{index}	γ_F	F_x [kN]	F_y [kN]	F_z [kN]	F_{res} [kN]	M_x [kNm]	M_y [kNm]	M_z [kNm]	M_{res} [kNm]
$F_{x,min}$	14	1.35	-0.26	0.01	-0.01	0.26	-0.00	-0.07	0.00	0.07
$F_{x,max}$	23, 24	1.35	0.34	-0.08	0.42	0.35	0.02	0.10	0.00	0.10
$F_{y,min}$	22, 29	1.35	0.02	-0.14	-0.00	0.14	0.04	0.01	-0.00	0.04
$F_{y,max}$	4	1.35	-0.22	0.04	-0.01	0.22	-0.01	-0.06	0.00	0.06
$F_{z,min}$	14, 30	1.35	-0.17	-0.02	-0.01	0.21	-0.00	-0.07	0.00	0.07
$F_{z,max}$	5	1.35	0.15	-0.06	0.78	0.16	0.02	0.04	0.00	0.05
$F_{res,max}$	7, 24	1.35	0.34	-0.08	0.42	0.35	0.02	0.10	0.00	0.10
$M_{x,min}$	4	1.35	-0.22	0.04	-0.01	0.22	-0.01	-0.06	0.00	0.06
$M_{x,max}$	22, 29	1.35	0.02	-0.14	-0.00	0.14	0.04	0.01	-0.00	0.04
$M_{y,min}$	14	1.35	-0.26	0.01	-0.01	0.26	-0.00	-0.07	0.00	0.07
$M_{y,max}$	24	1.35	0.33	-0.09	0.74	0.35	0.03	0.10	0.00	0.10
$M_{z,min}$	24, 8	1.35	0.21	-0.09	0.59	0.25	0.03	0.09	-0.00	0.09
$M_{z,max}$	25, 24	1.35	0.01	-0.04	0.76	0.23	0.01	-0.04	0.00	0.05
$M_{res,max}$	24	1.35	0.33	-0.09	0.74	0.35	0.03	0.10	0.00	0.10

Extreme loads at blade radius $R = 4.90\text{m}$

	LC_{index}	γF	F_x [kN]	F_y [kN]	F_z [kN]	F_{res} [kN]	M_x [kNm]	M_y [kNm]	M_z [kNm]	M_{res} [kNm]
$F_{x,min}$	14	1.35	-0.10	0.00	-0.00	0.10	-0.00	-0.01	0.00	0.01
$F_{x,max}$	23, 24	1.35	0.15	-0.03	0.20	0.16	0.00	0.01	0.00	0.01
$F_{y,min}$	22, 29	1.35	0.01	-0.04	-0.00	0.04	0.00	0.00	0.00	0.00
$F_{y,max}$	4	1.35	-0.08	0.01	-0.00	0.09	-0.00	-0.00	0.00	0.00
$F_{z,min}$	14, 30	1.35	0.01	-0.03	-0.00	0.03	0.00	0.00	0.00	0.00
$F_{z,max}$	5	1.35	0.08	-0.02	0.21	0.08	0.00	0.00	0.00	0.00
$F_{res,max}$	7, 24	1.35	0.15	-0.03	0.20	0.16	0.00	0.01	0.00	0.01
$M_{x,min}$	4	1.35	-0.08	0.01	-0.00	0.09	-0.00	-0.00	0.00	0.00
$M_{x,max}$	22, 29	1.35	0.01	-0.04	-0.00	0.04	0.00	0.00	0.00	0.00
$M_{y,min}$	14	1.35	-0.10	0.00	-0.00	0.10	-0.00	-0.01	0.00	0.01
$M_{y,max}$	24	1.35	0.15	-0.03	0.20	0.16	0.00	0.01	0.00	0.01
$M_{z,min}$	24, 8	1.35	-0.00	-0.04	0.00	0.04	0.00	0.00	-0.00	0.00
$M_{z,max}$	25, 24	1.35	0.15	-0.03	0.20	0.16	0.00	0.01	0.00	0.01
$M_{res,max}$	24	1.35	0.15	-0.03	0.20	0.16	0.00	0.01	0.00	0.01

B. Cost Analysis

In order to establish test setup, test fixture developed in Chapter 4 will be procured and required hydraulic and data acquisition system will be settled. Test fixture details will be procured in Ankara or Bursa and it costs about \$60000. The company that manufacture details provides laser tracker machine and serves assembly work. Controller and data acquisition system and software can be provided by local suppliers or MTS. Hydraulic service manifold can be provided from MTS. For hydraulic actuator, local supplier RotaTeknik Company is selected. Load cells are bought from Interface Company. Servo valve is also obtained from MTS and hydraulic piping, cabling is carried out by local supplier. The cost of infrastructural investment is estimated about \$200000. Cost of all items required are listed and approximate prices can be found in Table 0.1.

Table 0.1. *Estimated Cost for Equipment*

<i>Type</i>	<i>Quantity</i>	<i>Price (rough)</i>	<i>Remarks</i>
Test Fixture	1	\$ 60000	
Controller	1	\$ 50000	1 station, 12 channel
Data Acquisition System	1	\$ 20000	32 channel
Hydraulic Service Manifold (HSM)	1	\$ 12000	
Hydraulic Actuator	2	\$ 20000	
Load Cell	2	\$ 8000	
Servo Valve	1	\$ 3000	
Software	1	\$ 20000	AeroPro
Hydraulic Piping		\$ 3500	
Cable Set		\$ 2000	
TOTAL		~200.000 \$	

C. M16 Bolt Loads of Reaction Wall Assembly

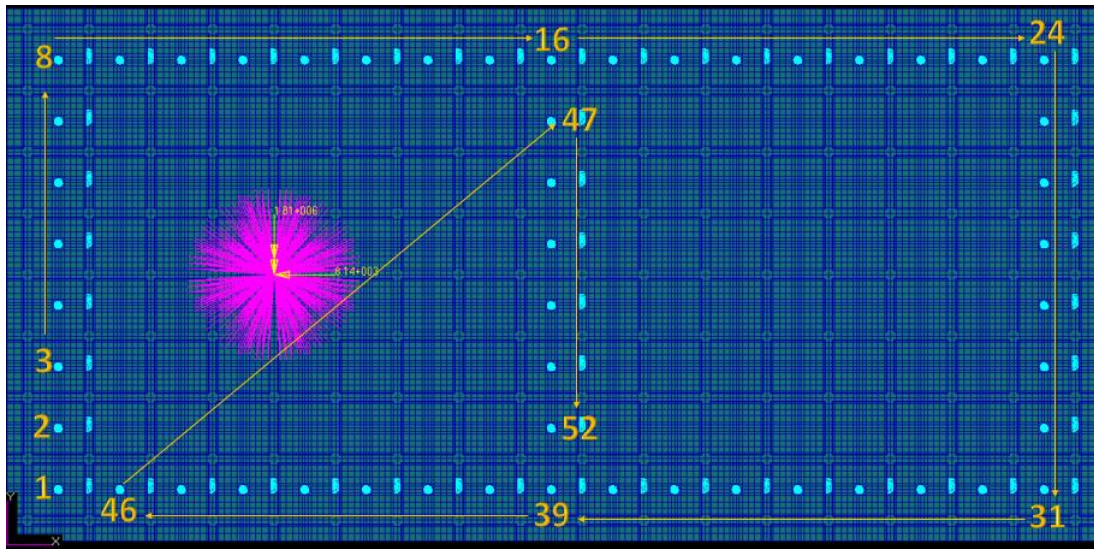


Figure 0.1. Bolt Number Guideline

Table 0.2. Bolt Loads Obtained from FE Results

Bolt #	Fx [N]	Fy [N]	Fz [N]	Radial [N]	Axial [N]
1	109.80	111.06	-76.32	110.01	-76.32
2	304.28	134.84	-13.24	304.32	-13.24
3	516.07	125.54	196.12	516.07	196.12
4	669.49	50.55	398.72	669.50	398.72
5	669.78	-50.41	399.69	669.78	399.69
6	516.40	-125.53	197.09	516.40	197.09
7	304.23	-134.90	-13.31	304.23	-13.31
8	109.72	-111.03	-76.39	109.74	-76.39
9	146.18	-234.05	28.41	146.21	28.41
10	195.49	-275.98	246.92	195.50	246.92
11	231.48	-145.17	152.81	231.53	152.81
12	236.33	90.22	-192.70	236.43	-192.70
13	207.76	238.60	-320.79	207.93	-320.79
14	163.12	237.14	-162.57	163.45	-162.57
15	104.87	164.47	41.91	105.56	41.91

Table 0.2. Bolt Loads Obtained from FE Results (cont'd)

16	73.27	59.22	64.92	74.36	64.92
17	27.90	14.52	9.19	31.45	9.19
18	22.91	12.71	11.95	63.53	11.95
19	18.16	12.06	5.38	165.56	5.38
20	14.00	10.42	2.17	237.73	2.17
21	10.23	8.51	0.62	239.15	0.62
22	6.98	6.74	-0.19	90.86	-0.19
23	4.38	4.82	-0.71	145.34	-0.71
24	2.49	2.14	-0.15	276.48	-0.15
25	6.43	2.76	-0.58	234.36	-0.58
26	9.17	2.13	0.43	71.67	0.43
27	10.34	0.79	1.25	65.62	1.25
28	10.34	-0.79	1.25	28.31	1.25
29	9.17	-2.13	0.43	27.83	0.43
30	6.43	-2.76	-0.58	65.10	-0.58
31	2.49	-2.14	-0.15	71.14	-0.15
32	4.38	-4.82	-0.71	4.38	-0.71
33	6.98	-6.74	-0.19	6.98	-0.19
34	10.23	-8.51	0.62	10.23	0.62
35	14.00	-10.42	2.17	14.00	2.17
36	18.16	-12.06	5.38	18.16	5.38
37	22.92	-12.71	11.95	22.92	11.95
38	27.91	-14.52	9.20	27.91	9.20
39	73.31	-59.26	64.92	73.31	64.92
40	104.98	-164.56	41.91	104.98	41.91
41	163.33	-237.32	-162.57	163.33	-162.57
42	208.06	-238.93	-320.83	208.06	-320.83
43	236.58	-90.59	-192.74	236.58	-192.74
44	231.63	145.27	153.28	231.63	153.28
45	195.61	276.47	247.22	195.61	247.22
46	146.41	234.27	28.23	146.41	28.23
47	206.69	71.08	29.76	206.69	29.76

Table 0.2. Bolt Loads Obtained from FE Results (cont'd)

48	341.67	64.80	-143.11	341.67	-143.11
49	429.35	26.35	-281.35	429.35	-281.35
50	429.41	-26.28	-281.35	429.41	-281.35
51	341.79	-64.78	-143.11	341.79	-143.11
52	206.81	-71.10	29.76	206.81	29.76

D. Hilti HAS – U 8.8 Anchor Loads for Ground Plate

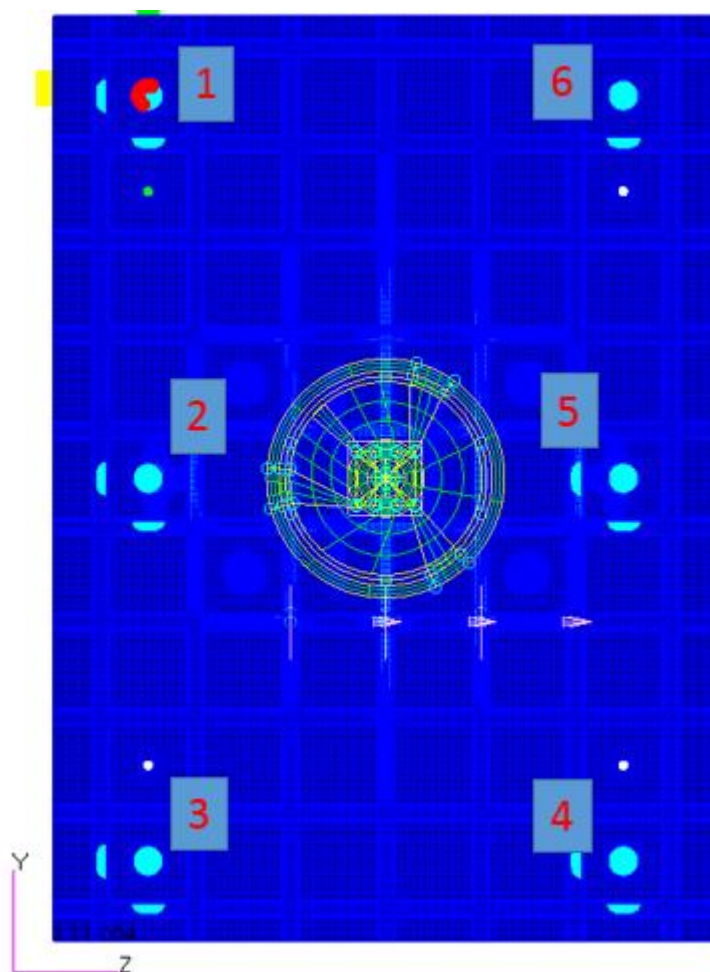


Figure 0.2. Ground Plate Anchor Rod Guideline

Table 0.3. Ground Plate Hilti Anchor Rod Loads

Bolt #	F_x [N]	F_y [N]	F_z [N]	Radial [N]	Axial [N]
1	-142.2	-2.5	108.7	108.7	-142.2
2	-1961.6	0.0	645.4	645.4	-1961.6
3	-142.2	2.5	108.7	108.7	-142.2
4	-142.2	-2.5	-108.7	108.7	-142.2
5	-1961.6	0.0	-645.4	645.4	-1961.6
6	-142.2	2.5	-108.7	108.7	-142.2

E. Hilti HAS – U 8.8 Anchor Loads for Reaction Wall Assembly

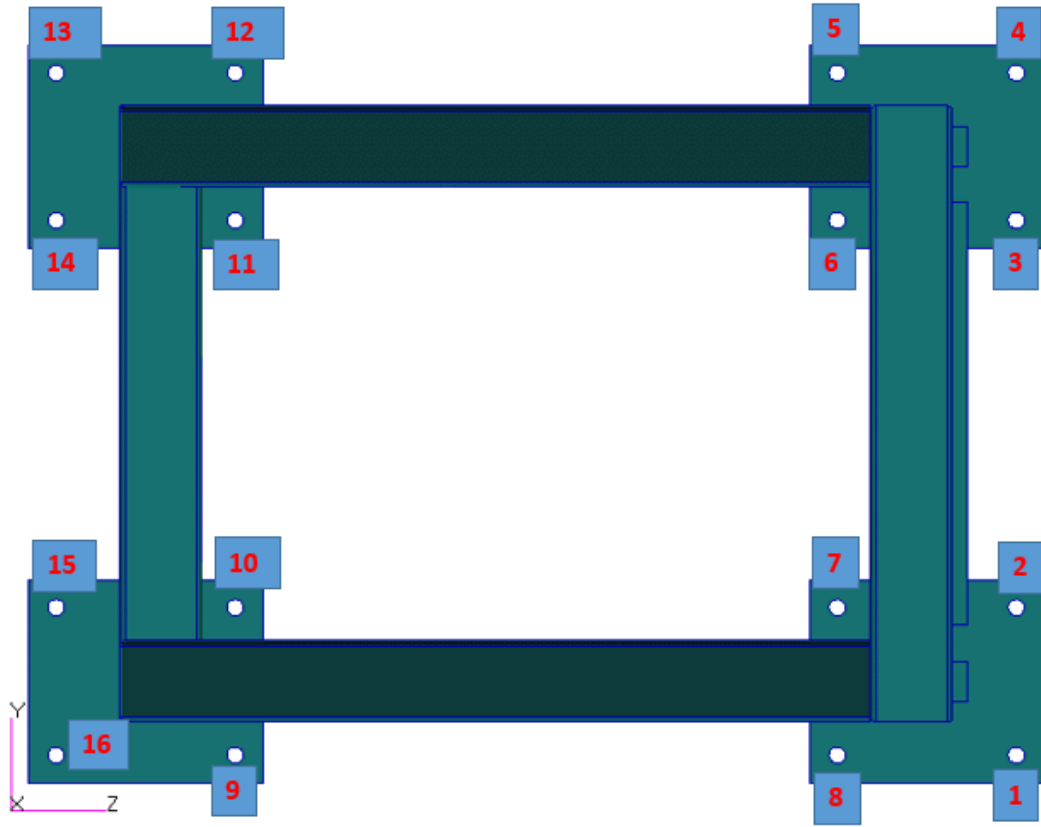


Figure 0.3. Reaction Wall Assembly Anchor Rod Guideline

Table 0.4. Reaction Wall Assembly Hilti Anchor Rod Loads

Bolt #	F _x [N]	F _y [N]	F _z [N]	Radial [N]	Axial [N]
1	925.1	-29.8	-63.7	70.4	925.1
2	898.0	-34.1	-166.4	169.9	898.0
3	901.7	33.9	-165.0	168.4	901.7
4	922.2	30.3	-63.1	70.0	922.2
5	2689.2	1053.3	-401.9	1127.3	2689.2
6	2669.9	-776.1	-446.8	895.5	2669.9

Table 0.4. *Reaction Wall Assembly Hilti Anchor Rod Loads (cont'd)*

7	2682.3	774.2	-450.6	895.8	2682.3
8	2683.8	-1051.6	-399.3	1124.9	2683.8
9	-809.7	61.0	312.2	318.1	-809.7
10	-1079.4	-354.5	54.5	358.7	-1079.4
11	-1078.0	351.8	58.4	356.7	-1078.0
12	-807.1	-58.9	311.9	317.4	-807.1
13	-498.9	-7.1	208.9	209.0	-498.9
14	-729.4	181.9	500.2	532.3	-729.4
15	-729.4	-182.0	500.9	532.9	-729.4
16	-499.1	7.7	209.8	210.0	-499.1